GENETIC EVIDENCE FOR NEURON-GLIA METABOLIC COUPLING IN THE CNS

DISSERTATION

in partial fulfilment of the requirements

for the degree *Doctor rerum naturalium* (Dr. rer. nat.)

in the GAUSS program

at the Georg August University Göttingen,

Faculty of Biology

submitted by

Lotti Marianna Supplie

born in Burg

Göttingen, July 2015

Thesis committee

Prof. Dr. Klaus-Armin Nave

Department of Neurogenetics, Max Planck Institute of Experimental Medicine

37075 Göttingen, Germany

Prof. Dr. Ernst A. Wimmer

Developmental Biology, Johann Friedrich Blumenbach Institute, University of Göttingen,

37077 Göttingen, Germany

Members of the Examination Board

First referee: ***Prof. Dr. Klaus-Armin Nave***

Department of Neurogenetics, Max Planck Institute of Experimental Medicine

37075 Göttingen, Germany

Second referee: ***Prof. Dr. Ernst A. Wimmer***

Developmental Biology, Johann Friedrich Blumenbach Institute, University of Göttingen,

37077 Göttingen, Germany

Further members of of the Examination Board

Prof. Dr. Ralf Heinrich

Cellular Neurobiology, Schwann-Schleiden Research Centre,

37077 Göttingen, Germany

Prof. Dr. Dr. Hannelore Ehrenreich

Clinical Neuroscience, Max Planck Institute of Experimental Medicine,

37075 Göttingen, Germany

Dr. Manuela Schmidt

Emmy Noether-Research Group Somatosensory Signaling,

Max Planck Institute of Experimental Medicine,

37075 Göttingen, Germany

Prof. Dr. Michael Sereda

Molecular and Translational Neurology, Max Planck Institute of Experimental Medicine,

37075 Göttingen, Germany

Date of the oral examination: 31.07.2015

Declaration

I hereby declare that I prepared the Ph.D. thesis "Genetic Evidence For Neuron-Glia Metabolic Coupling In The CNS" on my own and with no other sources and aids than quoted. I would like to gratefully acknowledge Dr. Ursula Fünfschilling who contributed a lot to the first part of my Ph.D. thesis and the collaborations with Dr. Don Mahad and Graham Campbell (serial COX and SDH histochemistry); Prof. Jens Frahm and Prof. Susann Boretius (proton magnetic resonance spectroscopy); Dr. Bastian Brinkmann and Prof. Michael Sereda (electrophysiology) and Dr. Wiebke Möbius and Torben Ruhwedel (electron microscopy).

Göttingen, 21.07.15   Lotti Marianna Supplie

TABLE OF CONTENTS

LIST OF FIGURES

PART II

PART III

ABBREVIATIONS

ADP	Adenosine diphosphate
ANLS	Astrocyte-to-Neuron-Lactate-Shuttle
APP	Amyloid precursor protein
AraC	Arabinofuranosyl cytidine
ATP	Adenosine triphosphate
bp	Base pairs
BG	Bergmann glia
BrdU	5-bromo-2'-deoxyuridine
CKIIα	CamKinaseIIalpha
CAP	Compound action potential
cc	Corpus callosum
CD3	Cluster of differentiation
con	Control
COX	Cytochrome c oxidase
Cox-4.1	ComplexIV, subunit 1
ctx	Cortex
CNS	Central nervous system
CNP	2',3'-cyclic 3'-nucleotide phosphodiesterase
Cre	Causes recombination
DAPI	Diamidino phenylindole
DIV	Days *in vitro*
DMEM	Dulbecco's Modified Eagle's Medium
DNA	Deoxyribonucleic acid
EdU	5-ethynyl-2'-deoxyuridine
EM	Electron microscopy
EYFP	Enhanced yellow fluorescent protein
Fig.	Figure
fl	flox
GABA	Gamma-Aminobutyric acid
GAPDH	Glyceraldehyde 3-phosphate dehydrogenase

DAPI	4',6-diamidino-2-phenylindole
GFAP	Glial fibrillary acidic protein
GFP	Green fluorescent protein
GLAST	Glutamate/ Aspartate Transporter
HSP	Heat shock protein
kDa	Kilo Dalton
LDHA	Lactate Dehydrogenase
LoxP	Locus of crossover of the bacteriophage P1
LTP	Long term potentiation
Mac3	Cluster of differentiation 107b
MAG	Myelin associated glycoprotein
MBP	Myelin basic protein
MEM	Minimum Essential Media
mito	Mitochondria
mL	Molecular layer
MOG	Myelin-oligodendrocyte glycoprotein
mRNA	Messenger ribonucleic acid
n	Number
NeuN	Neuronal nuclei
O4	Oligodendrocyte marker, sulfatide
o/n	Overnight
OL	Oligodendrocyte
Olig2	Oligodendrocyte lineage transcription factor 2
opt.n.	Optic nerve
OPC	Oligodendrocyte precursor cell
P	Postnatal day
PBS	Phosphate buffered saline
PB	Sodium phosphate buffer
PC	Purkinje cell
PCR	Polymerase chain reaction
PEP	Phosphoenolpyruvate

PF	Parallel fiber
PFA	Paraformaldehyde
PK	Pyruvate kinase
PKM1/2	Pyruvate kinase isozyme type M1/2
p-PKM2	PKM2 phosphorylated at tyrosine residue 105
PLP	Proteolipid protein
PNS	Peripheral nervous system
qPCR	quantitative Polymerase Chain Reaction
R26	Rosa26 locus
Rpl13a	Ribosomal protein L13A
Rplp0	Ribosomal protein, large, P0
RNA	Ribonucleic acid
RT	Room temperature
SEM	Standard error of the mean
SD	Standard deviation
S100ß	S100 calcium binding protein
tam	Tamoxifen
Tuj-1	Class III beta-tubulin
VDAC	Voltage-dependent anion channel
v/v	volume percent
w/v	weight per volume
wt	wildtype

1 SUMMARY

The active contribution of oligodendrocytes and astrocytes to sustain brain physiology was completely underestimated, but severe consequences of their dysfunction in various diseases and glia-specific mutants emphasized their importance in maintaining neuronal integrity and function. By the intimate interconnection between neurons, oligodendrocytes and astrocytes a network is established allowing bidirectional interaction. Improved techniques to analyze brain energy metabolism revealed that a high amount of glucose is not oxidatively metabolized. Thus, lactate, the end-product of aerobic glycolysis, is accepted to play an important role in fueling the brain. In this context, oligodendrocytes and astrocytes were assumed to produce lactate that is shuttled to neuronal compartments to benefit mitochondrial respiration and local energy requirements. To obtain supportive evidence for this hypothesis, conditional mouse mutants were generated by targeting COX10, essential to assemble COX (cytochrome c oxidase), the terminal complex of the mitochondrial respiratory chain. Consequently, *Cox10*-deficient cells can only survive by aerobic glycolysis or die. By using well-established Cre-driver mouse lines, selective recombination was achieved in oligodendrocytes and mature Bergmann glia, a cerebellar subpopulation of astrocytes, respectively. In both, disrupted oxidative phosphorylation did not affect the survival of *Cox10*-ablated cells. In the CNS, neurodegeneration, secondary inflammation or abnormal regeneration were not detected in both conditional mutants. Furthermore, the absence of oligodendroglial myelin defects and the normal appearance of synapses engulfed by Bergmann glia, respectively, reflect the ease of adaptation to aerobic glycolysis of these cells. Importantly, elevated lactate concentrations were detected in the living brain of oligodendroglial mutant and control mice by *in vivo* magnetic resonance spectroscopy. This was only reached when mice were exposed to isoflurane anaesthesia which blocks the pyruvate dehydrogenase complex. Furthermore, lactate accumulations immediately dropped by the end of anaesthesia to undetectable levels suggesting a model in which aerobic glycolysis products from oligodendrocytes are rapidly metabolized within white matter tracts in the healthy brain. To investigate a possible underlying mechanism, PKM2 expression was analyzed. This is an isozyme of the pyruvate kinase, specifically upregulated in cancers and highly proliferating cells. The shift of PKM1 to PKM2 is debated to promote aerobic glycolysis in cancer cells and thus tumor growth and proliferation. In adult wildtype mouse brains PKM2 was expressed in cells with oligodendrocyte-like morphology and protein analysis displayed high PKM2 expression abundance in white matter tracts. A possible regulatory mechanism controlling PKM2 activity and thus the velocity of glycolysis was unraveled by the detection of phosphorylated PKM2 in different adult brain regions. Taken together, these findings implicate specific metabolic properties of oligodendrocytes and astrocytes enabling a metabolic coupling to neurons that serves a physiological function.

2 INTRODUCTION

2.1 CELLS IN THE CENTRAL NERVOUS SYSTEM

Specialization of both neurons and glial cells and their persistent interactions are key features of evolution that allowed vertebrate species to develop fast and permitted rapid and coordinated responses to environmental changes. As brains became larger and more complex during vertebrate evolution, the proportion of glia increased and outnumbered the neurons (Sherwood et al., 2006). Despite the role of glia during development, their active participation in the physiology of the brain and the consequences of their dysfunction on the pathology of the nervous system has only been emphasized in recent years.

The mammalian central nervous system (CNS) comprises neurons and glial cells, which can be further divided into microglia and macroglia including oligodendrocytes and astrocytes. Neurons are very specialized cells appearing as heterogenous subpopulations throughout the CNS, but all of them have in common that they are responsible for processing and transmission of information. Electric impulses are conducted along axons to their synapses or other connections to cells, where the action potential is normally converted to a chemical signal. Like neuronal cells, oligodendrocytes and astrocytes derive from neuroepithelial cells and cover a variety of subclasses that are structurally and functionally highly diverse. Microglia, the macrophages of the CNS, which originate from hematopoietic stem cells, are the primary immune cells of the CNS. They respond to pathogens and injuries by becoming "activated" – a process in which they rapidly change morphology, proliferate and migrate to the site of infection/ injury where they phagocytose pathogens and remove damaged cells (Davalos et al., 2005; Dibaj et al., 2010). In the following I will focus only on astrocytes and oligodendrocytes, since both types of glial cells are hypothesized to be involved in the coverage of energetic demands of neurons.
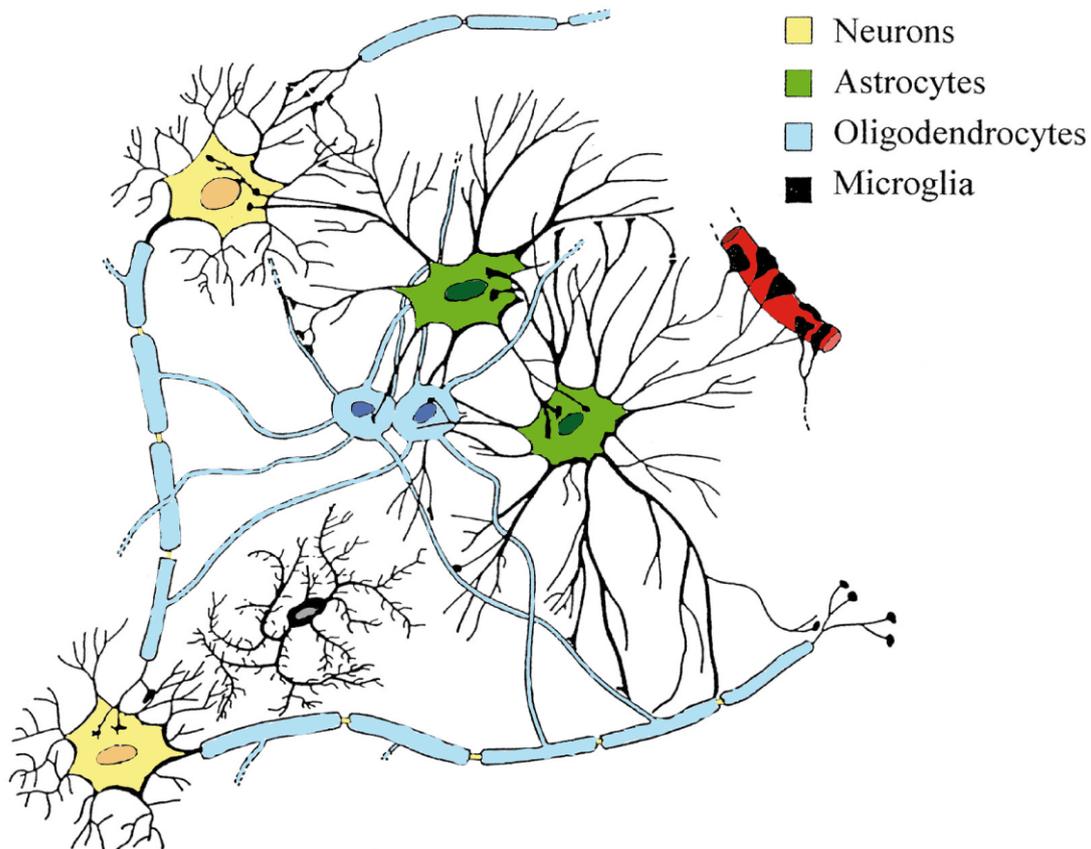
Fig. 1   Glial cells in the CNS

Scheme illustrates the tight interconnection between neurons and glial cells in the CNS. Myelinating oligodendrocytes enwrap up to 40 different axonal segments with myelin enabling fast propagation of action potentials, but also lead to the isolation of axons from the extracellular space. Astrocytes are in direct contact with blood capillaries and they are interconnected among each others and to oligodendrocytes *via* gap junctions. Additionally, astrocytic processes are coupled to nodes of Ranvier and surround many synapses. Microglia, the macrophages of the CNS, are involved in the immune defense. Picture adapted from Baumann and Pham-Dinh, 2001.

2.1.1 OLIGODENDROCYTES– NOT JUST PASSIVE INSULATORS MEDIATING MYELINATION

The best understood function of oligodendrocytes in the CNS and Schwann cells in the peripheral nervous system (PNS) is the myelination of axons, which is considered as the last true invention of vertebrate evolution in the architecture of the nervous system, allowing rapid impulse propagation and space economy. In contrast, in the invertebrate nervous system fast conduction of electric impulses is accompanied by increased axonal calibers. The myelin sheath constitutes the most abundant membrane in the vertebrate nervous system and is a spiral structure of lipid-rich plasma membrane extentions of myelinating glia, each of which contacts and repeatedly envelopes a stretch of axon with subsequent condensation (compact myelin). These insulating segments are called internodes which are separated by

gaps, also known as nodes of Ranvier. These are places where the axolemma is exposed to the extracellular environment, playing a major role in speeding up nerve impulse propagation and reduction of axonal energy consumption by enabling saltatory conduction velocity of action potential (Bunge, 1968; Peters, 1966; Nave, 2010), a prerequisite for the development of complex nervous systems operating quickly and efficiently (Zalc et al., 2008). Besides myelination, there is growing evidence that myelinating glia are not only passive insulators, but also have a crucial role in metabolic support of associated axons, which is important for the maintenance of axonal integrity and survival (Nave, 2010; Amaral et al., 2013; Morrison et al., 2013). Initial indications have emerged from mouse mutants carrying mutations in oligodendrocyte-specific genes and analysis of post-mortem brain tissue of patients with neurological diseases showing neurodegeneration.

The first indication that oligodendrocytes influence and support axonal function was uncovered by the study of mouse mutants lacking the proteolipid protein (*Plp1*), a tetraspan membrane protein in CNS myelin. In these mutants, oligodendrocytes assemble stable myelin and display only minor ultrastructural abnormalities. However, aged *Plp1*-null mutants suffer from insufficient axonal transport, followed by axonal swellings and Wallerian degeneration (Griffiths et al., 1998; Edgar et al., 2004). Additionally, MAG-deficient mice (myelin-associated glycoprotein, a non-compact myelin protein) are fully myelinated but exhibit a decrease in axon calibers and neurofilament spacing, which probably cause axonal loss (Yin et al., 1998). Similar neurodegenerative phenotypes could be observed in mouse mutants deficient of CNP1 (2',3'-cyclic nucleotide 3'-phosphodiesterase), which is localized in the non-compact myelin. Like PLP1, CNP1 is not essential for proper myelination, but is required for axonal integrity (Lappe-Siefke et al., 2003; Edgar et al., 2009). *Cnp1*-null mutant mice are more severely affected than *Plp1*-null mice, with an earlier onset of axonal swellings and neurodegeneration prior to defects of axonal transport, already detectable at P10 in the spinal cord (Fig. 2a, b). This axonopathy is progressive over age and results in premature death of *Cnp1*-null mutants at the age of 9 to 10 months. In striking contrast, shiverer mice lacking MBP (myelin basic protein, a compact myelin protein) display no axonal degeneration, although they are severely dysmyelinated (Rosenbluth, 1980). However, these findings strongly imply that axonal survival can be sustained despite the near loss of myelin, but not in the presence of ´unfunctional myelin´. Thus, myelin is not only a passive, electric insulator, but also benefits axonal survival and function by support mechanisms (Nave, 2010).
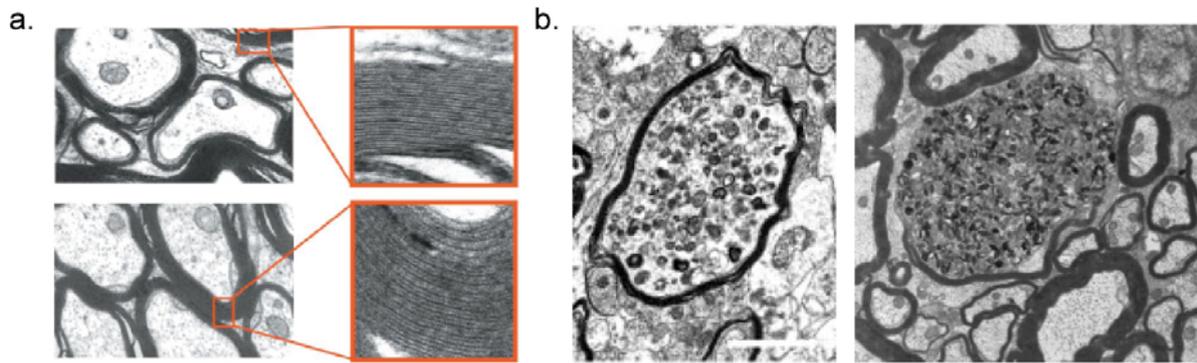
Fig. 2   *Cnp1*-null mutants develop a severe axonopathy and exhibit normal myelin

(a.) Electron micrographs and high power magnification of white matter tracts in spinal cord cross-sections of *Cnp1*-null mutant mice at 2.5 months display normally assembled myelin (lower panel) which is comparable to age-matched controls (upper panel). **(b.)** Depicted are spinal cord cross-sections of *Cnp1*-null mutants. Already at the age of P10 axonal spheroids as sign of axonal pathology are visible (left). This is progressive with age and characterized by the accumulation of membranous organelles and multivesicular bodies at 7 months (right). Pictures were taken from Edgar et al., 2009; Lappe-Siefke et al., 2003.

Many clinical phenotypes of neurological diseases in humans are caused by the loss of myelin. The best examined example is multiple sclerosis (MS), which has been historically assumed to be a myelin-specific autoimmune disease without affecting axons. However, this consideration has changed in the mid-1990s. Histological investigations of post-mortem brains from MS patients exhibited an early involvement of axons, characterized by transected axons and Wallerian degeneration already obvious with the onset of disease, which results in progressive axon loss and brain atrophy (Dziedzic et al., 2010; Peterson et al., 2001; Trapp et al., 1998). So far, the interplay between inflammation, demyelination, and neurodegenerative alterations that correlate best with clinical disability of patients are still not fully elucidated. It rather emphasizes the need to explore axon-glia interactions essential for neuronal survival and function.

To better understand the interdependence of oligodendrocytes and neurons it is important to have a detailed look at the ultrastructure of the myelin sheath that covers almost the entire surface of the axon serving for electrical insulation but also isolates the axon from the excess to nutrients from the extracellular space. In contrast, non-compacted regions of the myelin, which consist of the lateral endings of each myelin layer (known as "paranodal loops") and the inner tongue remain in close contact with the underlying axon forming cytoplasmic channels (Fig.3). Recently, Snaidero and colleagues (2014) could even show by electron microscopy of freshly highpressure frozen optic nerves that within the developing myelin sheath numerous cytoplasmic channels are located that changed the view of CNS myelin ultrastructure (Snaidero et al., 2014). Thus, a physical connection between myelin, especially

5
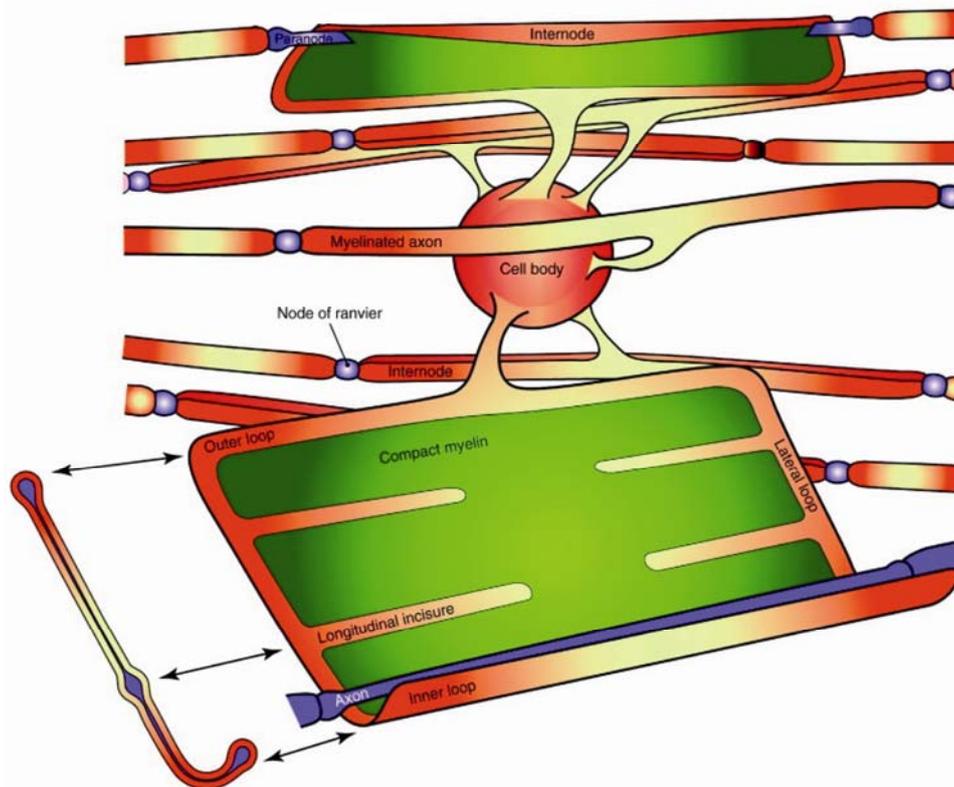
Fig. 3   Schematic view at the CNS myelin ultrastructure.

Myelinating oligodendrocytes form several processes that ensheath individual axonal segments with myelin (internodes). The illustration of an unwrapped myelin sheath reveals small areas of uncompacted myelin, which are the paranodal loops (lateral loops), inner and outer tongues (inner and outer loop) generating an interface between the oligodendroglial cytoplasm and the axonal surface. Figure taken from Aggarwal et al., 2011.

the non-compacted regions and its associated axon is generated. Additionally, astrocytes which are in direct connection to the blood-brain-barrier and therewith to nutrients of blood vessels are also contributors to the axo-glial interplay. They are partners of neurons by contacting them at the nodes of Ranvier and as well as of oligodendrocytes *via* gap junctions (Black and Waxman, 1988; Nagy et al., 2003).

Proper repetitive axonal firing causes massive sodium influx and requires subsequent repolarization that is mediated by energy-consuming Na^+-K^+-ATPases, which were shown to be distributed along the internodal axolemma (Young et al., 2008), where most of axonal mitochondria reside, which was validated by 3D-EM analysis of the optic nerve (Edgar et al., 2008; Ohno et al., 2011). Since mitochondria are the major source of ATP by oxidizing glycolysis end products, the internodal accumulation of stationary mitochondria may help to facilitate active, energy-dependent axonal transport and simply reflects high metabolic demands at these sites. More distal compartments like synaptic terminals and active growth

cones (Kang et al., 2008; Morris and Hollenbeck, 1993) require also much energy and are dependent on proper trafficking of glycolytic enzymes and mitochondria for the local maintenance of sufficient energy production. However, the anterograde travelling rates of cargoes, mitochondria and cytosolic proteins are comparably slow. Pulse-chase radiolabelling studies revealed that membrane-spanning or anchoring domains packaged into cargoes are conveyed *via* fast axonal transport at overall rates of 50–400 mm/ day (Perrot and Julien, 2009), whereas cytosolic proteins are shuttled much more slowly at rates of 1–10 mm/ day, (Brady and Lasek, 1981; Oblinger et al., 1988; Yuan et al., 1999). Considering the length, an axon can reach (motoneurons up to 100 cm in humans) and especially the sluggish transfer of cytosolic proteins, including glycolytic enzymes, the metabolic supply of the axon presents a logistical problem. This might be overcome by an oligodendroglial trophic support to neurons, e.g. by shuttling of glycolytic end products (lactate, pyruvate) to mitochondria in the axonal compartment, where their metabolization *via* oxidative phosphorylation benefits neuronal energy requirements (Nave, 2010; Amaral et al., 2013; Morrison et al., 2013). This hypothesis could also explain the length-dependent axon loss in many neurological diseases and mouse mutants with primary non-compacted myelin deficits.

Interestingly, a study of activity markers of glycolysis and oxidative phosphorylation in white matter tracts and cortex by Morland and colleagues revealed that glucose oxidation is low in normal white matter when compared to grey matter (Morland et al., 2007). Furthermore, the authors calculated that half of the glucose taken up by white structures might be processed glycolytically suggesting that white matter is a possible source of the glycolytic end products pyruvate and lactate for other cellular compartments.

Based on these data a new research direction has emerged recently assessing oligodendrocytes´ function not only as passive insulators, but has attracted attention to their possible metabolic importance supporting neuronal ATP demands. Two recent papers have shed new light on axonal support mechanisms.

Evidence for this hypothesis is provided by the group of Jeffrey D. Rothstein, who investigated the monocarboxylate transporter MCT1 which was shown to be the most abundant MCT in the CNS (Rinholm et al., 2011). MCT1 transports, along with the neuron-specific MCT2 and astrocyte-specific MCT4, monocarboxylic acids including lactate, pyruvate and ketone bodies. Hence, they might provide routes for glycolytic end products. By generating a MCT1 BAC transgenic mouse model they showed *in vivo* that MCT1 expression is almost exclusively found in oligodendrocytes and its downregulation led to axonal defects *in vitro* and *in vivo* (Lee et al., 2012). Treatment of spinal cord organotypic cultures with shRNA specific for MCT1 or its pharmacological inhibiton resulted in motor neuron loss

whereas oligodendroglial death could not be observed. Interestingly, neuron death could be prevented by adding exogenous lactate to the medium, supporting the hypothesis that failed lactate release from oligodendroglia and therewith its uptake into neurons is the cause for neurodegeneration. *Mct1*-null mutants are embryonically lethal. But more importantly, heterozygous *Mct1*-null mice, with 50% reduction in MCT1 expression or following lentiviral-mediated gene silencing in oligodendrocytes caused a late-onset axonopathy and neurodegeneration in brain and spinal cord (Lee et al., 2012). Notably, axon pathology in these mice is similar to *Cnp1*- and *Plp1*-null mice. Taken together, the results suggest that MCT1-regulated lactate export from oligodendroglia is a crucial component of the local energy supply to axons, and the disruption of this transport leads to axon dysfunction and ultimately to neuron degeneration. Thus, lactate release from oligodendrocytes is indeed essential for long-term axonal integrity.

In parallel, the group of Klaus-Armin Nave independently investigated the role of oligodendrocytes regarding a hypothetical metabolic coupling to axonal compartments (Fünfschilling et al., 2012). Parts of this PhD thesis contributed to this analysis and will be described in more detail in the results chapter. In short, conditional mouse mutants were generated, in which specifically mature oligodendrocytes fail to assemble stable cytochrome c oxidase, the complex IV of the mitochondrial respiratory chain. Thus, mutant oligodendrocytes are forced to live by glycolysis alone. Interestingly, oligodendrocytes lacking the ability to generate energy by oxidative phosphorylation survived. Moreover, no sign of brain pathology could be observed (Fünfschilling et al., 2012). This stands in striking contrast to mouse mutants, in which the same genetic modification driven selectively in a subset of projection neurons, suffering from severe neurodegeneration that caused premature death of mutants at around 4 months of age (Fukui et al., 2007) strongly indicating the dependence of neurons on mitochondrial energy production. However, proton NMR spectroscopic analysis of mouse brains, in which oligodendrocytes specifically lost their capacity for oxidative phosphorylation revealed significantly elevated lactate concentrations when compared to controls. In this context mice were anaesthetized with isoflurane, which is an inhibitor of mitochondrial metabolism, enabling detection of lactate accumulations by NMR. Importantly, at the end of anaesthesia the observed increase of lactate recurred to normal, undetectable levels, implying its rapid use by other cellular compartments (Fünfschilling et al., 2012).

These studies proposed a link between glycolytic metabolism in oligodendrocytes and axonal integrity and function. With regard to the broad spectrum of neurodegenerative diseases that are associated with myelin defects denotes the necessity to better understand the axo-glia interplay in order to develop new therapeutic approaches.

2.1.2 ASTROCYTES– MORE THAN JUST PASSIVE SCAFFOLDING CELLS

Historically, astrocytes were often considered as passive scaffolding cells of the mammalian CNS. However, work over the past 2 decades suggests that astrocytes play a more active role and are involved in a wide variety of complex and essential functions in the healthy brain. Astrocytes are specialized glial cells that are distributed throughout the CNS. According to their cellular morphology and location, astrocytes can be divided into two main classes, the protoplasmic and fibrous astrocytes. The latter are located in white matter tracts and are characterized by long, sparsely branched processes contacting nodes of Ranvier. Protoplasmic astrocytes, which are found in grey matter regions, have many branching processes, which envelop synapses (Cajal, 1909). As heterogenous as they are there are even more astrocytic subpopulations including Bergmann glia in the cerebellum, Müller glia in the retina, pituicytes in the neurohypophysis, cribrosocytes at the optic nerve head, and others.

Astrocytic endfeet project directly to blood vessels, therewith participating in the formation and maintenance of the blood-brain barrier and providing access to nutrients from the cerebral blood stream (Kacem et al., 1998), whose flow velocity can be adapted by astrocytes in response to changes in neuronal activity (Attwell et al., 2010; Gordon et al., 2007). Moreover, astrocytes are interconnected among each other in a coordinated syncytium and are coupled to oligodendrocytes *via* gap junctions (Giaume et al., 1991; Nagy et al., 2003). In this manner a highly organized network between neurons, astrocytes, oligodendrocytes and capillaries is generated that allows bidirectional communication and may provide routes for metabolites.

The relationship between astrocytes and neurons, assured by the intimate physical connection of astrocytic processes to synapses, starts already during neurogenesis when astrocytes guide neuronal migration, survival and process extension. Later they are involved in formation, maintenance and remodelling of synapses mainly through release of trophic factors such as brain-derived neurotrophic factor (Powell et al., 1999; Ullian et al., 2001a). There is growing evidence that in adulthood astrocytes are active partners of synapses. They express a plethora of transporters important for the clearance of neurotransmitters from the synaptic cleft (Genoud et al., 2006). Moreover, they were reported to be responsible for the recycling of synaptically released glutamate and GABA through the glutamate/GABA-glutamine cycle (Bak et al., 2006; Rothstein et al., 1996). A variety of receptors are expressed on astrocytes, which response to neuronal activity with an increase of intracellular calcium concentrations (Dani et al., 1992; Nimmerjahn et al., 2009). A specific consequence of astrocytic internal calcium elevations is the secretion of so-called gliotransmitters, including glutamate, adenosine triphosphate, GABA and d-serine (Parpura et al., 1994;

Zhuang et al., 2010; Panatier et al., 2006), which adapts synaptic transmission and plasticity (Gourine et al., 2010; Chen et al., 2012). This often results in several, often opposite types of effects, including stimulation or inhibition of synaptic transmission and participation in long-term potentiation or depression (Panatier et al., 2011; Yang et al., 2003; Shigetomi et al., 2013). The underlying mechanism how astrocytes release transmitters still remains a subject of debate (e.g. reviewed by Hamilton and Attwell, 2010; Araque et al., 2014). However, these findings have led to the concept of "tripartite synapse", which represents a functional view of synaptic physiology that considers astrocytes as active contributors controlling neuronal information transfer.

Concomitantly, another model has flourished implying that astrocytes also support brain activity by supplying neurons with energy metabolites. This concept was originally proposed by Magistretti and Pellerin in 1994 claiming "Glutamate uptake into astrocytes stimulates aerobic glycolysis" (Pellerin and Magistretti, 1994a). This publication could be considered as the cornerstone for the beginning of a new research field and the development of the "Astrocyte-to-Neuron-Lactate-Shuttle" (ANLS) hypothesis. Here, they described a tight metabolic connection between cortical synapses and their surrounding glial cell, in which the activity-dependent glutamate release in the synaptic cleft at glutamatergic synapses in the cortex is followed by the clearance of glutamate *via* glutamate transporters on astrocytes. The entry of sodium that is cotransported with glutamate activates astrocytic Na+/K+ ATPase, whose activity results in an enhancement of the glycolytic flux, hence the glucose uptake from the capillaries is stimulated. Lactate, the major end product of aerobic glycolysis, is released by astrocytes and taken up by neurons where it can be further metabolized in the tricarboxylic acid (TCA) cycle, thereby contributing to the energy budget of neurons (Pellerin and Magistretti, 1994). The rapid exchange of metabolites, such as lactate across the plasma membrane of cells requires expression of appropriate transporters. Monocarboxylate transporters (MCT) catalyze the proton-linked transport of glycolysis products pyruvate or lactate (Pierre and Pellerin, 2005). Three isoforms (MCT1, 2, and 4) are expressed in the CNS, whose distribution is heterogenous (Halestrap and Wilson, 2012). MCT1 and MCT4 were shown to be expressed by astrocytes, whereas MCT2 is preferentially expressed by neurons (Pellerin et al., 1998; Pierre et al., 2000, 2002), which is one prerequisite for lactate shuttling from astrocytes to neurons. Importantly, the disruption of actrocyte- or neuron-specific MCTs affects long-term memory *in vivo*, suggesting a trophically, supportive role of astrocytes for neuronal function (Suzuki et al., 2011).
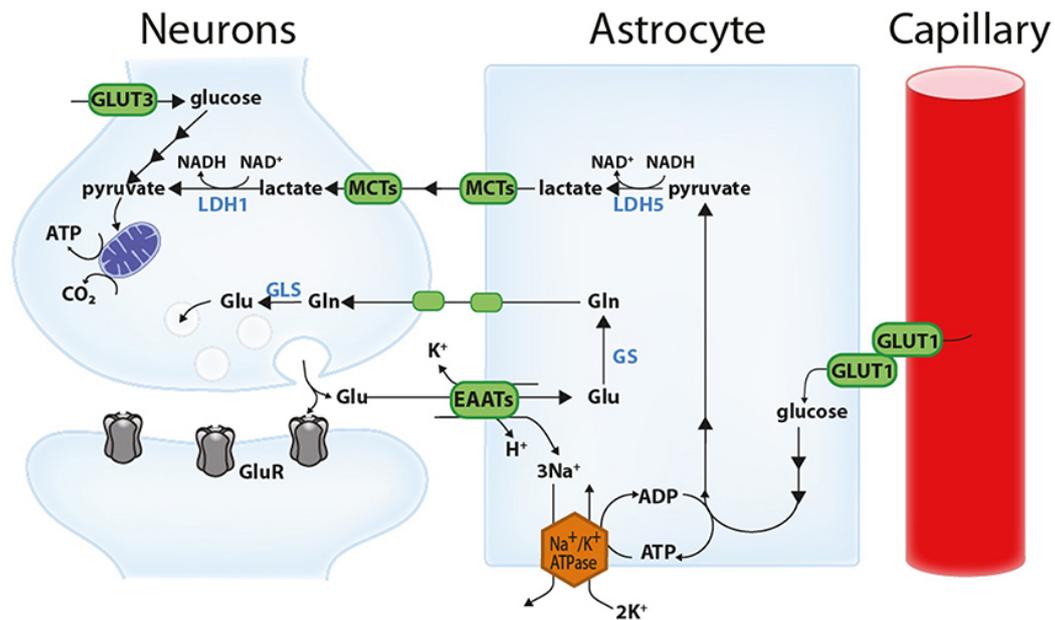
Fig. 4   Schematic representation of the ANLS hypothesis

Glutamate (Glu) release at the active synapse stimulates neuronal glutamatergic receptors (GluR). A large proportion of the glutamate is taken up by astrocytes *via* excitatory amino acid transporters (EAATs, more specifically GLT-1 and GLAST) together with sodium ions (Na^+). Na^+ is extruded by the Na^+/K^+ ATPase, consuming ATP which triggers nonoxidative glucose utilization in astrocytes and glucose uptake from blood vessels through the glucose transporter GLUT1. Pyruvate is converted to lactate by the lactate dehydrogenase 5 (LDH5) and shuttled to neurons *via* monocarboxylate transporters (MCT1 and MCT4 in astrocytes, MCT2 in neurons). In neurons, this lactate is metabolized to pyruvate (Pyr) by LDH1 and used as a metabolite to support the neuronal energy budget. Concomitantly, astrocytes participate in the recycling of synaptic glutamate by its conversion to glutamine (gln) by the glutamine synthetase (GS) and its subsequent transport to neurons, where it is converted back to glutamate by glutaminase (GLS). This figure is taken from Bélanger et al., 2011.

The concept of the ANLS based on several studies revealing striking metabolic differences between astrocytes and neurons. That neurons consume most of the energy during brain activation was already discovered in 1977 by positron emission tomography (PET) imaging of labelled F-fluoro-2-deoxyglucose (Sokoloff et al., 1977). Several PET studies in awake adult humans by Fox and Raichle, led to a fundamental rethinking of brain metabolism. They detected that the activity-dependent increases in blood flow and glucose uptake were only partly matched by parallel raises in oxygen utilization (Fox et al., 1988; Fox and Raichle, 1986). These investigations strongly indicate that neuronal activity stimulates aerobic glycolysis. Nonetheless, due to resolution limitations the cellular contribution remained elusive. However, studies on transcriptomic level of individually isolated cells revealed a different metabolic profile of neuronal and astrocytic cells indicating a prevalence of glycolytic pathways in astrocytes (Lovatt et al., 2007; Cahoy et al., 2008). In accordance with this, investigations of Itoh and Bouzier-Sore confirmed a higher glycolytic capacity in astrocytes

when compared to neurons in which oxidative metabolism predominates. Further, they figured out that astroglia metabolize glucose mainly to lactate which is released into the extracellular space and preferentially taken up and oxidized by neurons over pyruvate/ lactate produced intracellularly by glycolysis (Itoh et al., 2003; Bouzier-Sore et al., 2006). This lactate utilization was directly assessed in human brains by MRS imaging of ^{13}C-labeled lactate and was detected to be neuron specific (Boumezbeur et al., 2010). More important, lactate is able to maintain neuronal activity *in vivo* and even a preference of neurons to lactate over glucose in the presence of both metabolites is observed (Wyss et al., 2011).

However, the cellular origin and its possible contribution to the energy metabolism of the CNS are still issues of controversial debate. By now, direct *in vivo* evidence for the ANLS hypothesis is elusive and emphasizes the importance to further investigate the metabolic interactions between astrocytes and neurons.

2.2 THE WARBURG EFFECT– PKM2 MIGHT SERVE AS A MODULATOR OF GLYCOLYSIS

That mammalian cells metabolize glucose *via* glycolysis, citrate cycle and oxidative phosphorylation is an established dogma of cell biology and only few exceptions were made for cellular conditions in which only limited oxygen levels are available like in skeletal muscle cells during exercise. This was originally overcome by Otto Warburg who discovered that cancer cells rely on glycolysis for energy production, despite the presence of sufficient oxygen (Warburg, 1926). This phenomenon has been termed the Warburg effect or aerobic glycolysis. However, tumor growth is not always connected to a high rate of glucose conversion to lactate. It has been shown that several tumor cell lines are able to proliferate in media with low glucose supply without producing lactate *via* glycolysis (Mazurek et al., 1998; Mazurek, Michel, et al., 1997; Reitzer et al., 1979). Furthermore, aerobic glycolysis is not only an unique feature of cancer cells. In normal proliferating cells such as lung, fat, embryonic or adult stem cells a dependency on the glycolytic pathway was determined (McKeehan, 1982). This provides a dual advantage for dividing cells, including cancer cells, ensuring the supply with energy and glycolytic intermediates (phosphometabolites) that are required as precursors for the synthesis of nucleic acids, amino acids, lipids and additionally the regeneration of NADPH, which is needed for fatty acid synthesis (Mazurek et al., 1997; Dringen et al., 2007).
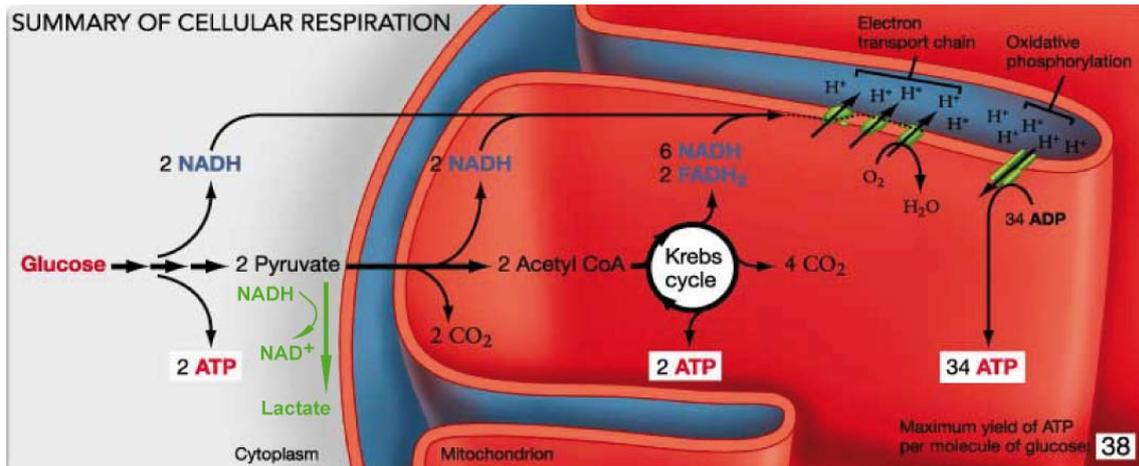
Fig. 5   Gross overview about glucose metabolism

After entering the cell, glucose is glycolytically converted in several steps into pyruvate that produces 2 molecules ATP. Normally, pyruvate is shuttled into the mitochondrium, where it is further metabolized *via* the Krebs cycle. By that reduction equivalents (NADH) are produced, whose electrons are transported along three pumps (complex I, II and III) of the respiratory chain, which are bound in the inner mitochondrial membrane. Finally, the electrons are transferred to oxygen. The electron conveyance leads to a proton flow from the matrix to the intermembrane space of the mitochondrium and generates a proton gradient, powering the ATPase to catalyze a huge amount of energy. By this process termed oxidative phosphorylation 34 molecules ATP per glucose molecule are produced. However, in some exceptions, energy metabolism is restricted to glycolysis. In that case pyruvate is converted to lactate, an absolutely necessary step regenerating NAD^+ that ensures continuous glycolysis. Debranching synthetic pathways were not considered in the depicted scheme. Picture adapted from Biochemistry, Volume 6.

Investigations of mechanisms controlling the Warburg effect of tumor metabolism put attention to the pyruvate kinase (PK), that catalyzes the conversion of phosphoenolpyruvate (PEP) to pyruvate, which is the last but rate-limiting step of glycolysis. Depending on metabolic requirements different isozymes of PK are expressed in various cells and tissues. In total four isozymic forms, consisting of type L, R, M1 and M2 are known to be present in the mammalian organism. PKL is found in tissues with high rates of gluconeogenesis such as liver and kidney (Domingo et al., 1992). Erythrocytes, in which mitochondria are absent, express type R (Rodriguez-Horche et al., 1987). PK isozymes type L and R are encoded by the same gene, but are under the control of different promoters. PKM1 expression is ubiquitous, but to a higher extent in tissues, in which rapid supply of large ATP amounts is important such as in muscle and brain.
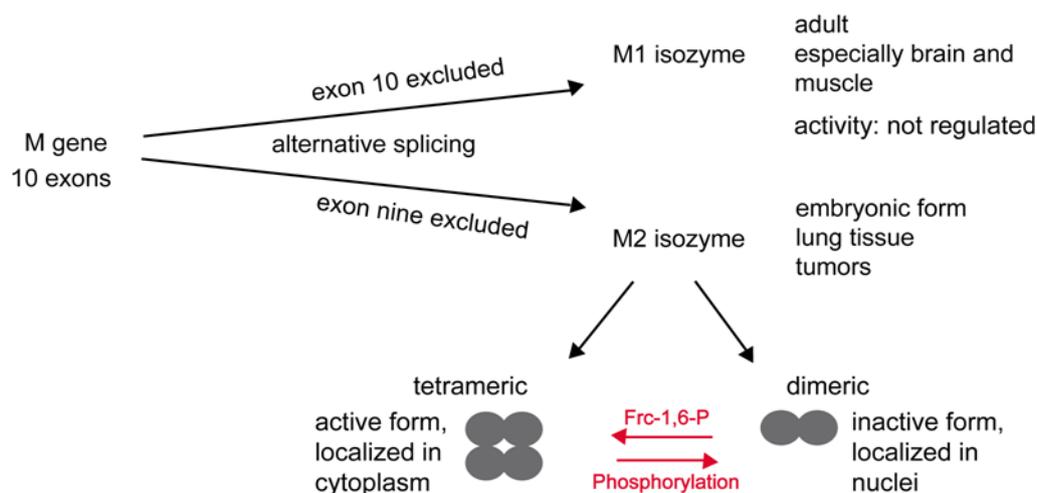
Fig. 6   Summary of PKM1 and PKM2 characteristics

PKM1 and PKM2 are alternative splicing transcripts originating from the same gene, but differing slightly in their exon composition. The majority of differentiated cells expresses PKM1 that has a high affinity to its substrate PEP and its activity can not be modulated. In contrast, the activity of PKM2 can be regulated by several posttranslational modifications such as phosphorylation that leads to the dissociation of active PKM2 tetramers, by what the glycolytic rate is slowed down. The accumulation of fructose-1,6-bisphosphate causes the tetramerization and activation of PKM2. The activity state of PKM2 is associated to its cellular localization. Whereas the dimeric, inactive form is found in the nucleus, the tetrameric PKM2 is distributed in the cytoplasm. PKM2 is strongly expressed in embryonic phases and is replaced in most cells by PKM1 during development. In still high proliferating, differentiated cells the cytoplasmic form of PKM2 is still present. In cancer cells PKM2 is strongly expressed and found to be translocated to the nucleus. Picture adapted from Mazurek, 2011.

PKM2 is expressed during embryonic development and in rapidly dividing cells, including lung cells, adult stem cells and especially tumor cells (Reinacher and Eigenbrodt, 1981; Eigenbrodt et al., 1985; Staal et al., 1991; Hacker et al., 1998). PK isozymes type M1 and M2 are differently spliced products of the same mRNA transcript (exon 10 is excluded in PKM1 and exon 9 is excised in PKM2) and differ in 22 of 531 amino acids (Noguchi et al., 1986; Tanaka et al., 1967).

In the following only on PKM1 and PKM2 will be focussed due to their (possible) importance in brain metabolism.

PK has been largely conserved throughout evolution and usually appears as a homotetramer composed of four identical subunits. However, PKM1 and PKM2 display various regulatory properties. PKM1 is constitutively active, efficiently converting PEP and ADP to pyruvate and ATP (Ikeda and Noguchi, 1998). In comparison, the modulation of PKM2 activity is controlled by a tightly woven regulatory network that decides the fate of glucose to promote either synthetic pathways or energy production. PKM2 can exist in an active tetrameric state, which is the common PKM2 appearance of normal proliferating cells (Mazurek and Eigenbrodt,

2003; Kumar et al., 2007). However, in response to different stimuli such as metabolic intermediates or oncogenes PKM2 tetramers dissociate into dimers, which are inactive and consequently slow down glycolysis and thus ATP generation. This allows accumulation of glycolytic intermediates used in anabolic pathways to build up amino acids, nucleotides and lipids. Importantly, the Pentose-Phosphate-Pathway (PPP), a debranching pathway of glycolysis, is indirectly coupled to fatty acid synthesis due to its delivery of NADPH by PPP that is crucial for the synthesis of fatty acids and cholesterol, two major lipids of myelin (Mazurek, Boschek, et al., 1997; Dombrauckas et al., 2005; Christofk et al., 2008; Gui et al., 2013). In addition, PPP-derived NADPH is needed for the function of glutathione that is important for the defense against oxidative stress (Hirrlinger et al., 2002).

Knockout studies with different cancer cell lines indicate a regulatory mechanism underlying the alternative splicing of the PKM gene controlled by c-Myc that mediates the expression of heterogeneous nuclear ribonucleoproteins hnRNPA1 and hnRNPA2. These hnRNPs bind repressively to the PKM sequence flanking exon 9, which results in exon 10 inclusion (David et al., 2010). Further, it was reported that the activation of epidermal growth factor receptor (EGFR) signalling promotes upregulation of PKM2 expression (Yang et al., 2011).

On protein level a key metabolite regulating the PKM2 tetramer/ dimer ratio is fructose-1,6-bisphosphate (FBP), an upstream intermediate of PEP. Binding of FBP leads to PKM2 tetramerization, whereas its release causes subunit dissociation into inactive dimers (Ashizawa et al., 1991). Furthermore, the interaction with different oncoproteins such as the E7 oncoprotein of human papilloma virus type 16 is described to induce dimer formation (Zwerschke et al., 1999). Apart from that, several posttranscriptional modifications, including phosphorylation, acetylation, oxidation and sumoylation are suggested to be involved in PKM2 dimer formation (Anastasiou et al., 2011; Hitosugi et al., 2009; Lv et al., 2011; Spoden et al., 2009). However, by a phosphoproteomic analysis of Hitosugi and colleagues (2009) it was demonstrated that specific phosphorylation of PKM2 at tyrosine residue 105 (Y105) masks the binding site of FBP and thus inhibits the association of PKM2 tetramers. Further, they figured out that in many human cancers PKM2 is phosphorylated at Y105 and observed a decreased growth rate when the tyrosine residue 105 was substituted by phenylalanine, but only under hypoxic conditions (Hitosugi et al., 2009). Therefore, this study proposes that phosphorylation and dephosphorylation kinetics at Y105 of PKM2 influence the velocity of glycolysis which regulates the cell proliferation index in tumors.

However, other residues of PKM2 were detected to be phosphorylated. An *in vitro* kinase assay containing PKM2 and active extracellular signal-regulated kinase 2 (ERK2) showed that ERK2 phosphorylates PKM2 specifically at serine residue 37, whereas mutated serine 37 remains unphosphorylated (Yang, Zheng, et al., 2012). Further, the authors

showed that upon EGF-induced ERK activation PKM2 translocates into the nucleus, whereas PKM1 is observed to remain in the cytoplasm (Yang, Xia, et al., 2012; Yang et al., 2011; Lv et al., 2013). Gel filtration chromatography indicated that nuclear PKM2 is completely dimeric, while the cytoplasmic PKM2 exists in both dimeric and tetrameric state and it could be determined that the malignancy grade of human cancer cell lines corresponds to a higher level of nuclear PKM2 (Gao et al., 2012). Further, there is emerging evidence that the nuclear PKM2 does not act as a pyruvate kinase anymore, but functions as a transcription factor. By now several independent studies displayed participation of PKM2 in activation of mek5, transcription 3 (STAT3), ß-catenin transcription leading to upregulation of LDHA, GLUT1 and PKM2 itself and thus promoting tumor growth and cell proliferation (Lv et al., 2013; Yang et al., 2011; Yang, Xia, et al., 2012).

Thus, PKM2 can be considered as a key enzyme responsible for keeping the balance of macromolecule formation (dimer) and energy production (tetramer) according to cell demands- at least in cancer cells. However, underlying regulatory mechanisms seem to be very complex and are still subject of controversial debate.

3 AIMS OF THE STUDY

Recently, several studies suggested that oligodendrocytes and astrocytes have a trophic function for the survival and integrity of neurons. Specifically, they are hypothesized to produce lactate to support neuronal energy requirements by shuttling lactate. To address this question, conditional mouse mutants were generated by targeting the *Cox10* gene, in which exon 6 is flanked by LoxP sites. *Cox10* is ultimately necessary to assemble COX, the terminal complex of the mitochondrial respiratory chain. Hence, in *Cox10* mutant mice, COX is cell-type specifically disrupted. Consequently, lactate needs to be generated to maintain the NAD^+/ NADH equilibrium ensuring continuous glycolysis. Hence, *Cox10*-deficient cells live by aerobic glycolysis or simply die.

Part I: To study the energy metabolism of mature oligodendrocytes and their dependency on oxidative phosphorylation, floxed *Cox10* mice were crossbred with the CNP1-Cre and the tamoxifen-sensitive PLP1-CreERT2 driver mouse lines mediating recombination specifically in myelinating glia. How the loss of mitochondrial respiration affects the structural and functional integrity of the PNS (Schwann cells) and the CNS (oligodendrocytes) are analyzed. In addition, magnetic resonance spectroscopy is performed in the living brain to investigate the cellular origin and contribution of lactate in energy metabolism and to get a better insight into the trophic function of oligodendrocytes.

Part II: To address the open question whether adult astrocytes *in vivo* are capable of providing lactate to neighboring synapses to support the local energy budget, floxed *Cox10* mice were as well used. By crossbreeding them with mice expressing the tamoxifen-sensitive Cre-recombinase from the GLAST (*Slc1a3*)-promoter, astrocyte specific deletion of *Cox10* was achieved. Since GLAST is expressed by the majority of Bergmann glial cells, a specific astrocyte subpopulation in the cerebellar cortex, the analyses mainly focussed on the cerebellum. How the disruption of mitochondrial function affects the integrity of the cerebellum is studied to draw conclusion to the origin and fate of lactate

Part III: The established presumably link between an aerobic glycolytic metabolism of oligodendrocytes and the maintenance of axonal integrity requires the understanding of underlying mechanisms. The pyruvate kinase isozyme PKM2 is highly discussed to be important for adapting cancer metabolism since the switch from PKM1 to PKM2 is involved in tumor growth and proliferation. To study whether PKM2 has a role in the modulation of aerobic glycolysis in glial cells, its expression is studied *in vitro* and *in vivo*. Moreover, expression levels of PKM1, PKM2 and PKM2 that is phosphorylated at tyrosine residue 105 in different brain regions at important developmental stages and in adulthood are evaluated.

4   PART I:

GLYCOLYTIC OLIGODENDROCYTES MAINTAIN MYELIN AND LONG-TERM AXONAL INTEGRITY

4.1   RESULTS

4.1.1   GENERATION OF CONDITIONAL *COX10* MUTANT MICE

To investigate whether oligodendrocytes in the living brain are dependent on oxidative phosphorylation we crossbred $Cox10^{fl/fl}$ mice, in which exon 6 of the *Cox10* gene is flanked by LoxP sites, with Cre driver mouse lines mediating recombination specifically in myelinating glia (oligodendrocytes and Schwann cells). *Cox10* encodes for a hemefarnesyl transferase that participates in the biosynthesis of heme α from the cytochrome c oxidase (COX), the terminal complex of the respiratory chain. Thus, by disruption of the *Cox10* locus functional COX can not be assembled, as successfully shown in other mouse models (Diaz et al., 2008, 2005a; Fukui et al., 2007). Hence, *Cox10*-deficient cells should fail to fully metabolize glucose by oxidative phosphorylation and therefore produce most energy glycolytically. Consequently, lactate needs to be generated to maintain the NAD^+/ NADH equilibrium for continuous glycolysis.

To target myelinating glia CNP1-Cre mice were used (Lappe-Siefke et al., 2003), whose promoter activity starts in oligodendrocytes (CNS) at early postnatal states and in the Schwann cell lineage (PNS) already during embryonic development (Gravel et al., 1998; Scherer et al., 1994). This Cre driver mouse line was crossbred with $Cox10^{fl/fl}$ mice (Diaz et al., 2005). Conditional $Cnp1^{Cre/+} * Cox10^{fl/fl}$ mice were phenotypically indistinguishable from controls at birth, but fewer mutant pups were born than expected (11% compared with 25% that were calculated according to Mendelian ratios, n=466). The prenatal death of some mice is best explained by CNP1 expression in a subset of neural precursor cells. Moreover, these mutants developed signs of muscle atrophy already at P21 that was progressive over age. By two months, mutants exhibited reduced weight, tremors, and hindlimb weakness. This neuropathological phenotype further worsened and led to complete hindlimb paralysis, severe muscle atrophy and forelimb paresis by the age of 9 months, at which time-point mutant animals had to be euthanized. Control mice were heterozygously and mutants homozygously floxed for the *Cox10* gene and both carryied Cre on one allele. In the following chapter data are from these control and mutant mice, unless otherwise stated.

Additionally, crossbreedings of $Cox10^{fl/fl}$ mice with tamoxifen-sensitive PLP1-CreERT2 mice (Leone et al., 2003) enabling recombination in a timely controlled fashion were performed. To truly recombine only mature myelinating glial cells after nearly finished myelination mice

received tamoxifen injections for 2 weeks, beginning at 1 month of age. Control mice were also homozygously floxed for *Cox10*, but they either lacked PLP1-CreERT2 expression and were injected with tamoxifen or expressed CreERT2 and got the vehicle only. *Plp1-CreERT2 * Cox10^{fl/fl}* mutants were obtained in normal Mendelian ratios, appeared normal, well groomed and were long-lived.

The recombination level of *Cox10* genomic DNA at 2 months was analyzed by qPCR and the subsequent long-term ablation of COX protein was examined by WB analysis at 14 months (Fig.I - 1a.).

For all investigated tissues a partial loss of exon 6 could be confirmed and thus an infunctional *Cox10* gene. Whole brain homogenates of both conditional mutants displayed a recombination rate of approximately 15% compared to control mice. In comparison mutant sciatic nerve and optic nerve samples revealed much higher recombination efficiencies (sciatic nerve around 67%, optic nerve around 45%), which correspond to the expected percentage of Schwann cells in sciatic nerves and oligodendrocytes in optic nerves (Burne et al., 1996; Herculano-Houzel and Lent, 2005; Nakao et al., 1997) and suggests that all Schwann cells and oligodendrocytes are targeted by recombination (Fig.I - 1b.,c.).

Indeed, the exon 6 excision of *Cox10* caused COX deficiency. Immunolabelling against subunit1 of COX resulting in a brown staining determined the lack of COX from many Schwann cells in mutant sciatic nerve cross-sections that was obvious already at P21. Axonal mitochondria of mutants and controls exhibited equally intense COX expression (Fig.I – 1d.). WB analysis of 14 months optic nerves of *Plp1-CreERT2 * Cox10^{fl/fl}* mutant mice validated a strong long-term reduction of subunit 1 of COX in comparison to age-matched controls. The quantification revealed a diminishment of around 45% compared to control optic nerves, which is in accordance with the estimated fraction of oligodendrocytes in this brain region (Fig.I - 1e.,f.).
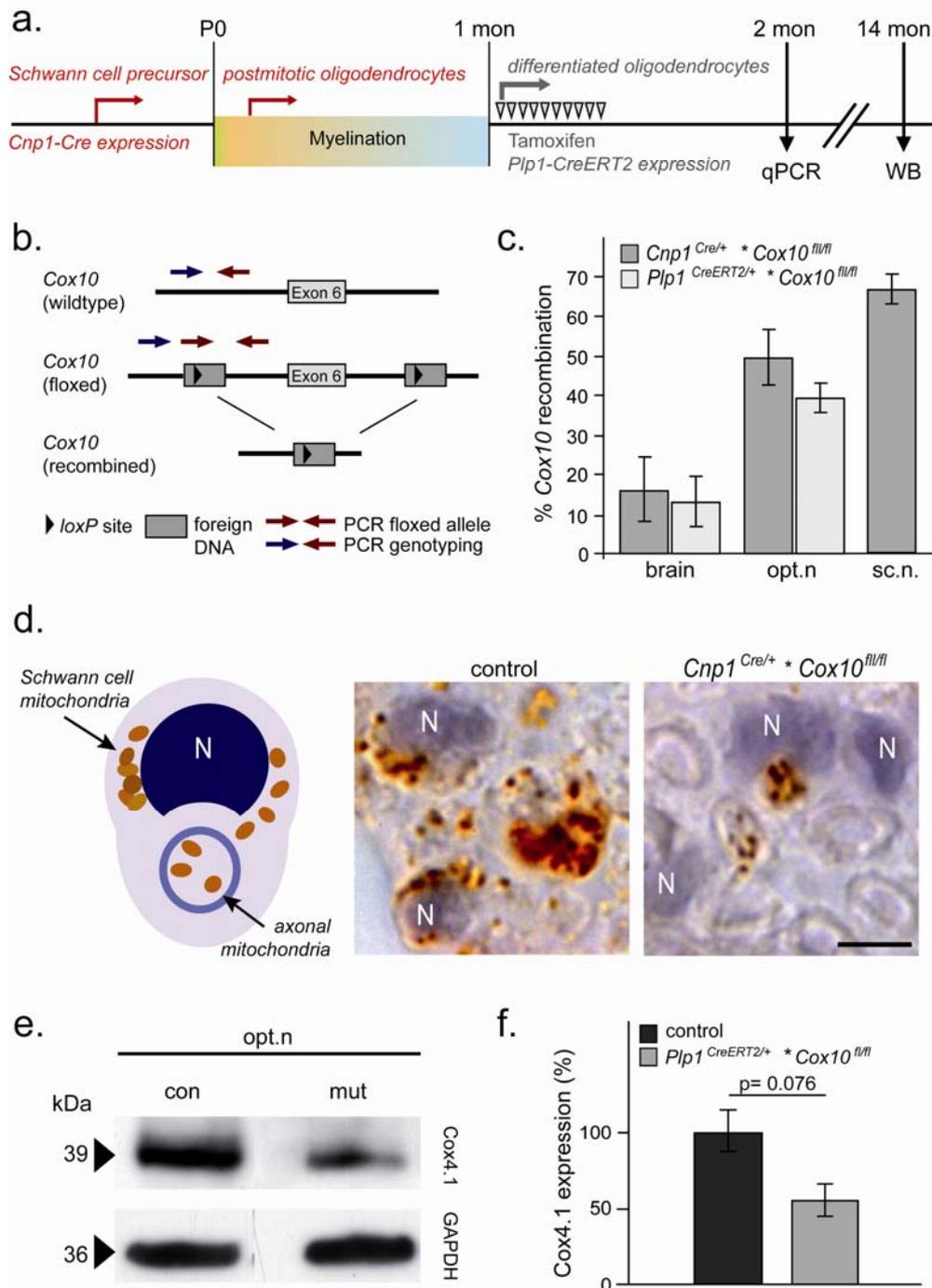
Fig. I - 1   Genetic targeting of *Cox10* leads to the loss of COX in myelinating glia

(a.) Time-scale indicating the conditional deletion of *Cox10* in Schwann cells and oligodendrocytes by using CNP1-Cre (denoted in red) and PLP1-CreERT2 (denoted in grey) driver mouse lines. Since the mitochondrial half-life is about 3 weeks, *Cox10* disruption is not followed by a rapid COX loss. *Cox10* deletion mediated by PLP1-CreERT2 was induced by tamoxifen administration at 1 month. To evaluate the deletion of *Cox10*, qPCRs on genomic DNA were performed at 2 months and the resulting COX loss was determined by WB analysis at 14 months using *Plp1-CreERT2 * Cox10^{fl/fl}* mutants. **(b.)** Conditional recombination of the floxed *Cox10* gene, deleting exon 6 flanked by LoxP sites. Arrows indicate the location of primers used for genotyping (blue/red) and qPCR (red/red), the latter amplifying only the floxed allele. **(c.)** Quantification of the floxed *Cox10* gene disruption in different tissues of both conditional mutants at 2 months. Highest percentage of *Cox10* disruption was

found in sciatic nerve (67 ± 4%), followed by optic nerve (49.9 ± 4% and 39.4 ± 4.0%) and total brain (15.9 ± 8.8% and 12.9 ± 7.1%). Mean percentages are ± s.d.; n= 3–5. **(d.)** Left: scheme of a Schwann cell and their corresponding axon to represent precise COX localization. Right panel: Already at P21 immunostainings with Cox4.1 of mutant sciatic nerves displayed the absence of COX (in brown) in Schwann cells, whereas COX is present in axonal compartments. In comparison, control sciatic nerves showed COX-positive signals in Schwann cells and axons. Schwann cell nuclei were visualized by haemalaun in blue. Scale bar, 10 µm **(e.)** Left: Obvious reduction of COX subunit1 in optic nerves of *Plp1-CreERT2 * Cox10$^{fl/fl}$* mutants at 14 months compared to age-matched controls revealed by western blot analysis. Right: Quantification determined a decrease of COX4-1 expression by 45 ± 10.6% in mutant optic nerves. Depicted are means ± s.e.m.; n= 3–5. opt.n., optic nerve; sc.n., sciatic nerve; N, nucleus; con, control; mut, mutant; mon, months In collaboration with Dr. Ursula Fünfschilling (recombination efficiency and immunohistochemistry).

4.1.2 THE PNS OF *COX10* MUTANTS DISPLAYS SIGNS OF A SEVERE NEUROPATHY

To assess the functional integrity of peripheral nerves, conduction velocities in mutant and control sciatic nerves were determined at P21. Nerves were electrically stimulated proximally at the sciatic notch and distally at the ankle. The compound muscle action potentials were recorded in the foot. Control animals showed a motor conduction velocity of about 15 m/s. In contrast, motor conduction velocities in all analyzed mutants could not be determined, because they displayed functional blocks upon proximal stimulation (Fig.I - 2a.). Distal stimulation elicited a compound muscle action potential also in the mutant animals, but the amplitude was significantly reduced by a factor of two compared to controls. This implies that mutant animals suffer from peripheral neuropathy with features of both axonal and glial defects already at the age of P21. The drastic electrophysiological defect could be due to loss of axons or, more likely, to a significant change in the myelination status of the nerve.

TdT-mediated dUTP nick end labelling (TUNEL) staining of semithin sciatic nerve sections at 6 months detected no evidence for Schwann cell death as possible cause of hypomyelination (Fig.I - 2b.). In fact, the number of endoneurial nuclei was increased by 25% in the mutants (Fig.I - 2c.), which is a common feature in dysmyelinated nerves (Sancho et al., 2001). By P21 the cross-sectional area of mutant sciatic nerves was significantly reduced compared to controls (Fig.I - 2d.) and the number of total myelinated axons was already decreased by 40% in mutants that further progressed by 9 months indicating axon loss (Fig.I - 2e.). Electron microscopic analyses revealed that C-fibers were not correctly sorted by Remak bundles by failing to envelop single axons in mutant sciatic nerves already at P21 compared to age-matched controls (Fig.I - 2f.). Further, many medium-sized axons remained completely unmyelinated although they corresponded to caliber size of above 1 µm and appeared next to sufficiently myelinated axons (Fig.I - 2g.). This implies that Schwann cells that still need to myelinate are dependent on ATP delivery by oxidative phosphorylation to fulfill their function.
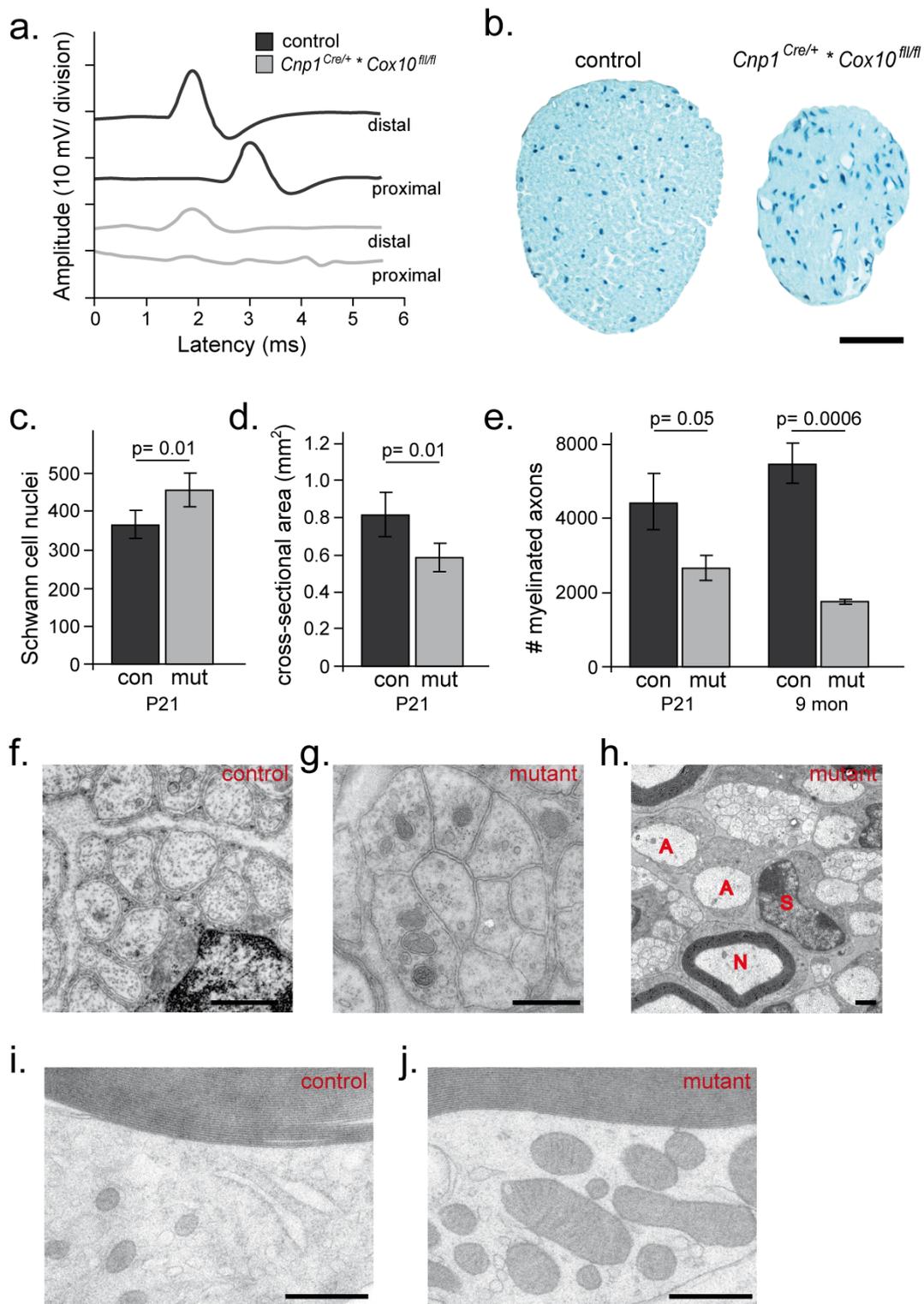
Fig. I - 2 *Cox10* mutant mice exhibit a severe peripheral neuropathy

(a.) Recordings of the amplitudes of sciatic nerve compound muscle action potentials of control and mutant mice at P21, which was strongly reduced after distal and almost not detectable after proximal stimulation in mutant sciatic nerves. **(b.)** TUNEL staining of sciatic nerves revealed no Schwann cell death at P21, but a strong reduction of the mutant cross-sectional area. Cell nuclei were counterstained with haemalaun (in blue). **(c.)** The Schwann cell nuclei number was significantly increased in mutant sciatic nerves (control, 361 ± 39.6; mutant 453 ± 42.1), **(d.)** and the cross-sectional area was significantly diminished at P21 (control, 0.808 ± 0.12 mm^2; mutant, 0.578 ± 0.088

mm^2). **(e.)** The absolute number of myelinated axons of sciatic nerves was reduced at P21 and further progressive by 9 months (control, 4376 ± 843, mutant, 2610 ± 383 at P21 and control, 5416 ± 582; mutant, 1744 ± 54 at 9 months). **(f.-j.)** Electron microscopic analyses. **(f.,g.)** In control Remak bundles, C-fibre axons were correctly engulfed by Schwann cell processes but not in mutants. **(h.)** Many unmyelinated medium-caliber axons were observed that appeared next to normally myelinated axons. Schwann cell nuclei were unaffected. **(i.,j.)** At higher magnification, myelin had developed morphologically normal, but mutant mitochondria were clearly enlarged and more abundant. Scale bars are 500 nm, besides from h., 2 µm. Numbers are mean ± s.d.. con, control; mut, mutant; A, unmyelinated medium-sized axon; N, normal myelinated axon; S, Schwann cell nuclei; mon, months. In collaboration with Dr. Ursula Fünfschilling (analyzed the data), Dr. Bastian Brinkmann (electrophysiology) and Dr. Wiebke Möbius (electron microscopy).

Indeed, already at P21 mutant sciatic nerve mitochondria appeared aberrantly large and abundant which is a hallmark of mitochondrial diseases pointing to mitochondrial defects going along with *Cox10* inactivation.

4.1.3 THE CNS OF *COX10* MUTANT MICE APPEARS NORMAL

To assess whether respiration-deficient oligodendrocytes were capable to myelinate, Gallyas´ silver impregnation on sagittal brain sections was performed at P21. Mutant brains seemed unaffected and white matter tracts such as corpus callosum, anterior commissure or cerebellar white matter were normally myelinated compared to controls (Fig.I - 3a.). Most likely, residual, but sufficient mitochondrial respiration of mutant oligodendroglial mitochondria ensures proper myelination. The discrepancy between PNS and CNS might be explained by different temporal activity patterns of the CNP1 promoter. In the PNS, CNP1 drives recombination in still proliferating Schwann cells during embryonic phases, which causes a fast dilution of mutant mitochondria to their progeny and hampers efficient myelination. In contrast, in the CNS, the CNP1-Cre-mediated *Cox10* elimination takes place in already postmitotic oligodendrocytes that does not disturb myelination. Since *Cox10* depletion is not followed by a direct COX loss due to the calculated mitochondrial half-life of 3 weeks, the *Cox10* inactivation in postmitotic oligodendrocytes rather leads to a functional ageing of mitochondria that preserves correct myelination.

Thus, we investigated mutant mice at 9 months, at which age they had to be euthanized because of severe features of peripheral neuropathy. Surprisingly, no white matter pathology could be detected by Gallyas´ silver impregnation of coronal brain sections. The mutants were normally myelinated compared to controls and exhibited no sign of morphological alterations (Fig.I - 3b.). Even at ultrastructural level, the mutant myelin appeared normal, no

evidence for demyelination or other abnormal features such as split or redundant myelin could be observed (Fig.I - 3c.). This suggests that mature, postmyelinating oligodendrocytes indeed tolerate COX deficiency and thus reduced mitochondrial function once myelination has occurred.
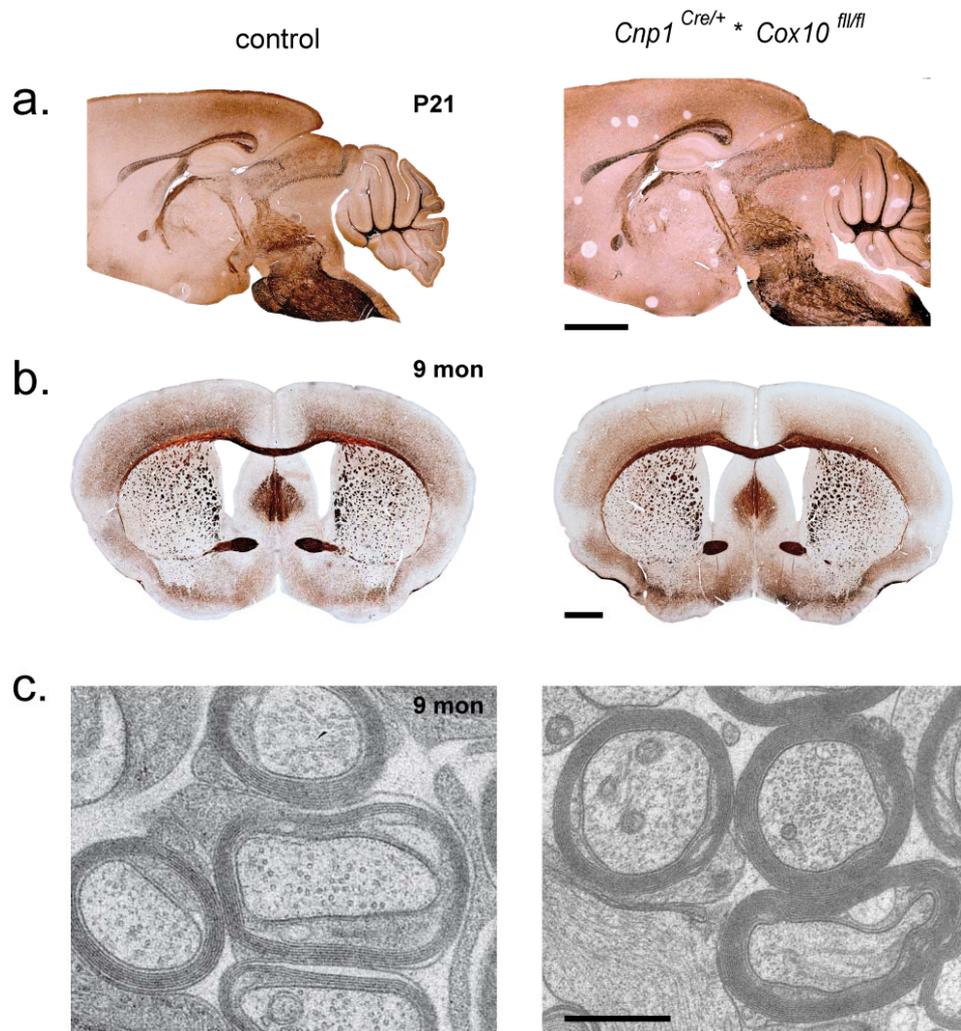
Fig. I - 3   The CNS appears normal and white matter tracts are preserved in *Cox10* mutant mice

Gallyas´ silver impregnation revealed **(a.)** no gross morphological or myelinic differences between mutant and control of sagittal brain sections at P21, **(b.)** and white matter tracts were still well preserved in mutant coronal brain sections at 9 months when compared to controls. Scale bars, 1 mm. **(c.)** The mutant myelin ultrastructure appeared normal and displayed no sign of hypo- or hypermyelination. Scale bar is 500 nm. mon, months. In collaboration with Dr. Wiebke Möbius (electron microscopy).

Alteration of cell size or cytoplasmic composition are known changes evoked by energy deprivation (Leist et al., 1997) or lactate accumulation. At ultrastructural level, no overt morphological variations of the nucleus or cytoplasm of respiration-deficient oligodendrocytes were visible and mitochondria seemed not to be affected in size or abundance (Fig.I - 4a.). WB analysis of VDAC (Voltage-dependent anion channel), a major protein of the outer mitochondrial membrane, revealed no protein expression difference between 14 months old optic nerves of *PLP1*-CreERT2 * *Cox10$^{flox/flox}$* mutants and controls, suggesting a normal amount of mutant mitochondria (Fig.I - 4b.,c.).
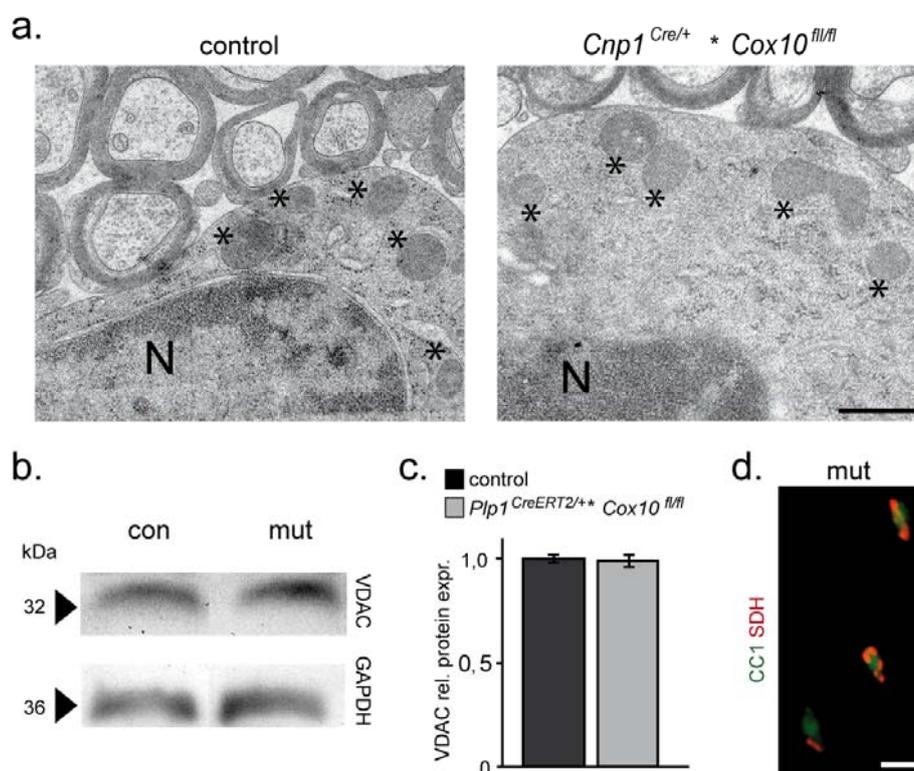
Fig. I - 4   Mitochondria of differentiated oligodendroglia were grossly unaffected in *Cox10* mutant mice

(a.) Ultrastructural analysis of mutant mitochondria in optic nerve cross-sections indicated normal morphology and abundance (mitochondria are marked by asterisks), **(b., c.)** the latter was as well confirmed by western blot examination of *Plp1-CreERT2 * Cox10$^{fl/fl}$* optic nerves at 14 months which showed equally intense signal for VDAC, a major mitochondrial protein, compared to controls. Numbers are mean ± s.e.m. **(d.)** Stainings against SDH detected abnormal enlargements of mitochondria of CC1-positive mature olgodendrocytes. Scale bar, 500 nm for a. and 10 μm for d. In collaboration with Dr. Don Mahad (immunohistochemistry).

However, immunostainings against succinate dehydrogenase (SDH), the complex II of the respiratory chain, clearly displayed an abnormal expansion of mitochondria of mature CC1-positive oligodendrocytes in mutant corpus callosum at 9 months, indicating functional deficits of mitochondrial respiration (Fig.I – 4d.).

Although SDH immunolabelling showed an abnormal expansion of mitochondria in differentiated oligodendrocytes, the loss of COX function remains to be elusive. To truly prove whether the lack of any CNS pathology might be caused by still functional mitochondria, sequential COX/ SDH histochemistry on sagittal brain cryosections was performed at age of P21 and 9 months. This is a widely used approach to study mitochondrial function (Mahad et al., 2009), in which COX activity leads to a brown precipitate that completely saturates mitochondria and prevents incorporation of a blue precipitate converted by SDH in a subsequent step. At P21 saturation with a brown precipitate that covers the entire area of the mutant corpus callosum was obvious and comparable to controls (Fig.I - 5a.). The absence of blue, COX-deficient mitochondria in the mutants emphasized functional mitochondria at that age, which is in line with the normal myelin appearance in white matter tracts in the CNS of *Cox10* mutants. Mitochondrial COX activity in the corpus callosum of 9 months old mutants yielded a brown saturation of cellular compartments and cells, such as axons and astrocytes. By successive SDH histochemistry COX-inactive cells could be detected by the accumulation of blue precipitate and were identified as oligodendrocytes by labelling with Olig2, a specific transcription factor of the oligodendroglial lineage. In age-matched controls evidence for blue, COX-inactive cells was neither present in the corpus callosum nor in any other brain region (Fig.I - 5b.). Thus, a long-term inactivation of COX was achieved by *Cox10* disruption specifically in differentiated oligodendrocytes.
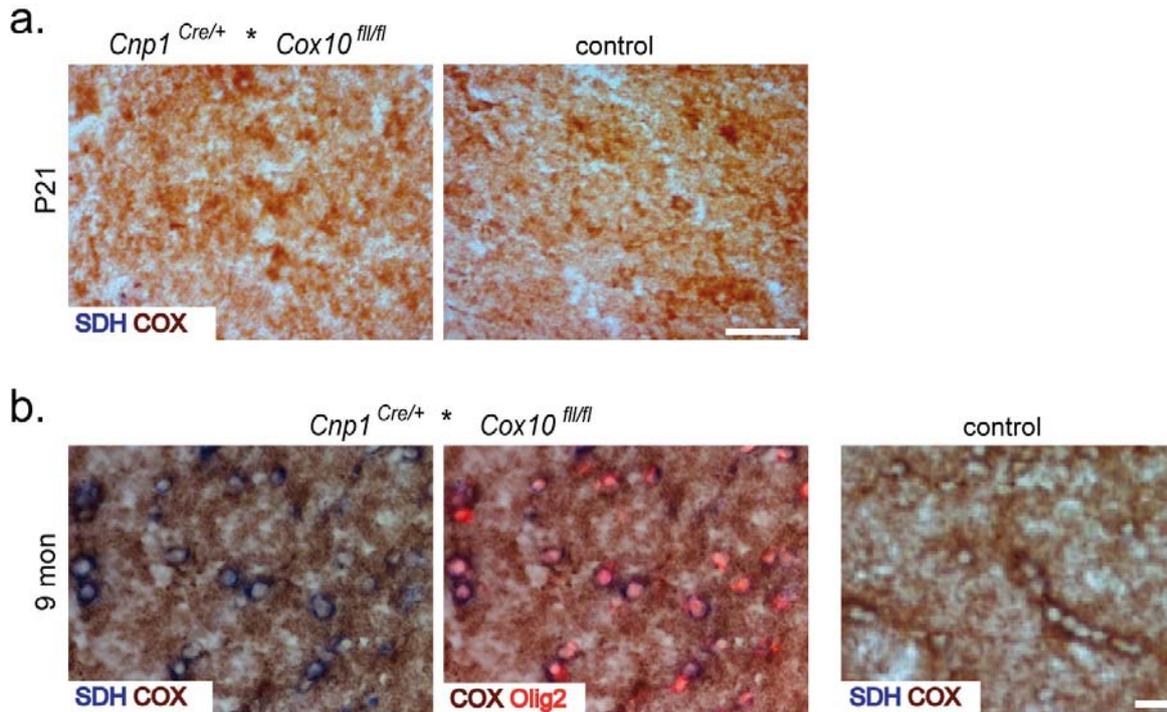
Fig. I - 5   Sequential COX/ SDH histochemistry proves the loss of COX activity in differntiated oligodendrocytes

(a.) At P21 all cells of mutant corpus callosum were homogenously saturated by a brown precipitate which verified COX activity and were comparable to age-matched controls. **(b.)** At 9 months the mutant corpus callosum showed the incorporation of a blue precipitate (left) in Olig2-positive cells (in red, middle) which validated the disruption of COX activity in differentiated oligodendrocytes. Other cellular compartments of the mutant corpus callosum were COX-active proven by brown saturation. The control corpus callosum showed persistend incorporation by the brown precipitate. Scale bars, 20 µm. mon, months. In collaboration with Dr. Don Mahad (serial SDH/ COX histochemistry).

Theoretically, white matter integrity could be preserved when newly synthesized oligodendrocytes would serve for steady myelination. These cells might survive and myelinate for several weeks after *Cox10* recombination. To get a first impression whether the oligodendrocyte ratio is changed in the mutants, immunostainings against Olig2, a marker for the whole oligodendrocyte lineage, were performed on spinal cord cross-sections at P21 and 9 months. Using an ImageJ Plugin the number of Olig2-positive oligodendrocytes was calculated and demonstrated no difference between mutants and controls at both ages (Fig.I - 6a.,b.). By this a constant dying of unfunctional respiration-deficient oligodendrocytes and their replacement by newly generated ones, that are indeed *Cox10* recombined, but still have functional mitochondria for a short time could not be excluded. Therefore the analysis was extended by a detailed determination of the oligodendrocyte proliferation index in the brain which was achieved by a daily treatment with BrdU (5-bromo-2'-deoxyuridine) for 4 weeks which was induced at 4 months of age. BrdU is a synthetic nucleoside and an analog

to thymidine that incorporates into newly synthesized DNA during cell replication. Histological investigations revealed that the proliferation rate of BrdU-positive cells in the fimbria of *Cox10* mutants and controls was nearly the same. Identification of BrdU-incorporated oligodendrocytes by co-immunolabelling with Olig2 revealed only sporadic double-positive cells (Fig.I - 6c.,d.). To directly evaluate cell death TUNEL staining was performed and exhibited no apoptotic cells in all white matter tracts of the mutant brain at 9 month (Fig.I - 6e., left and middle). This strongly indicates that mature oligodendrocytes do not depend on ATP delivery from oxidative phosphorylation for their survival. For comparison, when using CKIIα-Cre mice to delete *Cox10* in cortical neurons beginning at age P5–10 (CKIIα$^{Cre/+}$ * *Cox10*$^{fl/fl}$), we observed a massive apoptosis of projection neurons in the forebrain at 4 months (Fig.I – 6e., right). This confirms that neuronal survival strictly requires oxidative phosphorylation which is in contrast to the viability and function of mutant oligodendrocytes.

a. control   *Cnp1*[Cre/+] * *Cox10*[fll/fl]

b.

c. BrdU   Olig2   BrdU Olig2

control

Cnp1[Cre/+] * *Cox10*[fll/fl]

d.

e. control   *Cnp1*[Cre/+] * *Cox10*[fll/fl]   *CkIIα*[Cre/+] * *Cox10*[fll/fl]

TUNEL
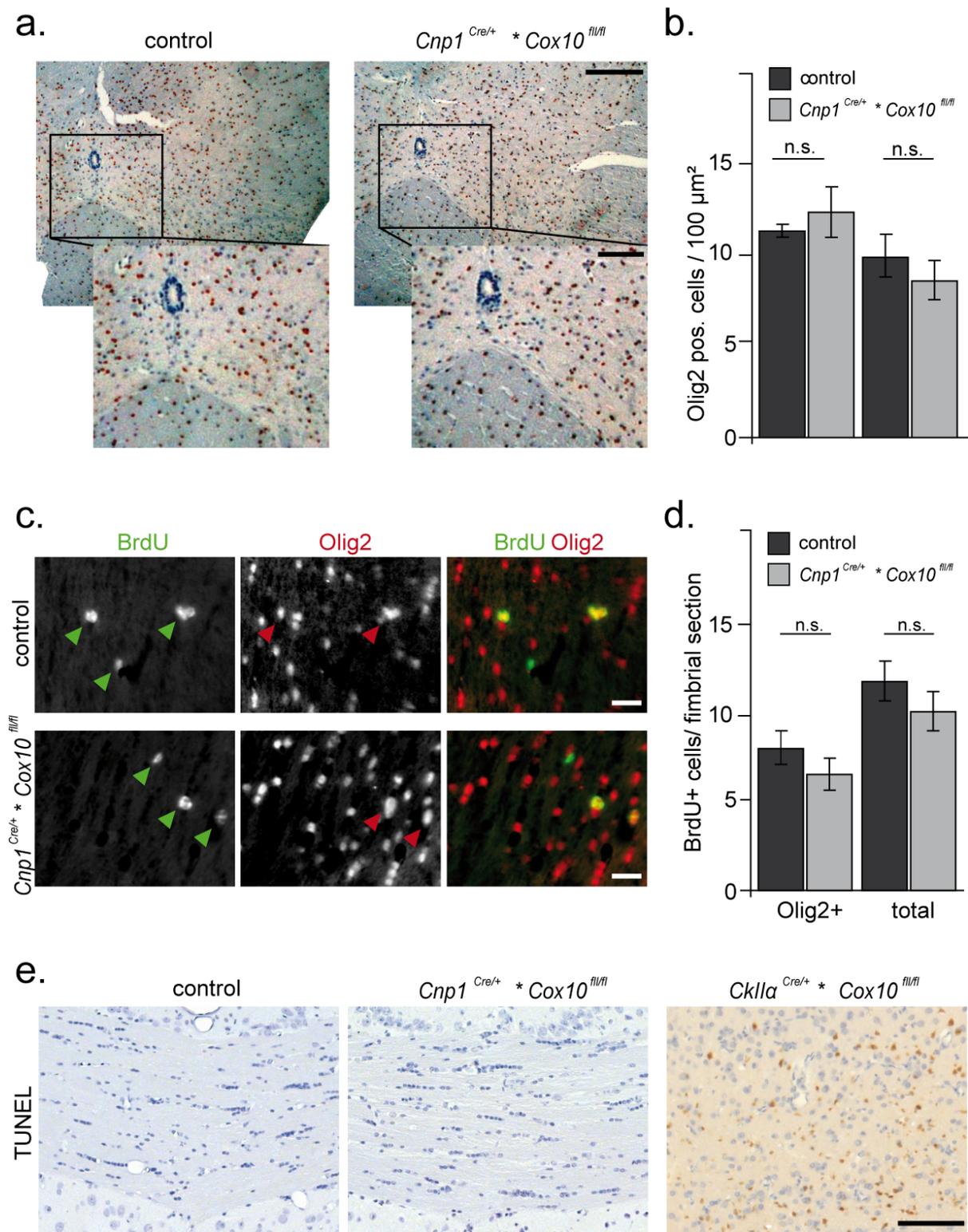
Fig. I - 6   Survival of oligodendrocytes in conditional *Cox10* mutant mice

(a.) By immunostaining against Olig2 of spinal cord cross-sections, the number of oligodendrocytes was determined at P21 and 9 months. Sections were counterstained with haemalaun (blue) **(b.)** The quantification of Olig2-positive oligodendrocytes in mutants was comparable to age-matched controls (at P21 controls, 11.3 ± 0.4; mutants 12.3 ± 1.4 and at 9 months controls, 9.8 ± 1.3 and mutants, 8.6 ± 1.0 Olig2-positive oligodendrocytes). **(c.)** Followed by daily administration of BrdU (denoted in green, arrows), a changed proliferation rate of mitotic Olig2-positive oligodendrocytes (depicted in red,

29

arrows) in the fimbria could not be observed in mutant mice. **(d.)** Significant differences were neither in BrdU-positive oligodendrocytes (7.8 ± 1.1 in controls and 6.4 ± 0.9) nor in the total number of BrdU-incorporated cells (11.6 ± 1.2 in controls and 9.8 ± 1.2) detected. **(e.)** TUNEL labelling revealed no apoptosis in the corpus callosum of 9 months mutants which was a feature of the positive control (*Cox10$^{fl/fl}$* * CKIIα-Cre, 4 months). All sections were counterstained with hemalaun (blue). Scale bars are 250 µm and 100 µm for a., 20 µm for b., 100 µm for c. Numbers are ± s.e.m. n.s., not significant.

Severe pathological features such as cell death as a consequence of potentially energy-deprived *Cox10*-deficient oligodendrocytes were not detected. However, neuroinflammation is a very sensitive sign of degenerative processes in the brain. To assess whether mutants at 9 months, the end-point of analysis, were affected, several inflammatory markers were tested on coronal brain sections. Astrogliosis was not observed in mutant corpus callosum when compared with controls, which was detected by immunostaining for GFAP (Fig.I - 7a.). No increase of activated microglia visualized by Mac3 immunosignals (Fig.I - 7b.) or invading CD3-positive T-lymphocytes (Fig.I - 7c.) were detected in the corpus callosum of conditional mutants compared to controls and were only sporadically found in both genotypes. Due to tight interconnection between oligodendrocytes and neurons the presence of APP-positive endosomes was examined. Accumulation of APP in axonal spheroids is a sign of disturbed axonal transport and was never observed in mutants and controls (Fig.I - 7d.).
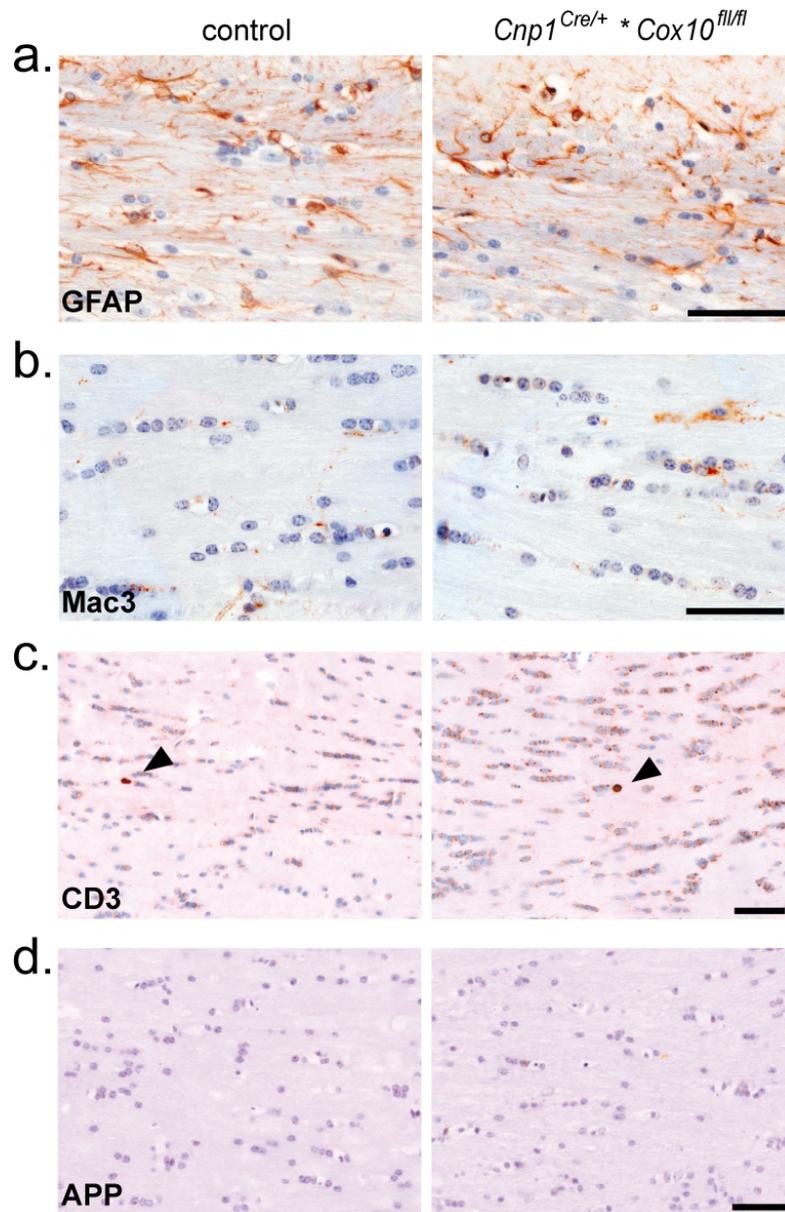
Fig. I - 7   No sign of inflammation or neurodegeneration in the brain of *Cox10* mutants

(a.) Immunostaining for GFAP (astrogliosis) of coronal brain sections revealed no difference between controls and mutant corpus callosum at the age of 9 months. **(b.)** Immunosignals for Mac3 (activated microglia) and **(c.)** for CD3 (invading T cells) exhibited a normal range in the corpus callosum and were comparable to controls (arrows pointing to single immunocells). **(d.)** APP positive plaques (axonal pathology) could not be detected in both controls and mutants (9 months). All sections were counterstained with hemalaun (blue) to display nuclei. Scale bars, 50 μm.

These findings described a normal CNS phenotype in mice harboring respiration-deficient oligodendrocytes were astonishing and led to the conclusion, that differentiated mutant oligodendrocytes survived by ATP supply from increased aerobic glycolysis. Thus, elevated lactate levels were predicted. Localized proton magnetic resonance spectroscopy (MRS) was performed to detect levels of different metabolites, among them lactate, in the living brain. Indeed, *Cox10* mutants showed a significantly increased lactate resonance compared with controls in both cortex and white matter at 6–7 months of age (Fig.I - 8a, red asterisks). Additionally, the detection of certain other metabolites further confirmed the absence of neurodegeneration and oligodendrocyte survival. This was supported by unchanged spectra of N-acetylaspartate (a marker of viable neurons and axons), choline-containing compounds (indicators of membrane turnover) and myo-inositol (an osmolyte and glial membrane constituent). However, it has to be emphasized that accumulated brain lactate was detectable only under isoflurane anaesthesia. This narcotic drug is known to inhibit the pyruvate dehydrogenase complex by blocking the entry of pyruvate into mitochondria, which shifts the glucose metabolism from oxidative phosphorylation towards lactate production and enables the enrichment of lactate. Under physiological conditions, lactate levels never reach MRS detectability *in vivo*, unless challenged by isoflurane anaesthesia. Thus, also in controls observable lactate concentrations in both analyzed regions could be displayed (Fig.I - 8a.). The analysis of mutant cortices and corpora callosa revealed approximately doubled lactate concentrations each in contrast to the control regions at both ages, suggesting that *Cox10*-ablated oligodendrocytes survive by enhanced aerobic glycolysis (Fig.I - 8b.). More important, control white matter displayed higher lactate levels than cortical regions, which implies that wildtype oligodendrocytes are best equipped to be lactate-producing cells since the corpus callosum is highly enriched with oligodendrocytes in comparison to cortices (Fig.I – 8b.). At the end of anaesthesia those lactate increases immediately fell very drastically within minutes and finally dropped to undetectable levels when mice woke up (Fig.I - 8c.). Hence, lactate that had accumulated under isoflurane anaesthesia was rapidly used by other cellular compartments when the narcosis was shut off.
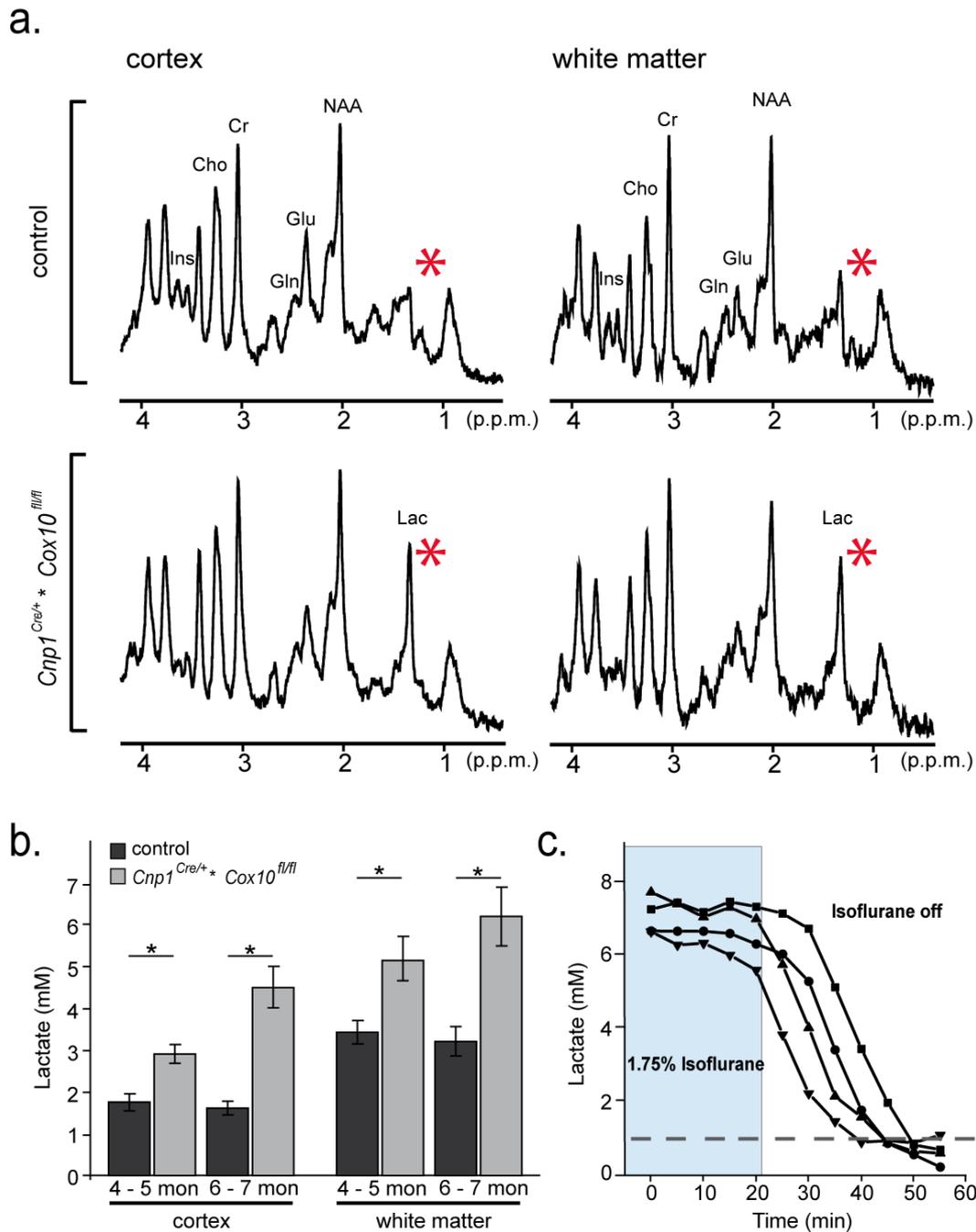
Fig. I - 8   Isoflurane-induced elevated lactate levels were rapidly used by cellular compartments after anaesthesia

(a.) Localized proton magnetic resonance spectroscopy of the cortex (left) and corpus callosum (right) from mutant and control mice at 6–7 months displayed spectra of different metabolites. In narcotized *Cox10* mutants lactate was highly accumulated in both regions. Red asterisks denote lactate. **(b.)** Lactate level quantification of the cortex (left) and white matter (right) exhibited an increase in mutant mice compared to controls under isoflurane anaesthesia. In control mice higher lactate concentrations were obtained in white matter than in cortices. **(c.)** At the end of isoflurane anaesthesia lactate levels dropped to undetectable levels within 30 min. Data are mean ± s.e.m.; n= 6–7 per genotype. Asterisks denote significance level (* p < 0.05). Lac, lactate; Cr, total creatine; Ins, myo-inositol; Glu; glutamate; Gln, glutamine; Cho, Choline; NAA, N-acetyl-aspartate; p.p.m., parts per million; mon, months. In collaboration with Prof. Jens Frahm and Prof. Susann Boretius.

4.2 DISCUSSION

For decades oligodendrocytes have been considered to be only passive cells that insulate their corresponding axons by enwrapping them with myelin. Thus a tight connection between oligodendrocytes and the axonal compartment is generated that physically isolates the axon from the extracellular space. This enables fast conduction velocity of action potentials, but also separates axonal compartments from access to nutrients. Investigations in recent years provided growing evidence that oligodendrocytes might as well metabolically support the integrity of neurons (Edgar et al., 2004; Griffiths et al., 1998; Lappe-Siefke et al., 2003). One highly discussed support mechanism is that oligodendrocytes might shuttle glycolytic end-products, namely pyruvate or lactate, to axons to promote neuronal energy requirements (Nave, 2010; Amaral et al., 2013; Morrison et al., 2013).

To shed light on this hypothetical metabolic coupling between oligodendrocytes and axons, we focused on the possible role of oligodendrocytes to serve as a source of energy-rich glycolytic metabolites. Therefore we asked whether oligodendrocytes in the living brain are dependent on oxidative phosphorylation and generated mouse models, in which oligodendrocytes that could not survive by aerobic glycolysis alone would simply die. This was achieved using *Cox10* mice (Diaz et al., 2005), in which exon 6 was flanked by loxP sites. The *Cox10* gene is evolutionarily highly conserved and exon 6 was identified to share sequence homology to the region that codes for part of the active site of the bacterial enzyme (Saiki et al., 1993). By crossbreeding them with well-established Cre driver mouse lines, the CNP1-Cre and the tamoxifen-sensitive PLP1-CreERT2 mice (Lappe-Siefke et al., 2003; Leone et al., 2003) recombination was specifically mediated in myelinating glia (oligodendrocytes and Schwann cells). *Cox10* is essential for the assembly of the cytochrome c oxidase (COX), which is the terminal proton-pumping complex of the mitochondrial respiratory chain. Thus, by disruption of *Cox10* functional COX can not be assembled. This has been successfully shown in other mouse models targeting hepatocytes, muscle cells or neurons (Diaz et al., 2008, 2005; Fukui et al., 2007). Consequently, COX10-deficient cells should fail to fully metabolize glucose by oxidative phosphorylation and produce most energy by aerobic glycolysis. Hence, lactate needs to be generated to maintain the NAD^+/ NADH equilibrium for continuous glycolysis. Indeed, elevated lactate levels have been observed by MRI analysis in many patients suffering from mitochondrial disorders due to defects in one of the complexes of the respiratory chain (Lebre et al., 2011).

Cox10 disruption in different tissues was reliably revealed in both mouse mutants by analyzing the exon 6 excision of the *Cox10* locus using qPCRs at the age of 2 months. The percentage of detectable *Cox10* elimination (in average; brain, 15%; optic nerve, 45% and sciatic nerve, 67%) was in accordance with estimated ratios of oligodendrocytes and

Schwann cells in the corresponding tissue (Ling and Leblond, 1973; Burne et al., 1996; Nakao et al., 1997; Sandell and Peters, 2002; Walhovd et al., 2014) and led to the conclusion that all oligodendrocytes and Schwann cells were targeted by Cre recombination. Already at P21 an obvious reduction of COX protein in sciatic nerve cross-sections, specifically from Schwann cells, was found and confirmed the loss of COX following *Cox10* ablation. COX deficiency was validated to be long-term as shown by WB analysis of 14 months optic nerves. Importantly, by sequential COX/ SDH histochemistry of brain sections the inactivity of COX and thus the disruption of oxidative phosphorylation could be clearly depicted specifically in postmyelinating oligodendrocytes.

By using the CNP1-Cre driver mouse line for targeting *Cox10*, mice appeared normally developed after birth. However, fewer mutants were obtained than expected indicating prenatal death of some mice that can be due to the known expression of CNP1-Cre in a subset of neuronal precursor cells (Lappe-Siefke et al., 2003). Phenotypical signs of a peripheral neuropathy were already detectable at P21 that worsened with increasing age and resulted in a premature death at around 9–10 months of age. Schwann cell mitochondria were found to be enlarged and increased in number, which is a common feature of mitochondrial dysfunction (Diaz et al., 2008; 2005). By ultrahistological analyses, we observed pathological features in the PNS already at P21, including dysmyelination of medium-sized axons and defects of Remak bundle sorting that was accompanied by axonal loss at older age. This indicated that myelination is an energy-consuming process relying on proper mitochondrial respiration and thus its immense ATP generation. Interestingly, no Schwann cell death could be detected implying that Schwann cells survive despite the lack of ATP generation by oxidative phosphorylation. In line with this another mouse model, in which the Schwann cell-specific deletion of the mitochondrial transcription factor A gene (*Tfam*), required for mitochondrial DNA transcription and replication (Larsson et al., 1998), caused a similar peripheral neuropathy (Viader et al., 2011). In that case the Cre-recombinase was expressed under the control of P0 promoter inducing recombination in Schwann cells starting at E13.5–E14.5 (Feltri et al., 1999). These mice were characterized by Remak bundle disruption and axonal degeneration, and also exhibited Schwann cell survival. In contrast, these mutants displayed no obvious dysmyelination (Viader et al., 2011), although mitochondria are known to be essential for the synthesis of cholesterol and fatty acids as building blocks of myelin (Aeberhard and Menkes, 1968; Matthieu et al., 1973; Saher et al., 2005). Indeed, mitochondrial diseases display a broad spectrum of clinical phenotypes in patients, but are often reported to affect the integrity of myelin in the brain and peripheral nerves that can result in the development of leukodystrophies (Cheon et al., 2002; Kumakura et al., 2009; Nishino et al., 1999). An example is the Leigh syndrome, a human neurodegenerative disease caused by various genetic defects in the respiratory chain,

including COX disorders (DiMauro et al., 1987; Cavanagh and Harding, 1994; Yiş et al., 2009). In patients it has been shown that *Cox10* is one of 3 genes responsible for COX defects (Valnot et al., 2000) and several missense mutations in the *Cox10* gene have been found in patients suffering from leukodystrophy or the Leigh syndrome (Antonicka et al., 2003; Valnot et al., 2000). The ablation of Tfam affects all mitochondrial-encoded proteins, thus every complex of the respiratory chain (Larsson et al., 1998). However, Tfam-deficiency leads to the disruption of the catalytic core of COX since this part is encoded by mitochondrial DNA (Capaldi, 1990). The best explanation for the initially normally developed myelin in conditional Tfam mouse mutants (Viader et al., 2011) is that mitochondrial function is not completely disrupted during the myelination process. The P0 promoter is indeed already active in premyelinating Schwann cells, but only to a very low extent (Feltri et al., 1999; Lee et al., 1997). Investigations of the temporal expression profile of different Schwann cell proteins, including CNP1 and P0 have clearly shown that P0 expression increases during postnatal states and peaks around P21 (Stahl et al., 1990). In comparison, CNP1 is the earliest marker of the Schwann cell lineage and represents high expression levels already during embryonic development (Chandross et al., 1999; Stahl et al., 1990). Thus, it is conceivable that many premyelinating Schwann cells escaped Cre-recombination due to insufficient early P0 promoter activity resulting from low expression levels at embryonic states. Regarding the averaged half-life of mitochondrial proteins of around 24–26 days (Beattie et al., 1967; Menzies and Gold, 1971), elimination of mitochondrial DNA is not accompanied by an immediate loss of mitochondrial function. Hence, myelination which occurs within the first weeks of age in mice should be preserved in conditional Tfam mutants (Foran and Peterson, 1992; Skoff et al., 1980; Sturrock, 1980). Further analyses by Viader and colleagues uncovered that Tfam-deficient Schwann cells were not energy depleted at 2 months although all complexes of the mitochondrial respiration are affected by the loss of Tfam. The authors found an activation of stress response and a shift in the lipid metabolism away from synthesis towards oxidation in respiration-disrupted Schwann cells as likely drivers of the demyelinating phenotype observed in these mice (Viader et al., 2013). Conditional *Cox10* mutants, in whose *Cox10* recombination is already induced by early CNP1 promoter activity led to a fast dispersion of infunctional mitochondria by mitotic expansion of mutant Schwann cell precursors. The progressive dysmyelinating pathology in the PNS of *Cox10* mutants is an indicator for Schwann cell dependency on functional mitochondria to maintain proper myelination.

The absence of affected myelin in the CNS of conditional *Cox10* mutants is as well explained by differences in the spatio-temporal expression pattern of CNP1, whose promoter activity starts remarkably later in development, when oligodendrocytes were already postmitotic. Due to a comparatively slow loss of mitochondrial COX, myelination defects should be prevented

by residual mitochondrial function of still myelinating *Cox10*-deficient oligodendrocytes. Since myelination itself requires cholesterol and fatty acid synthesis which takes place in mitochondria, it is conceivable that myelinating oligodendrocytes rely on proper mitochondrial function (Cuzner and Davison, 1968; Matthieu et al., 1973; Orth and Bellosta, 2012; Saher et al., 2005; Aeberhard and Menkes, 1968). This is as well suggested by the sensitivity of oligodendrocytes to the COX inhibitor sodium azide (Rinholm et al., 2011). These cells correspond to pre-myelinating oligodendrocytes *in vivo*, and it seems that metabolic properties of oligodendrocyte lineage cells change during maturation.

However, it remains remarkable that pathological alterations could not be observed in the adult CNS, even not in aged mice at 9 months when they had to be euthanized due to severe PNS neuropathy. At ultrastructural level, myelin appeared normal and oligodendrocytes were not obviously affected in conditional *Cox10* mutants. By EM analyses neither the density nor the morphology of mitochondria in oligodendrocytes seemed to be unchanged. However, mitochondria of 9 months old mutants displayed a clear abnormal expansion visualized by immunostainings against succinate dehydrogenase, also known as complex II of the respiratory chain, and indicated mitochondrial dysfunction. Nonetheless, inflammatory processes as a subtle response to the possible lack of ATP supply in oligodendrocytes were not a feature of the *Cox10* mutant CNS. These results strongly indicate that mature oligodendrocytes can easily adapt to aerobic glycolysis ensuring their survival and function.

Since high dynamics of oligodendrogenesis is a known compensating mechanism in many neurological diseases like MS (El Waly et al., 2014), a continuous replacement circle of mutant oligodendrocytes by newly synthesized cells that maintain normal oligodendrocyte function for several weeks after *Cox10* recombination could be a consequence of energy-deprived oligodendrocytes. Basically, there is no strong evidence for oligodendrocyte turnover during healthy young adulthood. Moreover, a recent study analyzing the integration of ^{14}C derived from nuclear bomb-tests in 1940 in post-mortem human brains revealed that the oligodendrocytic population is very stable throughout life (Yeung et al., 2014). However the possibility of replacement was proven by several experiments. The number of Olig2-positive oligodendrocyte lineage cells of conditional *Cox10* mutants at different ages was determined which was each comparable to age-matched controls. Direct tracing of proliferating cells by EdU incorporation revealed no alterations in the mutants in comparison to controls. Moreover, evidence for oligodendrocyte death or a general increased cell death could not be observed by TUNEL assessment, demonstrating survival of *Cox10*-deficient oligodendrocytes. These results verified that mature oligodendrocytes, once myelination is complete, are independent from energy supply by oxidative phosphorylation and able to maintain the integrity of myelin and their associated axons. That differentiated

oligodendrocytes survive by aerobic glycolysis similar to cancer cells was unexpected. Whether myelinating oligodendrocytes display the same metabolic properties remains to be elusive.

These findings are in agreement with a previous study providing evidence that in various white matter tracts of rodent adult brains the glycolytic activity significantly exceeded oxidative activity relative to those in grey matter (Morland et al., 2007). Similar, by MRI analysis of anaesthetized *Cox10* control mice elevated lactate levels were found in the corpus callosum when compared to cortical regions. Lactate is a surrogate marker for aerobic glycolysis and its stronger accumulation in the control corpus callosum as an oligodendrocyte-dense brain structure reflects a higher glycolytic rate in white matter tracts compared to the cortex. In Isoflurane-narcotized *Cox10* mutant brains significant higher lactate levels were observed in both CNS regions when compared to control mice, which might originate from mutant oligodendrocytes surviving by enhanced aerobic glycolysis. Of note, under physiological conditions lactate is normally not detectable by MRI resolution, unless challenged by isoflurane anaesthesia, which inhibits the pyruvate dehydrogenase complex and blocks the entry of pyruvate into mitochondria. Lactate production assures continuous glycolysis by concomitant NADH regeneration. The detection of lactate in anaesthesized control and mutant brains strongly implies that lactate is not disposed by the blood flow since isoflurane is described to slightly increase the cerebral blood flow velocity (Duong, 2007; Li, Patel, et al., 2013). Directly after switching off isoflurane narcosis lactate concentrations fell within minutes to undetectable levels. Thus, the rapid decline of observed lactate indicates that lactate, which is the necessary by-product of aerobic glycolysis, is not drained by the blood stream. It is more likely that the accumulated lactate is locally taken up by other cellular compartments. Therefore, we suggested a model, in which oligodendrocytes are metabolically coupled to axons by shuttling glycolysis products to support axonal energy demands.

Traditionally, glucose has been considered as the obligate energy substrate fueling the brain. More recent studies showing that neuronal activity can be maintained only in the presence of lactate in *ex vivo* optic nerve preparations (Wyss et al., 2011). Further, cytosolic proteins, to which glycolytic enzymes belong, are shuttled *via* slow axonal transport from neuronal cell bodies to more distal compartments (Brady and Lasek, 1981; Oblinger et al., 1988; Yuan et al., 1999). Considering the lengths some axons can reach, especially those of motoneurons, the sufficient metabolic equipment for glycolysis in distal parts of axons, like synapses, is a logistical problem. Thus, this might be overcome by the intimate physical connection of oligodendrocytes to axonal compartments enabling metabolic interaction in the axo-glia interface. The possibility of shuttling lactate between brain cell types in the living brain is

determined by the expression of monocarboxylate transporters (MCT) transferring monocarboxylates, including lactate and pyruvate. It has been shown that MCTs are not only expressed during suckling in the rodent CNS, when lactate is an important source feeding the brain, but also in the adult brain (Vannucci and Simpson, 2003). In fact, their concentration remains fairly constant throughout life indicating a necessity for the transport of glycolytic intermediates in the adult brain (Vannucci and Simpson, 2003). By immunogold labelling of MCT1 the precise oligondroglial expression domain could be assigned to ab- and adaxonal myelin regions and the inner tongue (Rinholm et al., 2011; Saab et al., in prep.), whereas MCT2 is restricted to myelinated neurons. Thus, a network of transporters is generated, which is a prerequisite for providing routes shuttling lactate between oligodendrocytes and their associated axons.

Moreover, MCT1 BAC transgenic mouse indicated that MCT1 is almost exclusively expressed by oligodendrocytes (Lee et al., 2012). The inhibition of MCT1 by specific shRNAs or pharmacological treatment of spinal cord organotypic cultures resulted in motor neuron loss, without affecting oligodendroglial survival. Importantly, neuronal death could be prevented by adding exogenous lactate. *In vivo* disruption of MCT1 genetically or by lentiviral knockdown specifically in oligodendrocytes caused a neuropathy in brain and spinal cord. This axonal pathology was characterized by swellings of myelinated axons without disrupting oligodendrocytic integrity (Lee et al., 2012). These results support the conclusion that the lactate transfer of oligodendrocytes is crucial for axonal integrity. The transport direction of MCTs is determined by intra- and extracellular concentration gradients of lactate and hydrogen (Merezhinskaya and Fishbein, 2009). Hypothetically, the neurodegenerative phenotype induced by MCT1 downregulation could also be caused by reduced lactate import into oligodendroglia. This possibility is unlikely because the lactate application into the media of organic cultures prevented the observed pathology. Further, no sign of oligodendroglial apoptosis could be found *in vitro* and *in vivo*. Thus, this analysis contributes to the emerging concept that oligodendrocytes support axonal survival and function independent from myelination (Nave, 2010; Amaral et al., 2013; Morrison et al., 2013) and provides insight that the underlying mechanism might rely on lactate supply from oligodendroglia to their corresponding axon (Lee et al., 2012).

These findings serve *in vivo* evidence that denotes a link between glycolytic metabolism of oligodendrocytes and axonal integrity and suggests a metabolic coupling in the axo-glia compartment essential to support the ATP budget of energy-deprived axons by shuttling energy-rich intermediates from oligodendrocytes to neurons (Lee et al., 2012, Fünfschilling et al., 2012). Thus, it will be important to unravel the complexity of metabolic capabilities of

oligodendrocytes to understand the contribution of insufficient metabolic support of oligodendrocytes to the development of neurodegenerative diseases.
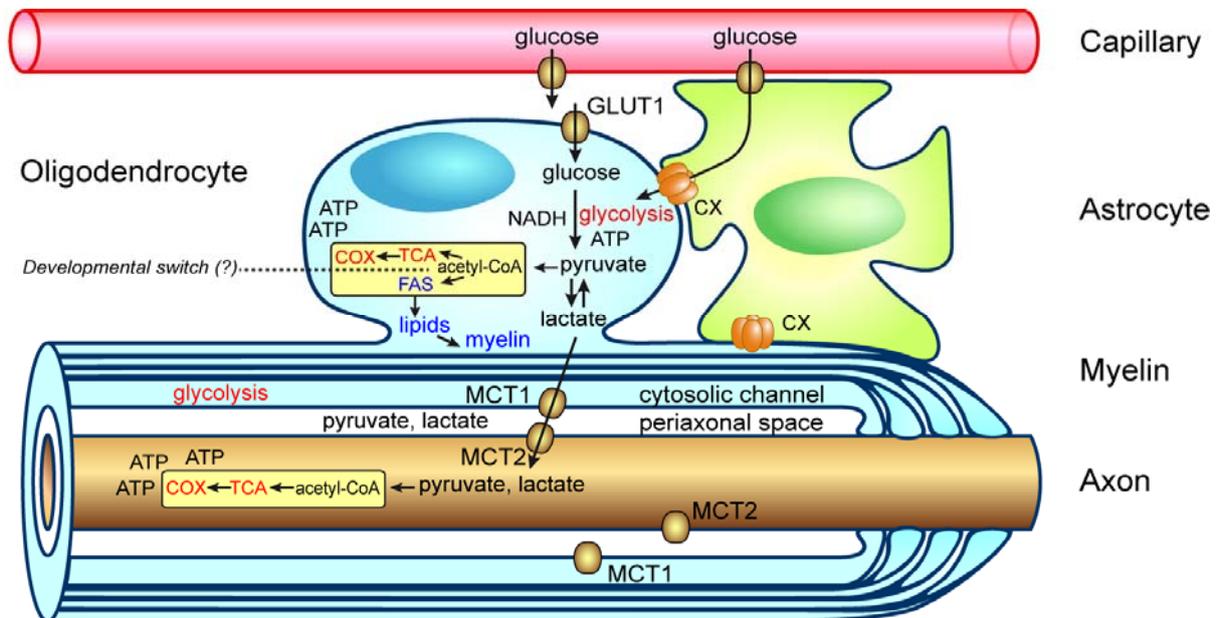
Fig. I - 9   Hypothetical model of the metabolic coupling in the axon-glia compartment

Oligodendrocytes import glucose via Glucose transporter 1 (GLUT1) and possibly from astrocytes through gap junctions (CX, connexins) for glycolysis. Pyruvate enters the mitochondria (yellow) and is used in the oxidative phosphorylation for immense ATP production (TCA, tricarboxylic acid cycle). With the onset of myelination glucose also contributes to the synthesis of fatty acids (FAS) and myelin lipids from acetyl-CoA. In post-myelinating oligodendrocytes aerobic glycolysis is sufficient to cover oligodendroglial energy needs. Glycolysis products (lactate) are used by myelinated axons when energy-deprived. Lactate can be directly shuttled to axons *via* monocarboxylate transporters (MCT1 and MCT2) that are expressed in the internodal myelin and axonal compartments. Picture is taken from Fünfschilling et al., 2012.

4.3 DETAILED SUMMARY

Oligodendrocytes ensheath their corresponding axons with myelin, a multi-lamellar, lipid-rich membrane enabling fast velocity of action potentials, but also isolates almost the entire axonal surface from nutrients in the extracellular space. Mice carrying myelin defects often develop neurodegenerative phenotypes in the presence of normal appearing myelin which argued for a crucial role of oligodendrocytes in maintaining axonal integrity. Myelin is not an impermeable layer. The connection between axons and oligodendrocytes is ensured by myelinic cytosolic channels and integrated glucose and monocarboxylate transporters which might serve as routes for energy-rich metabolites through the myelin sheath to support neuronal energy demands. To obtain supportive evidence for the trophic function of oligodendrocytes, conditional mutants were generated by crossbreeding mice floxed for the *Cox10* gene with mice expressing the Cre-recombinase from the CNP1 promoter which is cell type-specifically active in myelinating glia. Since *Cox10* is essential for the assembly of cytochrome c oxidase (COX), the terminal proton-pumping complex of the respiratory chain, its ablation leads to the gradual loss of mitochondrial function. In the PNS, *Cox10* mutant mice exhibited a severe neuropathy characterized by dysmyelination, abnormal Remak bundles and paralysis. Interestingly, in the adult CNS, no signs of myelin deficits, neurodegeneration, secondary inflammation or abnormal regeneration were observed in conditional *Cox10* mutant mice. The pathology in the PNS is most likely caused by the early activity of the CNP1 promoter when Schwann cells are still proliferating, whereas in the CNS CNP1 drives Cre-recombination in largely postmitotic oligodendrocytes, which presumably preserves myelinogenesis by residual mitochondrial function. However, it remained remarkable that the inactivation of oxidative phosphorylation did not affect the survival of mature oligodendrocytes indicating their independency of ATP supply by mitochondrial function. Importantly, by magnetic resonance spectroscopy enhanced lactate concentrations in the living brain were revealed only when isoflurane anaesthesia was applied. This narcotic agent is an inhibitor of the pyruvate dehydrogenase complex. The lactate accumulation in control and mutant mice upon isoflurane exposure and the rapid drop of lactate increases to undetectable levels by the end of anaesthesia implied that aerobic glycolysis products from oligodendrocytes are normally metabolized by other cellular compartments under physiological conditions. Since lactate can sustain neuronal spiking activity of myelinated axons, these findings suggest a model in which a link between an oligodendroglial glycolytic metabolism and the shuttling of energy-rich metabolites that derived from oligodendrocytes can be correlated with neuronal integrity

5   PART II:

SURVIVAL OF RESPIRATION-DEFICIENT ASTROCYTES BY AEROBIC GLYCOLYSIS *IN VIVO*

5.1   RESULTS

5.1.1   SURVIVAL OF ASTROCYTES AND DEATH OF NEURONS UPON INHIBITION OF THE MITOCHONDRIAL COMPLEX I BY ROTENONE *IN VITRO*

To compare the ability of cultured rat astrocytes and neurons to survive glycolytically in the presence of oxygen, purified cells were treated with rotenone (concentrations ranging from 10 nM to 40 nM), which is a plant-derived inhibitor of the mitochondrial respiratory chain complex I. The exposure of astrocytes to rotenone for 24 hours caused no obvious alteration of astrocyte morphology (Fig.II - 1a.) and no signs of cell death, as quantified by Trypan Blue exclusion (Fig.II - 1b.). In contrast, neurons responded very sensitive to the loss of complex I. Already the application of 10 nM rotenone led to a striking loss of Tuj1-expressing processes and apoptosis as revealed by pycnotic cell nuclei. At higher rotenone concentrations (20 and 40 nM) complete neuronal loss was observed within 24 hours (Fig.II - 1c.).
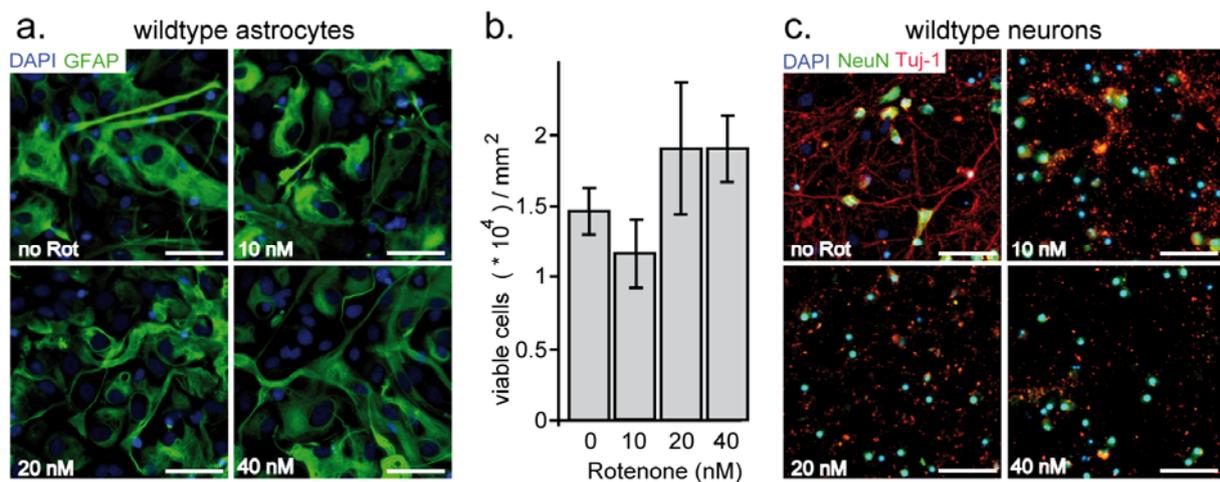
Fig. II - 1   Cultured astrocytes resist Rotenone treatment that is toxic for neurons

(a.) Rotenone treated astrocytes (concentrations as indicated) were indistinguishable regarding density and morphology from untreated astrocytes shown by GFAP immunolabelling (green). **(b.)** Rotenone did not affect astrocyte survival as quantified by Trypan Blue exclusion. The number of viable cells was obtained as followed: $1.47 \pm 0.17 * 10^4$ (untreated), $1.18 \pm 0.24 * 10^4$ (10 nM Rotenone), $1.92 \pm 0.46 * 10^4$ (20 nM Rotenone) and $1.91 \pm 0.24 * 10^4$ (40 nM Rotenone). **(c.)** Rotenone treatment was absolutely toxic to neurons shown by reduction in Tuj-1 expression (red) and pycnotic neuronal nuclei (NeuN in green, DAPI in blue). Scale bars, 50 µm. Numbers are ± s.e.m.

Since rotenone also causes mitochondria to generate reactive oxygen species (ROS) (Li, Fang, et al., 2013), it could mask respiratory chain energy defects and be more toxic for neurons than for astrocytes, which are even protective to neurons in mixed cultures in the presence of rotenone (Chang et al., 2013). Therefore we turned to a long-term *in vivo* analysis and to mitochondrial complex IV, whose functional loss is only associated with the delayed generation of ROS (Diaz et al., 2012).

5.1.2 GENERATION OF AN INDUCIBLE AND ASTROCYTE-SPECIFIC *Cox10* MUTANT MICE

In order to analyze whether adult astrocytes in the living brain are dependent on oxidative phosphorylation we crossbred $Cox10^{fl/fl}$ mice with tamoxifen-sensitive GLAST-CreERT2 mice selectively targeting astrocytes in a temporally controlled fashion. By disruption of the *Cox10* gene functional COX can not be assembled. This was shown in other mouse models, in which mutant cells either die or survive by aerobic glycolysis (Fukui et al., 2007b; Fünfschilling et al., 2012b). Astrocytes that fulfill their own ATP needs in the absence of respiration must generate lactate in order to maintain the NAD^+/ NADH equilibrium for continuous glycolysis.

Mice received daily tamoxifen injections for 5 consecutive days, beginning at postnatal day 30 (P30). Age-matched control mice were homozygous for the floxed *Cox10* gene, but either lacked GLAST-CreERT2 when injected with tamoxifen or expressed GLAST-CreERT2 but received the vehicle only. Considering the calculated half-life time of mitochondrial proteins of 3 weeks in the brain (Beattie et al., 1967b; Menzies and Gold, 1971b) histological and electron microscopic analyses were performed at the age of 3 months when a significant loss of mitochondrial COX function is expected. Additionally, long-term effects in *Cox10* mutant mice were investigated at about one year of age (Fig.II - 2a.). All mutant mice were obtained at the expected Mendelian ratio, indistinguishable from control littermates regarding phenotypical appearance, cage behaviour, and life-span.

Recombination of the floxed *Cox10* locus was confirmed by PCR analysis of genomic DNA purified from the cerebellum and the cerebrum (Fig.II - 2b.,c.). For both regions the loss of *Cox10* exon 6 could be detected, implying the absence of functional *Cox10*. In brain genomic DNA from control mice no corresponding PCR product was detectable at 3 months (Fig.II - 2c.)

Recombination efficiencies were determined by crossbreeding $Cox10^{fl/fl}$ * *Glast-CreERT2* to reporter mice R26R-EYFP that express the yellow fluorescent protein YFP upon Cre-mediated excision of a *loxP*-flanked transcriptional "stop" sequence (Srinivas et al., 2001a)
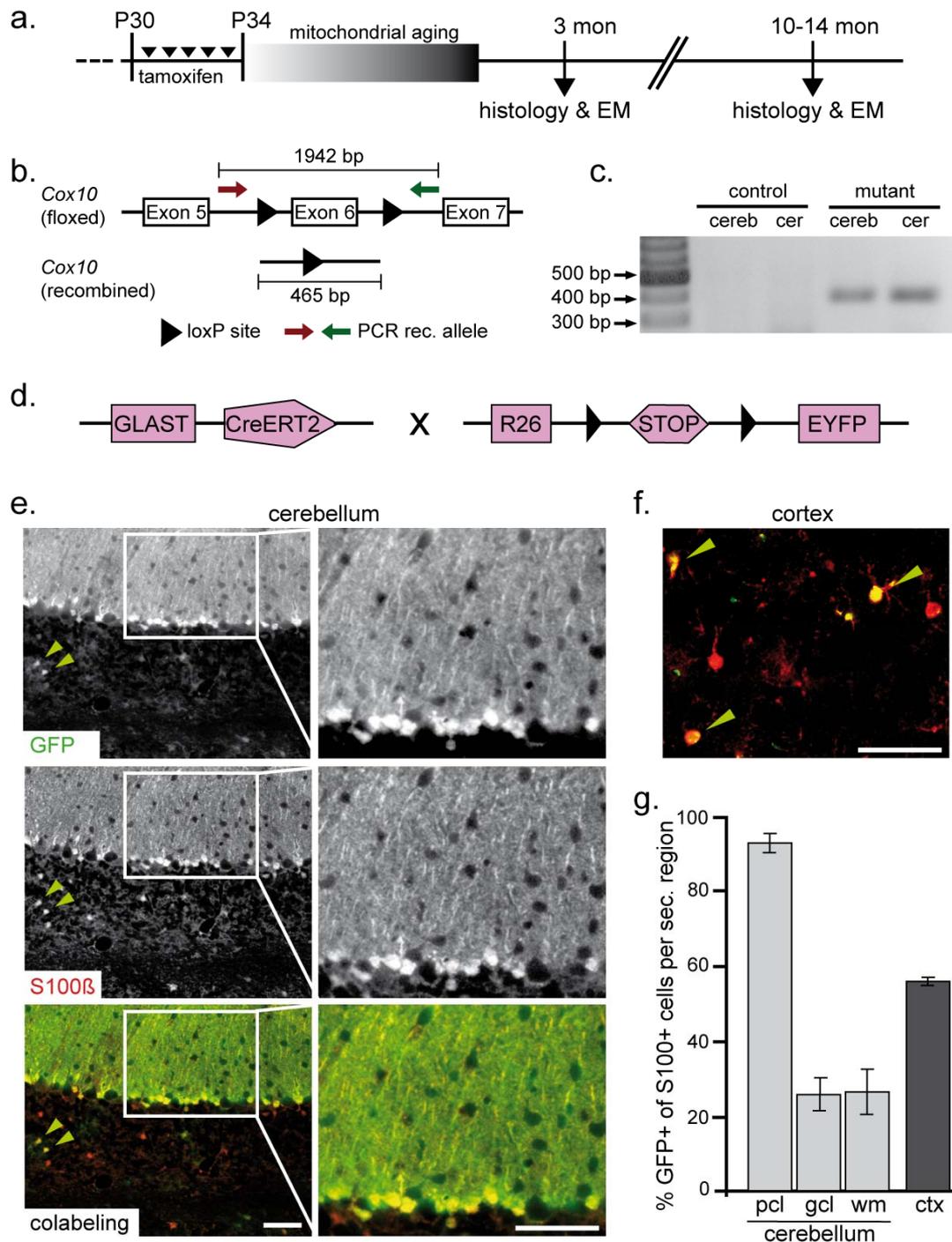
Fig. II - 2 Inducible deletion of *Cox10* and specific reporter gene recombination

(a.) Mice were tamoxifen injected for 5 consecutive days beginning at P30 to circumvent developmental defects. Since the estimated mitochondrial half-life is around 3 weeks, first analysis was performed at 3 months. **(b.)** Conditional mutagenesis of the floxed *Cox10* gene, deleting exon 6, results in PCR product of 465 bp. Arrows indicate the position of primers for the amplification of the recombined allele. **(c.)** Detection of recombined *Cox10* allele from cerebral (cereb) and cerebellar genomic DNA (cer) from mutant animals (3 months), but not from age-matched controls. **(d.)** To confirm recombination efficiency, *Cox10* mutants were crossbred with a reporter mouse line expressing EYFP upon successful recombination. **(e.)** Virtually all Bergmann glia in the cerebellar Purkinje cell layer (labeled with S100β, red) were targeted for recombination as demonstrated by intense Cre-sensitive expression of the reporter signal EYFP (green, enhanced with anti-GFP

labelling), whereas considerably fewer astrocytes in the underlying granule cell layer and white matter were recombined (denoted by green arrowheads). **(f.)** The recombination of cortical astrocytes was quite mosaic. Green arrowheads pointing to recombined astrocytes (labelled with S100ß, red). **(g.)** Quantification revealed an astrocyte recombination ratio of 93.0 ± 2.4% in the pcl; 25.9 ± 4.6% in the granule cell layer and 26.4 ± 6.1% in the white matter and 56.2 ± 1.1% in the somatosensory cortex. Data are mean ± s.e.m. All scale bars are 50 µm. cer, cerebellum; ml, pcl, Purkinje cell layer; gcl, granule cell layer; wm, white matter.

(Fig.II - 2d.). Identification of astrocytes was achieved by colabelling YFP+ cells with S100ß, a calcium binding protein and widely used astrocytic marker. As expected, inducible Glast-CreERT2 expression was mosaic throughout the brain (Mori et al., 2006). In the cerebellum, the highest degree of recombined astrocytes (93 ± 2.4%) was found in the Purkinje cell layer. These cells were characterized as Bergmann glia (BG) by their localization, shape and S100ß-expression. In contrast, in the underlying cerebellar granule cell layer and white matter tracts only about 25% of all S100ß-positive astrocytes were targeted by Cre recombination (Fig.II - 2e.,g.). In the somatosensory cortex only 55% of S100ß-marked astrocytes were recombined (Fig.II - 2f.). Due to high recombination efficiency of BG further analyses mainly focussed onto this subgroup of astrocytes.

To show long-term functional loss of mitochondrial respiration in mutant glial cells, sequential COX and succinate dehydrogenase (SDH, also known as mitochondrial complex II) histochemistry was performed on brain sections at the age of 14 months. This is a widely used approach to study mitochondrial dysfunction (Mahad et al., 2009; Campbell et al., 2011; Fünfschilling et al., 2012), in which COX activity results in a brown precipitate that completely saturates mitochondria and prevents incorporation of a blue precipitate converted by active SDH in a subsequent step. In cerebellar sections of controls the tissue was saturated with the brown precipitate, evidence that all cells harbored functional and active COX (Fig.II - 3, left). In mutant cerebella the absence of COX activity from *Cox10*-deficient BG cells was validated by the emergence of a blue precipitate (arrows), which was almost absent from other cell types. Few bluish spots in the mutant granule cell layer were observable, that most likely belong to recombined astrocytes in this region (Fig.II - 3, middle). The scheme illustrates the precise localization of mutant, respiration-deficient (blue) BG and astrocytes in the granule cell layer of the cerebellum (Fig.II - 3, right).
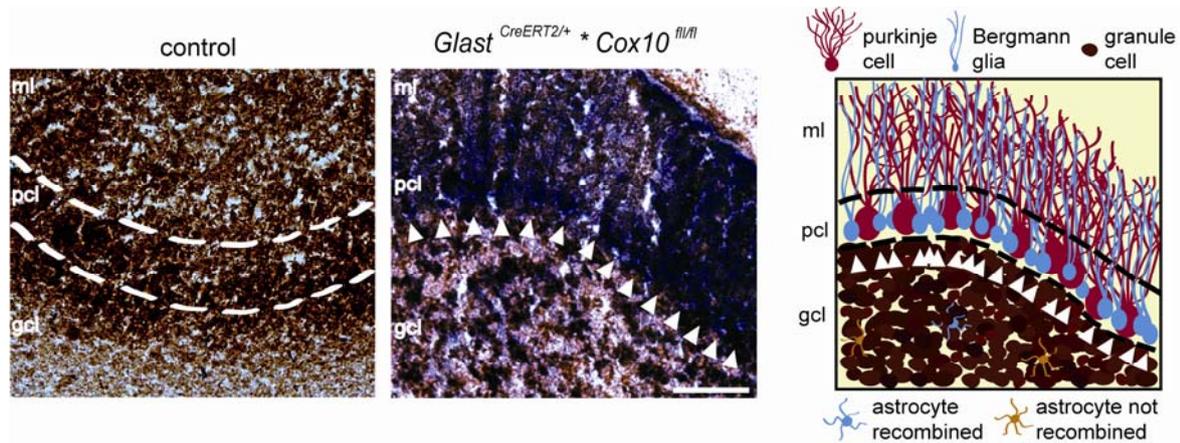
Fig. II - 3 Serial COX and SDH histochemistry proves the loss of COX activity in Bergmann Glia

In controls (left) mitochondrial COX activity yielded a brown precipitate in all cells of the cerebellum at 14 months. In age-matched mutants (middle) cells with BG characteristics were visibly stained by active SDH revealing COX inactivity (blue precipitate, white arrows). Bluish spots in the granule cell layer indicating recombined astrocytes in this region. Scheme illustrating the precise localization of mutant BG in the Purkinje cell layer (in blue, arrows), where as well Purkinje cells (brown, COX active) are resided. ml, molecular layer; pcl, Purkinje cell layer; gcl, granule cell layer. In collaboration with Dr. Don Mahad and Graham Campbell (serial COX/ SDH histochemistry).

5.1.3 THE CEREBELLUM OF CONDITIONAL *Cox10* MUTANT MICE APPEARS NORMAL

To assess whether the conditional lack of COX activity from astrocytes affects the gross organization of cerebella hemalaun stainings of cerebellar sections at 3 and 14 months were performed. At both ages the cerebellar cytoarchitecture and size (and any other brain region) were unchanged in mutant mice (Fig.II - 4a.). Co-immunolabelling with S100ß and GFAP displayed unchanged BG morphology and their many processes had properly developed. No overt differences of BG cell density could be observed in conditional *Cox10* mutants, implying that respiration-deficient BG cells were not affected (Fig.II - 4b.). At ultrastructural level BG identified by glycogen inclusions appeared normal and their mitochondria were unaltered in size and number (Fig.II - 4c.), which suggests that BG cells do not rely on oxidative phosphorylation for survival, very similar to myelinating oligodendrocytes in the CNS white matter (Fünfschilling et al., 2012).

.
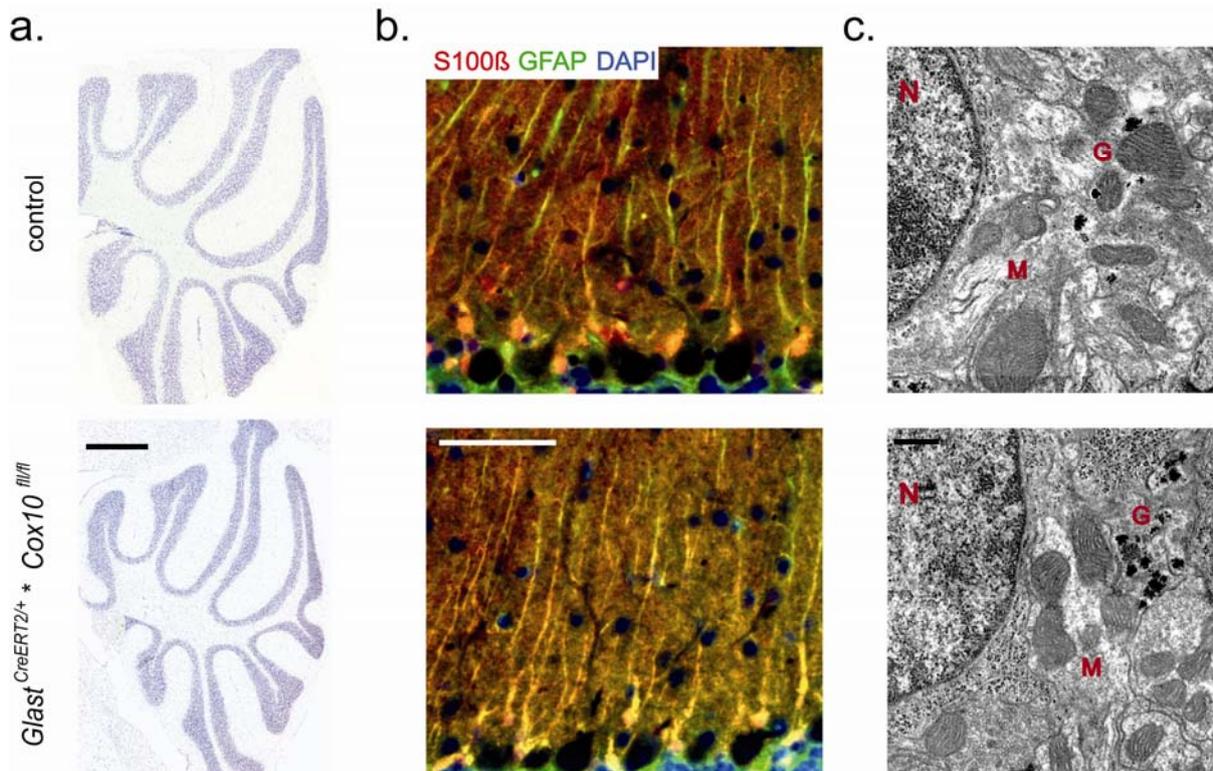
Fig. II - 4   The cerebellum and Bergmann glia cells appear normal in *Cox10* mutant mice

(a.) The cerebellum appeared normally in mutant mice revealed by haemalaun staining (14 months). **(b.)** BG co-stained with antibodies against S100ß (red) and GFAP (green) were morphologically not affected. **(c.)** Electron microscopy of healthy Bergmann glia nuclei identified by surrounding glycogen inclusion showed an unchanged glycogen content and mutant mitochondria were unaltered in size and number comparable to controls (10 months). Scale bars are 500 µm for a., 100 µm for b., 500 nm for c. G, glycogen; N, nucleus; M, mitochondria

Inflammatory processes can be subtle responses to metabolic deprivation of astrocytes (Xanthos and Sandkühler, 2014). However, no evidence for astrogliosis by GFAP immunostaining of brains from 14 months old *Cox10* mutant mice could be found (Fig.II - 5.a.). Furthermore, staining with Mac3, a marker for microgliosis, demonstrated no alterations compared to controls (Fig.II - 5b.). Only a few invading T-cells, positive for CD3 could be observed in brain sections, but comparable to controls (Fig.II - 5c.). Considering tight interactions between neurons and astrocytes, it is conceivable that altered function of astrocytes can cause CNS pathologies. Therefore, APP immunostainings were performed to check for APP-positive endosomes in axonal spheroids, which is evidence for a disturbed axonal transport. The presence of APP plaques in *Cox10^{fl/fl}* * CKIIα-Cre mice driving
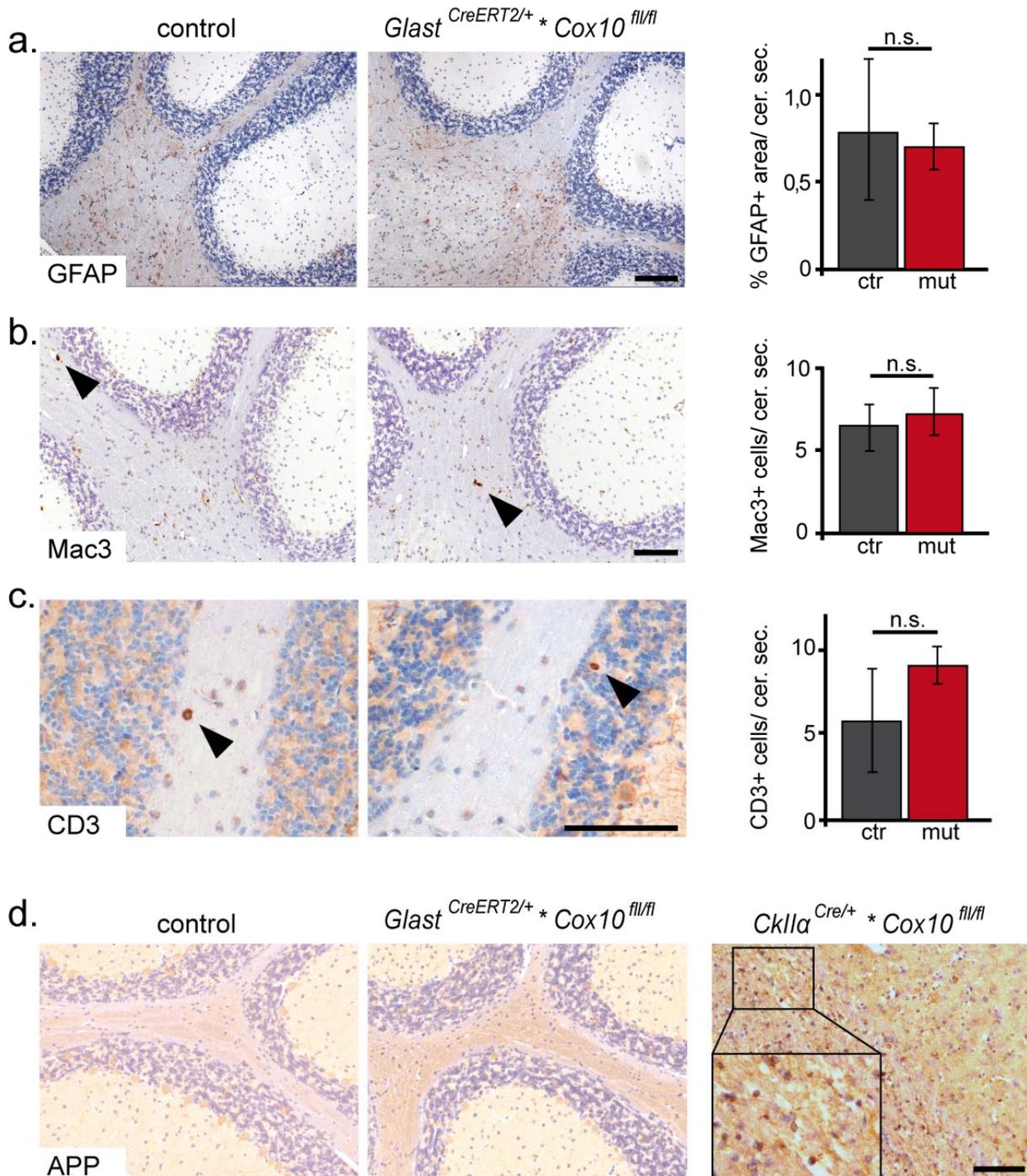
Fig. II - 5 No sign of inflammation or neurodegenerative processes in *Cox10* mutants

(a.) Immunostaining for GFAP (astrogliosis) in sagittal cerebellar sections revealed no significant difference between controls and mutant mice at the age of 14 months. The GFAP-positive cerebellar area of sections accounted for 0.79 ± 0.4% in controls and 0.70 ± 0.1% in mutants. **(b.)** Staining for Mac3 (activated microglia) displayed no significant alteration between mutants (7.17 ± 1.5) and controls (6.5 ± 1.5) per section. **(c.)** Immunolabelling for CD3 displayed no increase of invading T-cells in the 14-month-old mutants (9.0 ± 1.2) compared to age-matched controls (5.8 ± 3.1) per section. Arrowheads point to single immunocells. **(d.)** APP positive plaques (axonal pathology) could not be detected in controls and mutants (14 months), whereas APP positive plaques were accumulated in the forebrain of CKIIα-Cre*Cox10$^{fl/fl}$ mice at 4 months. All sections were counterstained with hemalaun (blue) to display nuclei. Scale bars, 100 µm. Numbers are ± s.e.m. n.s., not significant.

recombination in cortical projection neurons starting from P5–P10 was a key feature of the neurodegenerative pathology in these mice. In comparison, even aged conditional *Cox10fl/fl* * GLASTcreERT2 mutant mice (14 months) did not exhibit any sign of APP accumulation (Fig.II - 5d.).

5.1.4 NO EVIDENCE FOR ABNORMAL REGENERATION OR CELL DEATH

CNS integrity could theoretically be preserved when *Cox10* mutant astrocytes are rapidly replaced by newly generated astrocytes that have escaped Cre recombination. Therefore, the proliferation index of astrocytes after a 2-week treatment with EdU (5-ethynyl-2'-deoxyuridine) beginning 50 days after tamoxifen-induced deletion of *Cox10* was explored. Histological analysis detected a normal proliferation rate in mutants compared to controls (Fig.II - 6a.,b.). Moreover, co-immunolabelling with S100ß bared only sporadic dividing astrocytes in mutants and controls. To directly investigate apoptosis in the cerebellum TUNEL staining was performed. Neither in the brains of mutant mice nor in age-matched controls evidence for increased apoptotic cell death at 3 months and 14 months of age could be found (Fig.II - 6c.). In contrast, *Cox10*-deficient cortical projection neurons, using *Cox10fl/fl* * CKIIα-Cre mice showed massive apoptosis in the forebrain confirming strict dependency of neurons on oxidative phosphorylation (Fig.II - 6d.).
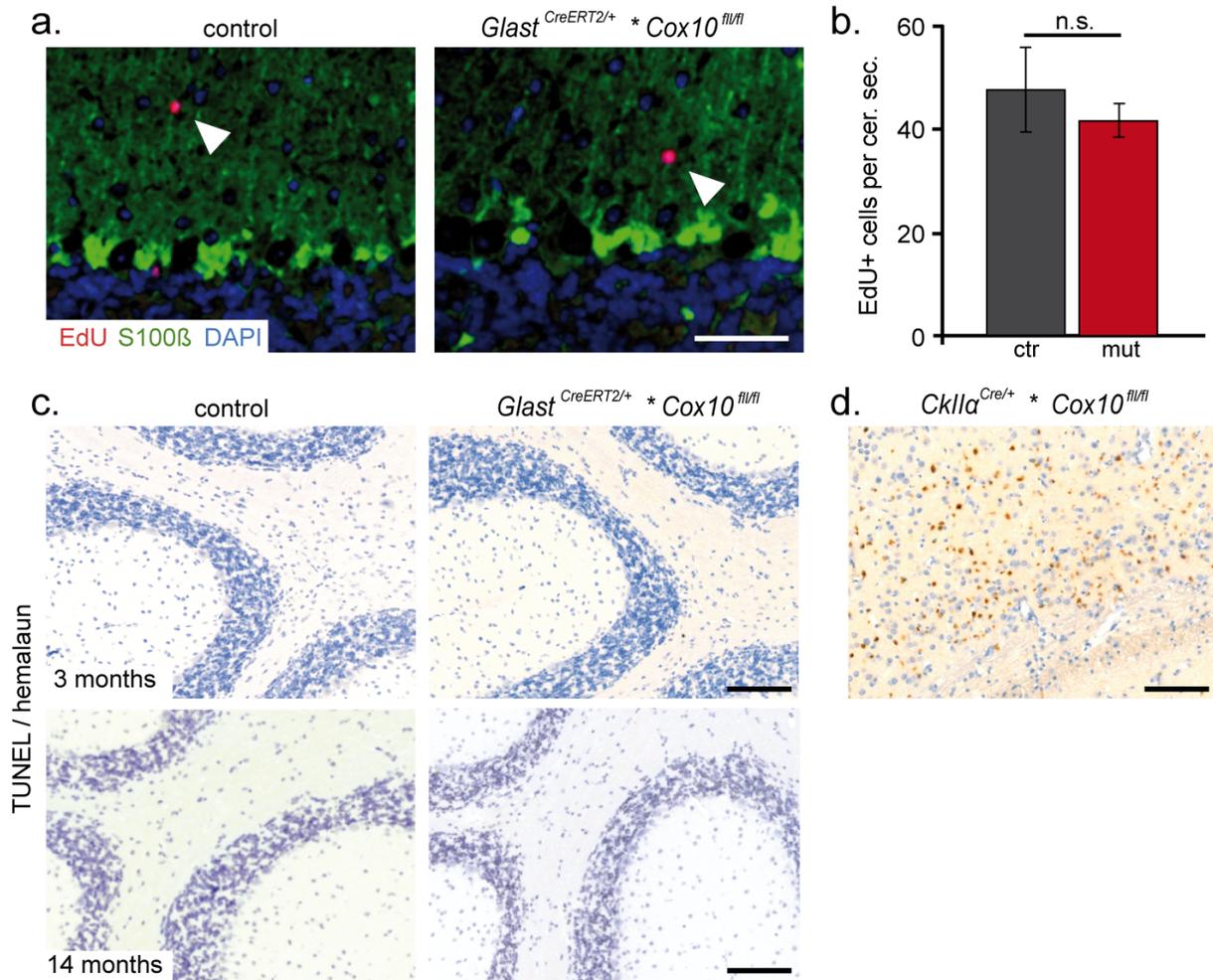
Fig. II - 6 Survival of Bergmann glial cells of *Cox10* mutant mice

(a.) Proliferation index was determined by EdU (red) administration. Mitotic S100ß+ cells (green) in the cerebellum of mutant mice and controls were almost absent. Asterisks denote dividing non-astrocytic cells. **(b.)** Similarly, there was no significant difference in the total number of EdU positive cells (47.7 ± 8.3 in controls and 41.75 ± 3.1 in mutants). Scale bar, 20 µm. Numbers are ± s.e.m. **(c.)** By TUNEL labelling of the cerebellum at 3 and 14 months, control and mutant mice revealed no apoptotic cells, **(d.)** which were easily detectable in a positive control (forebrain of $Cox10^{fl/fl}$ * CKIIα-Cre at 4 months). Scale bar, 100 µm. cer.sec., cerebellar section; n.s., not significant.

5.1.5 NORMAL BERGMANN GLIA MORPHOLOGY AND SYNAPSE DENSITY

Astrocytes contribute to the formation and maintenance of synapses and are thought to be involved in the regulation of synaptic transmission and plasticity (Chen et al., 2012; Gourine et al., 2010; Ullian et al., 2001a) The close proximity of astrocytic processes to synapses allows a bidirectional communication between both cellular compartments. To assess whether respiration-deficient BG cause morphological changes of the tripartite synapse compartments consisting of parallel fiber (PF) projecting to Purkinje cell spine (PC) and their ensheathing BG process ultrastructural analysis were performed. Quantification of PF-PC
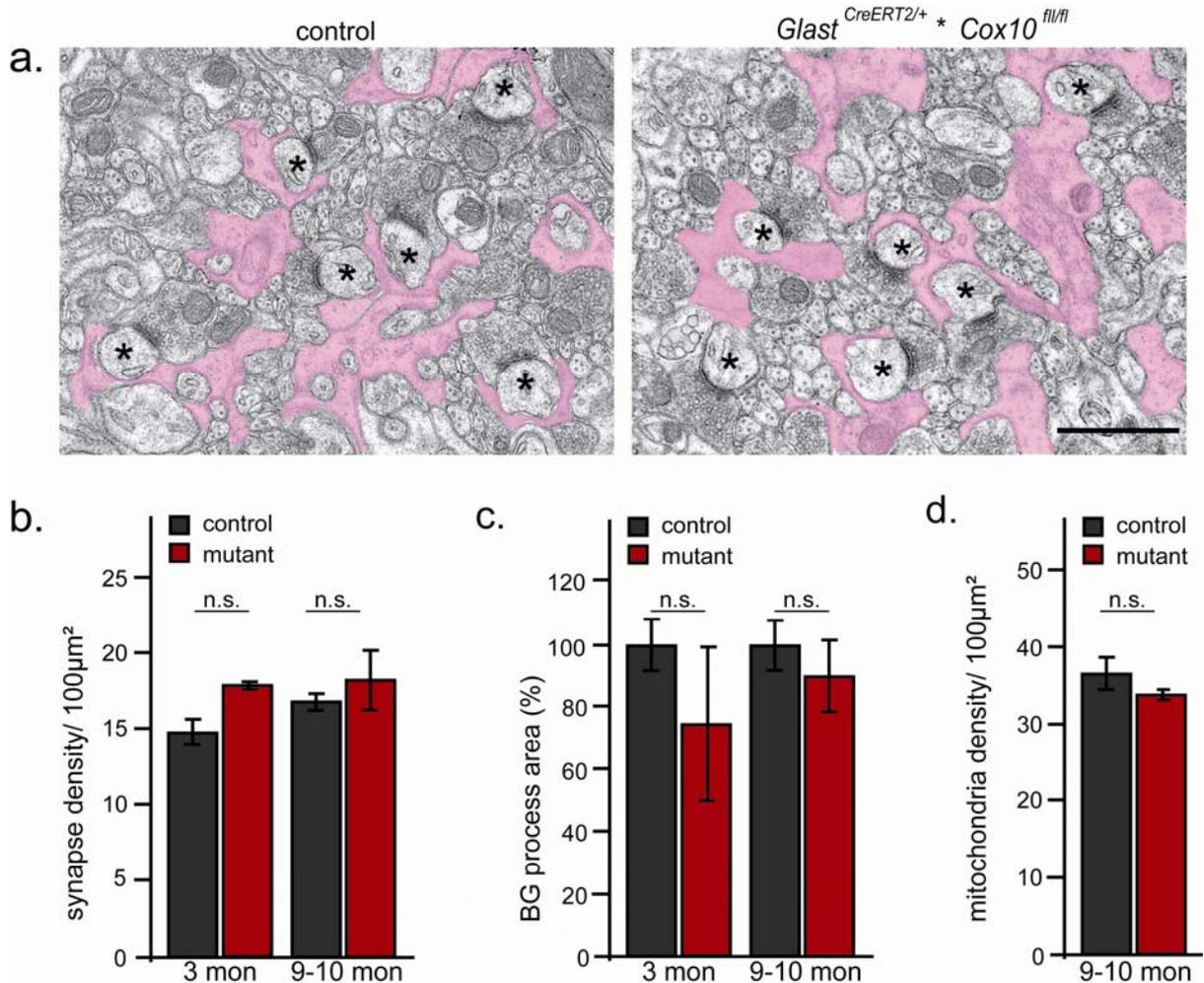
Fig. II - 7 Normal synapse density and BG process coverage in *Cox10* mutant mice

(a.) EM images of the upper third of the ML from control and mutant mice at 9–10 months of age. BG processes are false-colored pink and synapses are indicated with asterisks. Scale bar, 1 μm. **(b.)** PF-PC synapse density was quantified in randomly acquired EM images. At both timepoints no significant differences could be observed between control and mutant mice. At 3 months, controls revealed a synaptic density of 14.7 ± 0.9; mutants 17.8 ± 0.2 and at 9–10 months, 16.8 ± 0.6 in controls and 18.2 ± 1.9 PF-PC synapses in mutants each per 100 μm². **(c.)** Mutant PF-PC synapses were normally covered by BG processes (pink) when compared to controls at both timepoints analyzed (at 3 months, controls 100 ± 8.4%, mutants 74.7 ± 24.3% and at 9–10 months, controls 100 ± 7.8%, mutants 89.8 ± 11.9%). **(d.)** The mitochondrial density in mutant BG processes was normal compared to controls at 9–10 months and displayed per 100 μm² 36.4 ± 2.1 in controls and 33.7 ± 0.9 mitochondria in mutants. Numbers are ± s.e.m. n.s., not significant

synapses in the upper part of the molecular layer displayed normal synaptic densities in conditional Cox10 mutant mice in comparison to controls (Fig.II - 7a.,b.). Further, BG processes surrounding PF-PC synapses were investigated. Swollen BG processes can be an indicator for accumulated lactate and thus acidosis, and process retraction is reported to be associated with synapse dysfunction (Saab et al., 2012). The calculation of BG process area of mutant relative to control mice revealed no differences at 3 and 10 months of age (Fig.II - 7a.,c.). Moreover, the mitochondrial density in BG processes was normal in mutants compared to age-matched controls (Fig.II - 7d.). This is in agreement with the finding that glycolytic   astrocytes   maintained   normal   brain   functions   in   vivo.

5.2 DISCUSSION

The cellular origin and fate of lactate and its contribution to brain energy metabolism are important, and still open issues and led to diverse hypotheses mainly based on conflicting *in vitro* data (Pellerin and Magistretti, 1994; Bouzier-Sore et al., 2013; Dienel, 2012; DiNuzzo et al., 2010; Hertz et al., 2014; Magistretti and Allaman, 2015; Patel et al., 2014). More than 30 years ago as the discovery of the misbalance between cerebral oxygen utilization, blood flow and glucose consumption during brain activation was unraveled using improved neuroimaging techniques (Fox et al., 1988; Fox and Raichle, 1986) a new research direction was introduced, which finally originated in diverse concepts by today. There are two main models facing each other. Studies by Dienel and Cruz implied that lactate, wherever generated, is detrimental for the CNS and is rapidly disposed of by the blood stream (Dienel and Cruz, 2003). That lactate is a by-product of active synapses, which is dispersed *via* gap junction coupled astrocytes into capillaries, was specified by Gandhi and collegues (Gandhi et al., 2009). Controversely, the observation has been made that glutamate, the main neurotransmitter in the CNS, can be taken up by astrocytes which stimulates glucose uptake. This triggers the production of lactate by aerobic glycolysis, which is in turn shuttled to glutamatergic synapses to cover neuronal energy requirements (Bouzier-Sore et al., 2006; Pellerin and Magistretti, 1994; Pellerin et al., 1998). However, direct *in vivo* approaches to determine the role of endogenously generated lactate are difficult to implement technically.

To address the open question whether astrocytes *in vivo* are capable of providing lactate to neighboring cells to support neuronal energy demands, a new mouse model was generated. Therefore, the mitochondrial complex IV (COX) was indirectly inactivated by targeting the *Cox10* allele (Diaz et al., 2005) in adult astrocytes by using the tamoxifen-inducible GLASTcreERT2 mouse line (Mori et al., 2006). Successful recombination by Cre activity was displayed by intense reporter EYFP expression of almost all Bergmann glial cells in the cerebellum (Srinivas et al., 2001), and called for further analyses of this brain region. *Cox10*-mutant astrocytes are forced to live glycolytically, whereby lactate as a necessary by-product needs to be generated to retain the NAD+/ NADH equilibrium ensuring continuous glycolysis. Elevated lactate levels as a consequence of *Cox10* ablation have been reported in conditional mouse mutants harboring *Cox10*-deficient oligodendrocytes and in patients with *Cox10* germline mutations (Valnot et al., 2000; Antonicka et al., 2003; Fünfschilling et al., 2012).

Conditional *Cox10^{flox/flox}* * GLASTcreERT2 mutants were obtained at expected Mendelian ratios. They appeared normal and were phenotypically indistinguishable from controls up to an old age of 14 months. Long-term effects of *Cox10* disruption was proven by sequential COX/ SDH histochemistry at the age of 14 months which revealed the absence of COX

activity from BG cells. Notably, histological analysis exhibited a normal cerebellar structure at 3 months (when COX ablation in BG is expected) as well as at 14 months. Morphology or density of BG cells themselves were not altered, which is in good agreement with the survival of cultured rotenone-treated astrocytes. Astrocytes are normally not postmitotic in the healthy brain, but it is conceivable that mutant astrocytes could be replaced by newly generated astrocytes, which have escaped Cre-recombination. However, evidence for apoptosis or elevated astrogenesis could not be detected in mutant mice. Thus it is more likely that astrocytes survive as glycolytic cells and are still able to fulfill their functions. Additionally, glycogen, which is the astrocyte-specific storage form of glucose and largest energy reserve the in the adult brain (Brown et al., 2004; Magistretti et al., 2008), was normally distributed in conditional mutants. It has been shown that astrocytic glycogen mobilization is essential to sustain neuronal firing in optic nerve preparations (Brown et al., 2005; Tekkök et al., 2005) and *in vitro* studies suggested that glycogenolysis results in lactate release (Brown, 2004; Dringen et al., 1993). Moreover, pharmacological blocking of glycogen breakdown interferes with hippocampal long-term memory formation, which also suppresses the increase of lactate that is normally associated with memory formation (Suzuki et al., 2011).

Importantly, no sign of mitochondrial morphological abnormalities was detected, such as swellings, a feature of mitochondrial dysfunction in *Cox10*-deficient skeletal muscle cells, hepatocytes and Schwann cells (Diaz et al., 2005, 2008; Fünfschilling et al., 2012). This indicates that a physiological adaptation has taken place, possibly as a result of normal astroglial differentiation. Unfortunately, the relative percentage of Bergmann glial cells to the total cell number of the cerebellum is too small for the application of ^{3}H-NMR spectroscopy as a tool to quantify the cerebellar lactate concentration.

Axonal swellings, APP accumulation and neuroinflammation comprise a sensitive response to neurodegenerative processes. The absence of any tested neuroinflammatory marker suggests that mutant Bergmann glia (and their neighbors) are not distressed by the conditional lack of mitochondrial respiration. Bergmann glia, which are in intimate contact to synapses play an important role in the maintenance of synapses *in vitro* (Ullian et al., 2001). Moreover, it has been shown that Bergmann glia are necessary to retain physiology and plasticity between parallel fiber (pf) and Purkinje cell (pc) synapses (Saab et al., 2012). Morphological alterations of astrocytic processes engulfing their corresponding synapse would be indicators for astrocyte-derived energy disturbances (Saab et al., 2012). However, mutant cerebellar PF-PC synapse densities or the area of astrocytic processes enwrapping PF-PC synapses were comparable to control mice.

This suggests that astrocytes can live by aerobic glycolysis alone, as already exhibited by the survival of cultured astrocytes upon rotenone treatment. More importantly, the lack of any

pathological alteration in the living brain of conditional *Cox10* mutants confirmed their independency of ATP generation by mitochondrial respiration. In striking contrast, cultured neurons responded very sensitive to rotenone-induced complex I inhibition and led to massive apoptosis. Importantly, genetic targeting of *Cox10* in a subset of neurons using CamKinaseIIα-Cre driver line (Minichiello et al., 2002) resulted in severely affected conditional mutants. CamKinaseIIα expression is restricted to cortical projection neurons of the forebrain, starting at P5–P10 and showed an activity peak phase around P60 in mice. These neuronal mouse mutants were obtained in normal Mendelian ratio, but showed already at age P21 signs of neurodegeneration, which were progressive with age resulting in complete paralysis of fore- and hindlimbs and the premature death by the age of 4 months. Histological analysis at this final timepoint revealed vigorous axonopathy determined by APP accumulations that were accompanied by severe neuronal cell death. Bearing in mind that *Cox10* depletion is not followed by an immediate loss of mitochondrial function, predicted to take around 1 month (Beattie et al., 1967; Menzies and Gold, 1971) and the comprehensively late postnatal CamKinaseIIα-mediated Cre-expression might explain the relative late onset of prominent features of neuropathy by 2 months in neuronal *Cox10* mutant mice. However, the severity of neurodegeneration is remarkable since only a small subpopulation of neurons is targeted by Cre-recombination. This highly emphasizes the absolute dependency of neurons on mitochondrial ATP production (Fukui et al., 2007, own observation). Both conditional mutants develop different phenotypes, ranging from not (astrocytes) or severely (neurons) affected. This is in perfect agreement with previous transcriptome analyses displaying variations of the metabolic enzyme profiles of neurons and astrocytes, and even an astrocytic preference for glycolytic pathways (Lovatt et al., 2007; Cahoy et al., 2008). Moreover, nitric oxide-stressed neurons in culture are unable to respond with enhanced glycolysis due to missing glycolytic activators in their enzymatic repertoire (Almeida et al., 2001). Interestingly, genetic and pharmacological approaches both leading to the upregulation of glycolytic activators in cultured neurons and thus to an increased rate of glycolysis, concomitantly caused massive neuronal apoptosis (Herrero-Mendez et al., 2009). The observed neuronal cell death is explained by the diversion of glucose towards glycolysis and away from Pentose-Phosphate-Pathway (PPP) resulting in oxidative stress-induced apoptosis. The authors further concluded that neuronal consumption of glucose by the PPP to maintain their antioxidant status may take priority over the use of glucose to fulfill their energetic requirements (Herrero-Mendez et al., 2009). Thus this finding is in good accordance to the ANLS concept proposing that neuronal compartments are metabolically supported by shuttled lactate which derived from astrocytes.

The rapid exchange of metabolites across the plasma membrane of cells requires expression of appropriate transporters. By the close contact to blood vessels and the expression of

glucose transporters (GLUT) astrocytes are best positioned and equipped to excessively take up glucose from the blood stream. In fact, it has been shown that the blood flow velocity can even be adapted by astrocytes due to neuronal activity (Gordon et al., 2007; Attwell et al., 2010). Moreover, MCTs are expressed on glia and neurons, which serve as routes for monocarboxylates like lactate and pyruvate, and remained stably expressed in adulthood (Vannucci and Simpson, 2003). Importantly, the shRNA-mediated loss of MCT1 and MCT4 from astrocytes, or MCT2 from neurons perturbed long-term memory formation, whereas short-term memory appeared independent of lactate shuttling (Suzuki et al., 2011). These data denote the importance of lactate transport between cells for the establishment of higher brain functions, but remain to a high extent indirect with respect to the *in vivo* source of brain lactate. Since the transport direction of MCTs is dependent on lactate and hydrogen concentration gradients, these investigations do not serve as a clear *in vivo* proof for the ANLS hypothesis. However, it has to be mentioned that MCT1 was detected to be as well expressed by oligodendrocytes (Lee et al., 2012). Thus, the metabolic consequence of blocking MCT1 of oligodendrocytes was not considered in this study. Indeed, Suzuki and colleagues demonstrated that the inhibition of glycogen breakdown, which is exclusively found to be stored in astrocytes, reduced long-term memory establishment (Suzuki et al., 2011). However, the interconnection between astrocytes and oligodendrocytes has been shown to be important for maintaining brain physiology. This was reflected by the premature death of mice by 3 months, caused by the disruption of astrocyte-oligodendrocyte by the selective loss of their gap junctions (Tress et al., 2012). The specific ablation of astrocyte–oligodendrocyte connection results in hypomyelination of white matter tracts and revealed indications of osmotic problems within the oligodendroglial compartment at ultrastructural level (Tress et al., 2012). Moreover, mutations in gap junctions are known to contribute to the development of the Charcot-Marie-Tooth disease, an inheritated peripheral neuropathy and as well the Pelizaeus-Merzbacher disease, which is a severe leukodystrophy (Uhlenberg et al., 2004; Kleopa and Scherer, 2006). Although the function of astrocyte-oligodendrocyte gap junctions is not well understood, they are able to shuttle energy metabolites such as glucose (Rouach et al., 2008) and possibly could also transport lactate. This emphasizes the importance of proper coupling of neurons, astrocytes and oligodendrocytes and implied that the rapid exchange of metabolites within different cell types is essential for their function and survival.

Our findings provide *in vivo* evidence that the survival of respiration-deficient Bergmann glia is ensured by ATP generation by aerobic glycolysis alone, which contributes to the general understanding of brain metabolism. While of interest as an artificial experimental situation, the data also imply that these astrocytes must be a continuous source and not a sink of lactate, and this not for short time but for a year and more. In the cerebellum, this applies to

more than 90 % of all Bergmann glial cells, in the absence of any sign of pathology or cerebellar dysfunction. These *in vivo* data are no *in vivo* proof, but in perfect agreement with the original ANLS hypothesis.

However, this work provides new insights and raised further questions to the understanding of brain metabolism. Further investigations are needed to clarify metabolic capabilities of oligodendrocytes and the trophic interconnection of oligodendrocytes and astrocytes to neurons and among each other. This is important to fully reconstruct the contribution of glial cells to the onset of neurodegenerative diseases, which is the basis to develop novel therapeutic approaches.

5.3 DETAILED SUMMARY

Glucose is assumed to be the major energy metabolite of the adult brain. With the discovery of an uncoupling between cerebral oxygen utilization, blood flow and glucose consumption during brain activation, the participation of lactate as an important energy substrate to fuel the brain has been widely accepted in recent years. Astrocytes that are in intimate contact to synapses are widely discussed to support local energy requirements at glutamatergic synapses by shuttling glucose-derived lactate. However, the cellular origin and fate of lactate and its contribution to CNS energy metabolism are important and still open issues and led to diverse hypotheses mainly based on conflicting *in vitro* data.

To address the open question whether astrocytes *in vivo* are capable of providing lactate to neighboring cells to satisfy neuronal energy demands, conditional mouse mutants were generated. Therefore, the mitochondrial cytochrome c oxidase (COX) was indirectly disrupted by targeting the *Cox10* allele. COX10 is an essential assembly factor for COX and its ablation causes the gradual ablation of mitochondrial function. Hence, mutant astrocytes can survive by aerobic glycolysis or simply die. Cell type-specific *Cox10* inactivation in adult astrocytes was achieved by using the tamoxifen-inducible GLASTcreERT2 mouse line, which drives Cre-recombination in the majority of Bergmann glia, a specific astrocyte subpopulation in the cerebellum. This was confirmed by Cre-mediated reporter expression. However, conditional mouse mutants were fully viable and long-lived. Respiration-deficient astroglial cells showed no sign of cell death or any morphological alterration. Interestingly, using the same genetic modification conditional mouse mutants with *Cox10*-ablated projection neurons were apoptotic emphasizing their strict dependency on ATP generation by oxidative phosphorylation. In the astroglial mutants, not even unspecific indications of inflammatory processes and abnormal proliferation were detectable. Furthermore, synapses between parallel fibers and Purkinje cells were present in normal number and were normally covered by Bergmann glia processes when compared to control mice.

This work provides *in vivo* evidence that the physical survival of respiration-deficient Bergmann glia is ensured by ATP supply by aerobic glycolysis alone and strongly indicates that astrocytes must be a continuous source and not a sink of lactate and this applies to more than 90% of all Bergmann glial cells in the cerebellum. These *in vivo* data are no final proof yet, but further strengthen the original ANLS hypothesis and contribute to the general understanding of energy metabolism of the brain.

6   PART III:

PKM2- A MODULATOR OF THE BALANCE BETWEEN GLYCOLYSIS AND OXIDATIVE PHOSPHORYLATION

6.1   RESULTS

The pyruvate kinase, a key enzyme of the glycolysis, exists in several isoforms catalyzing the conversion of phosphoenolpyruvate (PEP) to pyruvate. The most active isozyme is PKM1, which is ubiquitous expressed, whereas the other forms show cellular and developmental specificity. PKM2, whose activity is described to be adjustable, displays strong expression during embryonic phases when cells are highly mitotic and is replaced by PKM1 expression in postnatal states. However, it has been shown that PKM2 is still present in highly proliferating tissues like lung or fat tissue. Moreover, an abundant PKM2 expression was detected in cancer cells, which are the most prominent glycolytically living cells, and has caught much attention by cancer research. There is emerging evidence that PKM2 is necessary for tumor growth and proliferation (Mazurek et al., 2005; Christofk et al., 2008; Spoden et al., 2009; Sun et al., 2011).

We hypothesize that oligodendrocytes are not only responsible for myelination, but might as well provide metabolites, most likely glycolytic end products, to their associated axons to locally support neuronal energy requirements. The underlying mechanism how oligodendrocytes can adapt to a rather glycolytic metabolism remains to be elusive. Therefore we focused our PKM2 due to its role in adapting cancer metabolism.

6.1.1   PKM2 IS EXPRESSED IN DIFFERENT CELL TYPES *IN VITRO*

To get a first impression whether PKM2 is expressed by brain cells *in vitro*, immunolabelling of PKM2 was performed on isolated glial and neuronal cells obtained from rats. In neurons, PKM2 was detectable in the cytoplasm and axons. By strong colocalization with NeuN, a neuron-specific transcription factor, a nuclear PKM2 expression could not be excluded (Fig.III - 1a.). A prominent PKM2 expression was found in astrocytes. The signal was homogenously distributed in astrocytic cytoplasm and cell processes, whereas the nuclear DAPI-positive area was only sparsely covered with PKM2-positive staining, indicating that this weak PKM2 signal might rather derive from the above located layer of cytoplasm than to a true nuclear expression (Fig.III - 1b.). Oligodendrocytic PKM2 expression was investigated at different developmental states. For the more immature state, oligodendrocytes were just grown for 12 h in the differentiation medium SATO to achieve the polydendrocytes status. To obtain differentiated oligodendrocytes that already developed myelin sheaths, cultures were left for 6 days in SATO medium. Microscopic analysis of immunolabeled cells indicated a
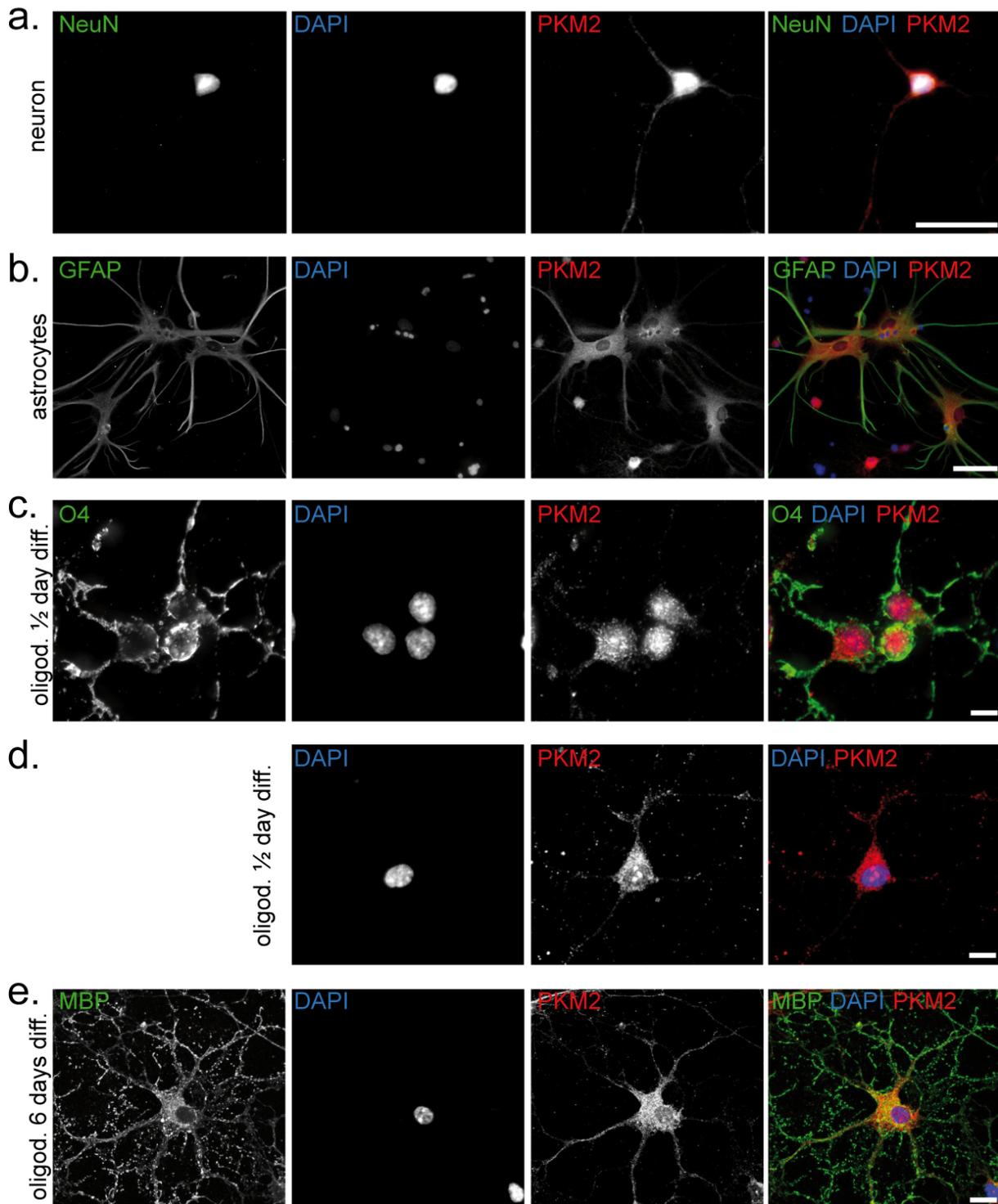
Fig. III - 1 PKM2 is expressed by main CNS cell types *in vitro*

Microscopic inspection of cultured **(a.)** neurons identified by NeuN expression, **(b.)** astrocytes positive for GFAP and **(c.)** immature oligodendrocytes visualized by O4 signal revealed co-immunolabelling of PKM2 (red). Confocal microscopic analysis of **(d.)** immature oligodendrocytes confirmed partly the microscopically observed nuclear PKM2 expression and **(e.)** differentiated oligodendrocytes identified by MBP expression exhibited PKM2 signals mainly distributed in the cytoplasm and processes. Scale bars are for a., b., 50 μm; c., d., 5 μm; and e., 10 μm. oligod., oligodendrocyte; diff., differentiation.

shift in the expression pattern between immature and more differentiated oligodendrocytes. In polydendrocytes, immuno-positive for O4 (sulfatide, an oligodendroglial surface marker), PKM2 expression seemed to be restricted to the nucleus (Fig.III - 1c.). To get a better insight into true localization of PKM2 expression, confocal analysis was performed. For more immature oligodendrocytes, a partial nuclear accumulation of PKM2 could be confirmed, while a cytoplasmic distribution was as well observable (Fig.III - 1d.). However, differentiated oligodendrocytes still revealed a cytoplasmic and myelin-associated localization, and only weak PKM2 expression in the nucleus (Fig.III - 1e.). Several studies describe a correlation between the cellular expression domain of PKM2 and its activity state. It has been reported that nuclearly expressed PKM2 had dissociated to dimers resulting in less affinity to its substrate PEP and thus a reduced activity. In comparison, PKM2 expression found to be localized in the cytoplasm is a strong indication for a tetrameric, full-active kinase (Dombrauckas et al., 2005; Gui et al., 2013; Yang et al., 2011). Hence, an alteration of the PKM2 expression pattern is a hint that oligodendrocytes change their metabolic program with regard to their differentiation state. This could mean that polydendrocytes which are at the beginning of myelination might slow down their glycolytic rate to accumulate glycolytic intermediates that are needed to build up macromolecules by other debranching pathways. In turn, when oligodendrocytes have already synthesized myelin sheaths, PKM2 associates to active tetramers promoting glycolysis and thus energy production.

6.1.2 PKM2 IS EXPRESSED IN THE LIVING BRAIN

To evaluate whether PKM2 is as well expressed in the living brain, immunolabelling against PKM2 on sagittal sections of wildtype mice (3 months) was performed. Throughout the brain, PKM2-positive cells could be observed. In all grey matter regions including hippocampus, striatum and hindbrain PKM2-labeled cells of similar size and morphology characteristics were found. All of them displayed a prominent PKM2 signal in the cytoplasm and processes. The highest density of PKM2 expressing cells was distributed over the cortex (Fig.III - 2a.,b.). Microscopic analysis of wildtype optic nerve samples (1 month), where oligodendrocytes make up to 60% of all residing cells, revealed that many cells expressed PKM2 in the cytoplasm (Fig.III - 2c.). Theses cells were often located in a row, which is a typical feature of oligodendrocytes. Due to missing co-labelling these cells can not be reliably classified as a specific cell population in the brain. However, that PKM2 is at all expressed in the adult brain is remarkable. So far, PKM2 expression was mainly described being exclusively restricted to embryonic, highly proliferating, mature cells and tumors.
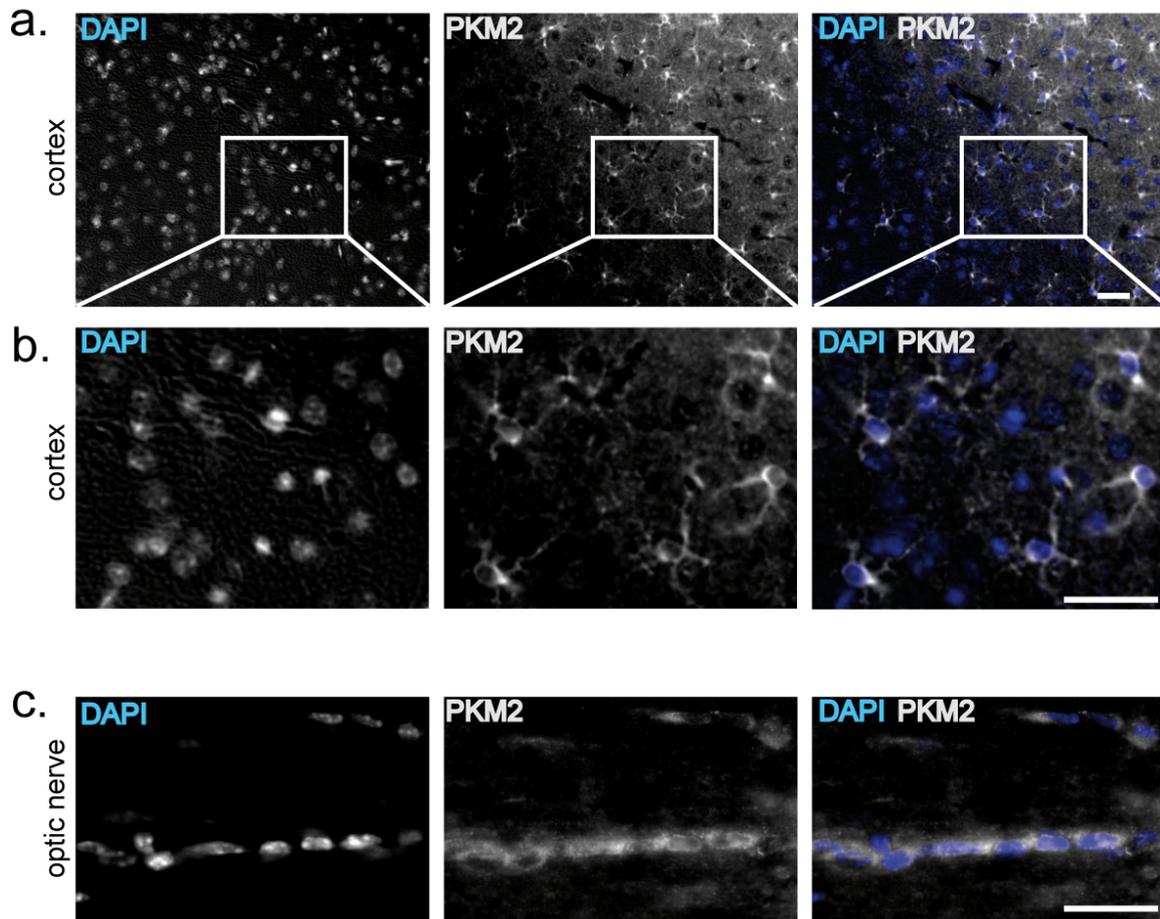
Fig. III - 2 PKM2 is expressed in the adult mouse brain *in vivo*

(a.) Microscopic analysis of sagittal brain sections of 3 months old wildtype mice showed PKM2-positive cells throughout the brain. The cortical region is exemplarily depicted, where the highest density of PKM2-expressing cells of all grey matter areas was observed. **(b.)** High power magnification of **(a.)** showing single PKM2-labeled cells. PKM2 expression was detectable in cytoplasmic regions and processes. **(c.)** Microscopic inspection of longitudinal optic nerve sections of 1 month old wildtype optic nerves revealed PKM2-expressing cells, lined up in a row, which is a characteristic of oligodendrocytes. Scale bar 50 µm was applied for all images.

6.1.3 PKM1/ PKM2 TRANSCRIPT EXPRESSION PATTERN OVER AGE

PKM2 is expressed in adult cells of the rodent brain. To extend this analysis with regard to PKM2 time course expression, transcript levels of PKM2 in different tissues at various developmental states were investigated by quantitative RT-PCR. Therefore, optic nerves as oligodendrocyte-enriched and cortices as a neuron-dominated region were examined. The focus was set on the analysis of P8 tissue (when myelination is at its starting point), P15 (a peak phase of myelination), P24 (when almost all axons are covered with myelin) and 3 months old tissue (when myelination is finished). PKM1, which is described to be the ubiquitous form of the pyruvate kinase, and total amounts of PKM transcripts were as well studied. Therefore, specific primer pairs were designed which were located to span

alternatively spliced exons. To quantify specifically PKM1 transcripts primers were positioned in exon 9 and 11 (exon 10 is excized) and for PKM2 in exon 8 and 10 (exon 9 is excluded). To detect both isozymes (total PKM) forward and reverse primers were located in exon 11, which is never spliced (Fig.III - 3a.). As

The analysis of total PKM transcripts revealed that its expression in optic nerves was stable at all timepoints tested and showed only a little increase over age (Fig.III - 3b.). Considering only PKM1 mRNA expression, optic nerves revealed a significant reduction between P8 and P15, which is a developmental state characterized by high myelinogenesis. In older ages a strong and significant rise of PKM1 transcripts could be detected (Fig.III - 3c.). In turn, PKM2 transcript expression in optic nerves was slightly elevated from P8 to P15, dropped significantly in P24 optic nerve samples and was found to be significantly raised again by the age of 3 months (Fig.III - 3d.).

In comparison, cortical samples showed a clear elevation of total PKM transcripts during development, which was even significant between P8 and P15 as well as P15 and P24 (Fig.III – 3e.). PKM1 mRNA levels were also continuously enhanced in cortical homogenates over age, but the significance was not as strong as in optic nerves (Fig.III - 3f.). Comparable to optic nerves similar PKM2 mRNA expression patterns could be detected in cortices with high significance between all analyzed timepoints (Fig.III - 3g.).
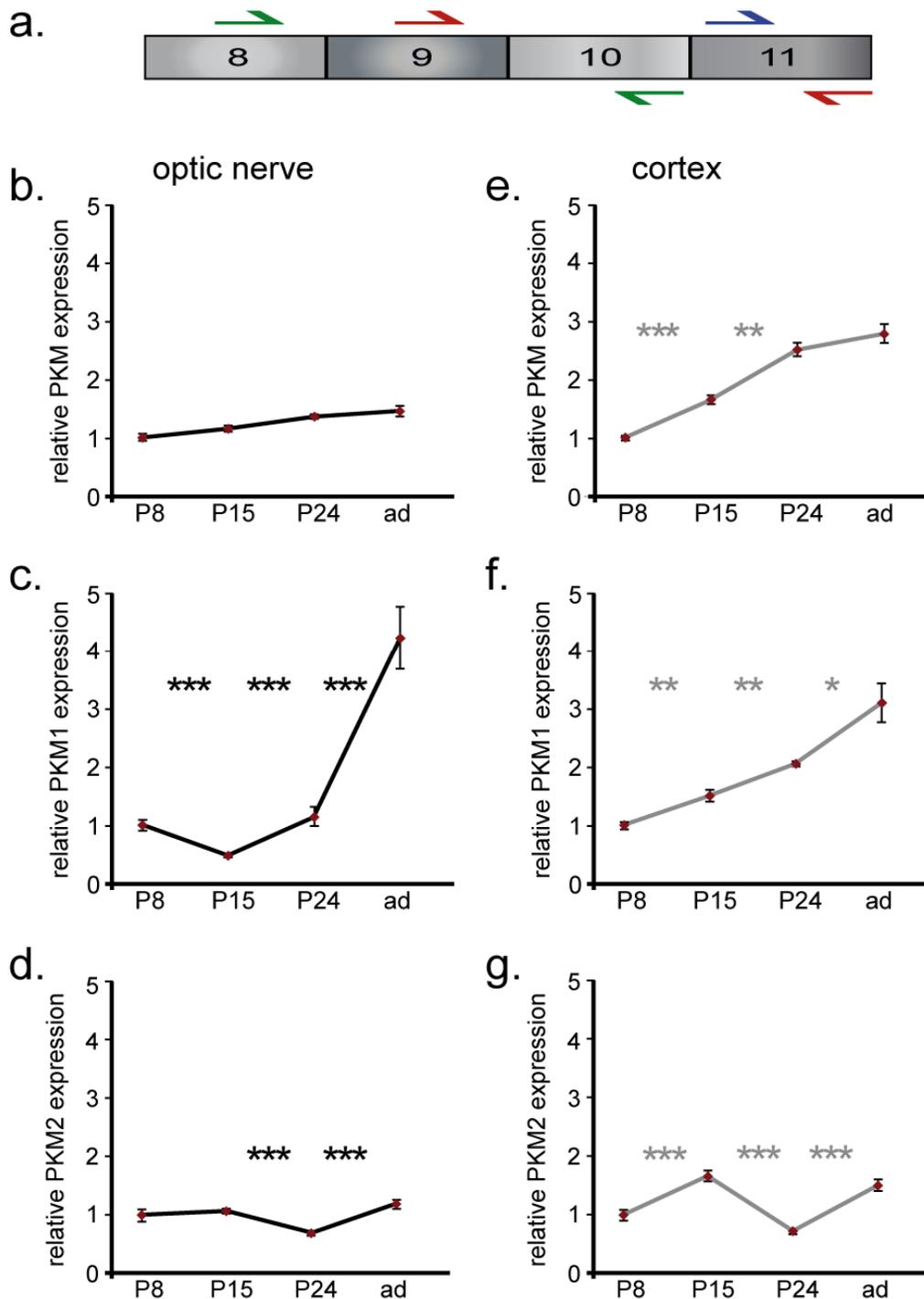
Fig. III - 3 PKM, PKM1 and PKM2 mRNA expression in cortex and optic nerve of at different ages

(a.) Scheme representing the localization of primer pairs for specific detection of relative mRNA expression levels of PKM (blue/red), PKM1 (red/red) and PKM2 (green/green). **(b.)** In optic nerves PKM mRNA expression remained mainly constant, only a slight trend to an increase of PKM transcripts could be observed over age (P8, 1 ± 0.034; P15, 1.15 ± 0.033; P24, 1.36 ± 0.014; ad, 1.46 ± 0.046). **(c.)** PKM1 mRNA expression in optic nerves dropped from P8 to P15 (P8, 1 ± 0.096; P15, 0.47 ± 0.027), whereas a significant raise could be observed in older states (P24, 1.13 ± 0.168; ad, 4.22 ± 0.548). **(d.)** PKM2 transcript levels were constant from P8 to P15 (P8, 1 ± 0.107; P15, 1.08 ± 0.039), decreased by P24 and exhibited a rise in adult states of optic nerves (P24, 0.68 ± 0.03;

ad, 1.2 ± 0.078). **(e.)** PKM mRNA expression in cortical regions revealed a significant increase over age (P8, 1 ± 0.026; P15, 1.66 ± 0.055; P24, 2.53 ± 0.077; ad, 2.8 ± 0.103), **(f.)** which was also true for the analysis of PKM1 mRNA expression in cortices showing similar expression patterns (P8, 1 ± 0.064; P15, 1.51 ± 0.102; P24, 2.06 ± 0.04; ad, 3.11 ± 0.335). **(g.)** PKM2 transcript levels in cortical regions increased from P8 to P15 (P8, 1 ± 0.088; P15, 1.7 ± 0.099), dropped by P24 and rose again by adulthood (P24, 0.73 ± 0.047; ad, 1.53 ± 0.11). Transcript levels of PKM, PKM1 and PKM2 are relative data that were normalized to averaged Rpl13a and Rpl0 mRNA expression. Asterisks denote significance level (* $p < 0.05$; ** $p < 0.01$; *** $p < 0.001$) and referred to the flanking time points each. Depicted are averaged means ± s.e.m of grouped tissues from individual wildtypes (n=3–10).

6.1.4 PKM/ PKM1/ PKM2 PROTEIN EXPRESSION IN THE BRAIN

To get better insights into PKM2 protein expression quantities, western blot analysis was performed. Therefore, different brain regions displaying varying cell type compositions were investigated. Optic nerve and corpus callosum homogenates served as oligodendrocyte-enriched tissues and cortices were used as neuron-dominated region. Moreover, the expression level between developmental states (P15) when myelination reaches its peak phase and adult animals (3 months) were compared. Since PKM2 is not the only isozyme in brain and PKM2 activity can be negatively modulated by phosphorylation at tyrosine residue 105, the expression of PKM1 and p-PKM2 was as well explored (Hitosugi et al., 2009).

The analysis of PKM1 demonstrated abundant expression in all examined tissues at both time points when compared to GAPDH signal used as loading control and for normalization. A trend of stronger PKM1 expression in adult samples of both corpus callosa and optic nerves when compared to their corresponding P15 time point and in comparison to adult cortical homogenates was clearly visible, but without significance. In neuron-enriched cortices no alterations of PKM1 expression could be observed between P15 and adult stages (Fig.III - 4a.). These results were in good accordance with the data obtained from the PKM1 mRNA expression study.

In contrast, optic nerve and corpus callosum homogenates of P15 and adult animals showed a high abundance of PKM2 signal when compared to GAPDH signal and cortical PKM2 expression levels. Quantification of western blots uncovered a 4-fold (for P15) and a 5-fold (for adult) stronger PKM2 signal in optic nerves compared to the corresponding cortical time point. Similarly, strong PKM2 expression, but to a lesser extent, was found for corpus callosum homogenates, where a 3-fold (for P15) and 4-fold (for adult) more abundant PKM2 signal was detected in contrast to respective cortical time points. A significant higher expression level was obtained in P15 optic nerves compared to P15 corpora callosa.
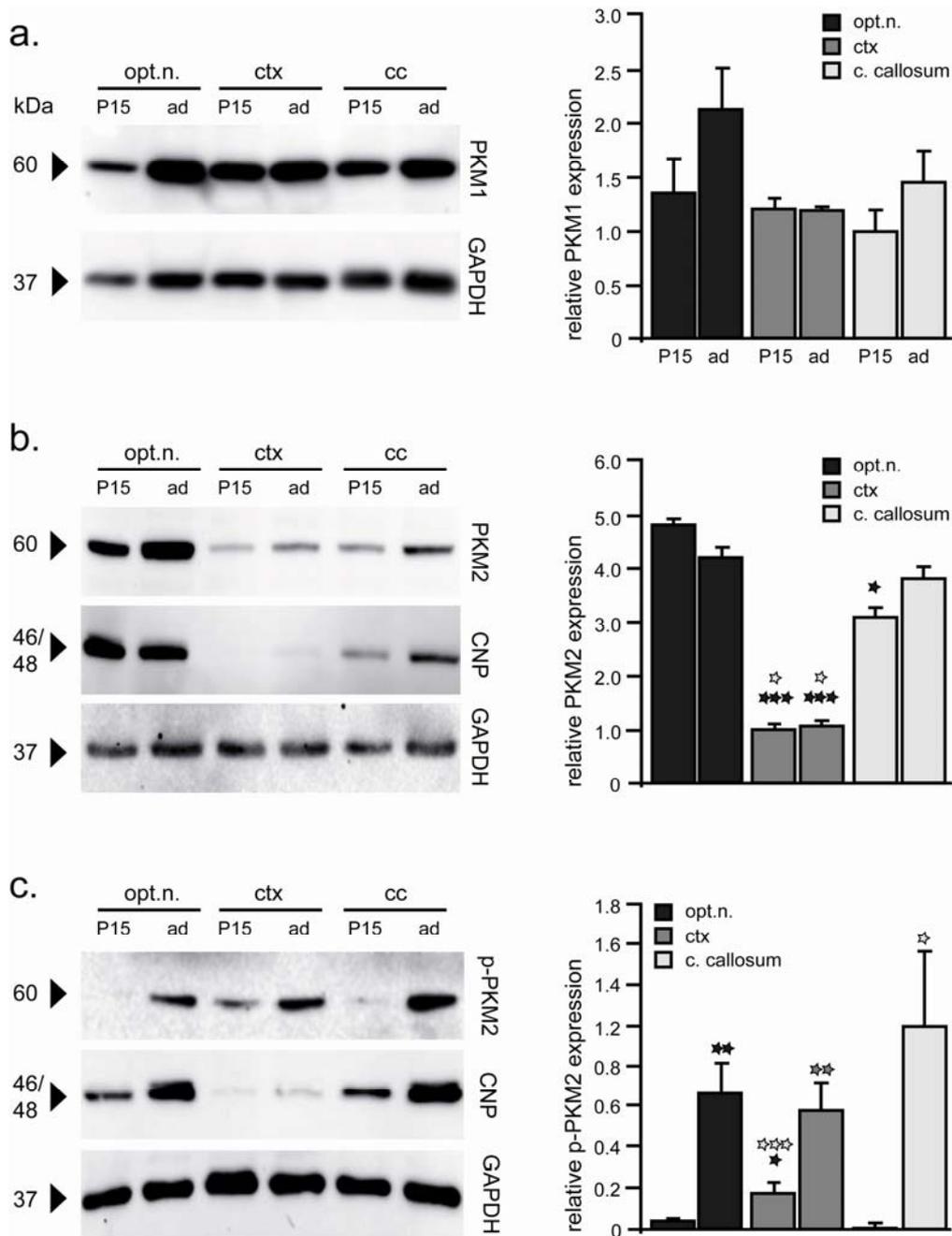
Fig. III - 4 Protein expression of PKM1, PKM2 and p-PKM2 in mouse white matter tracts and cortical samples at P15 and adult states

(a.) PKM1 western blot analysis revealed a slight enrichment of PKM1 expression in adult optic nerves and adult corpora callosa homogenates in comparison to adult cortices. Quantification of PKM1 expression levels displayed: P15, 1.36 ± 0.34; adult, 2.13 ± 0.38 for optic nerves; P15, 1.21 ± 0.13; adult 1.19 ± 0.03 for cortices; P15, 1 ± 0.19; adult, 1.45 ± 0.3 for corpora callosa. **(b.)** Strong PKM2 protein abundance was obvious in optic nerves and also in corpus callosum homogenates. Cortical samples exhibited weak PKM2 expression. Quantification numbers were P15, 4.82 ± 0.12; adult, 4.20 ± 0.20 for optic nerves; P15, 1 ± 0.10; adult 1.08 ± 0.1 for cortices; P15, 3.1 ± 0.16; adult, 3.8 ± 0.22 for corpus callosa. **(c.)** Strong p-PKM2 expression was detected in all adult tissues compared to the corresponding P15 region. In comparison to P15 optic nerve samples the p-PKM2 level was more abundant in P15 cortices and weaker in P15 corpora callosa. Quantification revealed: P15, 0.08 ± 0.03; adult, 0.67 ± 0.18 for optic nerves; P15, 0.18 ± 0.05; adult 0.59 ± 0.14 for cortices; P15, 0.02 ±

0.03; adult, 1 ± 0.37 for corpus callosa. Asterisks depict significance level (* p < 0.05; ** p < 0.01; *** p < 0.001). Asterisk colour referred to the compared tissue and comparison was performed between time points of the same tissue or between tissues at the same age. GAPDH was used as loading control and for normalization. CNP indicated content of myelin. Numbers are ± s.e.m. opt.n., optic nerve; ctx, cortex; cc, corpus callosum; P15, postnatal day 15; ad., adult.

When comparing both time points of each tissue, no difference in PKM2 abundance could be revealed (Fig.III - 4b.), which is, at least for cortical regions, in agreement with the PKM2 transcript analysis. However, the strong PKM2 expression found in white matter tracts (dominated by oligodendrocytes) might be related to oligodendrocytes and suggests that oligodendrocytes might exhibit the enzymatic prerequisite to balance between energy production and synthetic pathways.

To detect the status of PKM2 activity that is regulated by posttranscriptional modulation, the phosphorylation of PKM2 at tyrosine residue 105 (p-^{Y105}-PKM2) was investigated. In all adult tissues tested a significant stronger p-^{Y105}-PKM2 expression in comparison to the corresponding P15 time point could be quantified, with similar abundance in both white matter regions and in cortical homogenates. Compared to P15 optic nerve samples the p-PKM2 protein level was more abundant in P15 cortices and weaker in P15 corpora callosa (Fig.III - 4c.). Of note, in contrast to GAPDH, the p-PKM2 signal was in general not as strong as obtained for PKM1 and PKM2 (Fig.III - 4a.,b.).

6.2 DISCUSSION

There is emerging evidence that oligodendrocytes are not only responsible for myelination, but might as well provide metabolites, most likely glycolytic end products, to their associated axons to locally support neuronal ATP demands in the adult brain (Nave, 2010; Amaral et al., 2013; Morrison et al., 2013; Lee et al., 2012; Fünfschilling et al., 2012b). Recently, a link between a glycolytic metabolism of mature oligodendrocytes and the maintenance of axonal function and integrity was identified, which emphasizes the importance to investigate the oligodendroglial energy metabolism (Fünfschilling et al., 2012b). Generation of ATP mainly by aerobic glycolysis requires mechanisms controlling the shift away from mitochondrial oxidative phosphorylation. Since Otto Warburgs´ discovery that cancer cells cover their own ATP demands by enhanced glycolysis in the presence of O_2, a central dogma of cell biology was disproved and opened a new research direction exploring underlying mechanisms (Warburg, 1956). Initial work considered mitochondrial defects as the reason for the onset of tumors and the concomitant increase of glycolysis as a necessary adaptation to the lack of ATP generation by oxidative phosphorylation. Recently, it was shown that mitochondrial damage is rare in cancer tissue (Fantin et al., 2006; Frezza and Gottlieb, 2009). Moreover, enhanced glycolytic rates cover basic needs of rapidly proliferating tumor cells to facilitate construction of new cells by ensuring energy production and the synthesis of macromolecules at the same time. Similarly, aerobic glycolysis is a characteristic of many highly dividing normal tissues (Vander Heiden et al., 2009).

Microarray studies of different human and rodent cancers revealed an upregulation of glycolytic genes, including a significant elevation of pyruvate kinase transcript that catalyzes the rate-limiting final step of glycolysis (Altenberg and Greulich, 2004; Majumder et al., 2004). In mammals, four isozymes of pyruvate kinase (PK) exist: L and R isozymes are found in liver and red blood cells, respectively (Domingo et al., 1992; Rodriguez-Horche et al., 1987). The M1 form is expressed in most adult tissues, whereas the expression of its splice transcript M2 is spatio-temporally restricted to cells during embryonic development, highly proliferating cells in adulthood, like in lung or fat tissue and especially in cancer cells (Hacker et al., 1998; Reinacher and Eigenbrodt, 1981). Normally, PKM2 appear in an active, tetrameric state, which is the usual form of all PK forms, but exclusively in cancer cells PKM2 is present in an inactive, dimeric state (Yamada and Noguchi, 1999; Zwerschke et al., 1999, 2003) leading to the accumulation of glycolysis intermediates due to a decreased glycolytic rate. Thus, PKM2 can be considered as key enzyme balancing the direction of glucose metabolism dependent on cell requirements for macromolecule biosynthesis or ATP generation. Several studies with cancer cell lines strongly indicate that the switch from PKM1 to PKM2 expression in tumors is an essential mechanism adapting anabolic and catabolic

metabolism according to the needs of tumor growth and proliferation (Christofk et al., 2008; Mazurek et al., 2005; Spoden et al., 2009; Sun et al., 2011). It has been shown that downregulation of PKM2 diminished the ability of human tumor cell lines to proliferate and, moreover, the replacement of PKM2 by PKM1 reduced the ability forming tumors in nude mouse xenografts (Christofk et al., 2008).

To proof whether PKM2 might function as a possible modulator, regulating the glycolytic flux in oligodendrocytes, analyses concerning PKM2 expression in wildtype mouse brains were performed. Interestingly, immunostainings with PKM2 in adult brain sections revealed that many cells throughout the CNS were clearly positive for PKM2. This was intriguing and in contrast to the widespread belief that expression of the PKM2 isoform is restricted to rapidly dividing cells in adulthood (Cairns et al., 2011; Christofk et al., 2008; Gui et al., 2013; Vander Heiden et al., 2010). In fact, only sporadic PKM2-positive cells were found in the subventricular zone and dentate gyrus, which represent the regions of adult neurogenesis in the CNS. However, PKM2 expression was already detected in two independent studies (Bluemlein et al., 2011; Jahn et al., 2009). By mass spectrometry Blümlein and colleagues showed that PKM2 is expressed in several terminally differentiated tissues, including kidney, lung and liver, whereas the brain remained unstudied by this analysis (Blümlein et al., 2011). More important, proteome analysis of purified myelin samples identified the presence of PKM2 and further exhibited that about 5% of all myelin proteins are referred to glycolysis or gluconeogenesis (Jahn et al., 2009).

This is in line with our observation that PKM2 is expressed in cells of CNS white matter tracts of adult mice that possess morphology characteristics of oligodendrocytes. So far, cell type-specific PKM2 expression patterns in the brain could not be surely validated. *In vitro*, PKM2 was expressed by neurons, astrocytes and oligodendrocytes, which did not reflect its expression in the living CNS, where only a subset of cells showing similar shape and size was labelled by PKM2. However, immunocytochemistry indicated another important aspect of PKM2 expression. When comparing cultured polydendrocytes with more differentiated oligodendrocytes, that already developed myelin sheaths, an alteration of PKM2 localization was indicated. It seems that in younger developmental stages PKM2 was at least partially expressed in the nucleus of polydendrocytes, whereas more mature oligodendrocytes displayed a widespread PKM2 signal distributed over the cytoplasma, including myelin compartments. Importantly, localization of PKM2 expression is correlated to its activity state. Whereas cytoplasma-specific PKM2 expression is associated to an active quaternary structure, a nuclear localization is linked to inactive PKM2 dimers (Dombrauckas et al., 2005; Lv et al., 2013; Yang et al., 2011; Yang, Zheng, et al., 2012). These findings suggest that oligodendrocytes change their metabolic program according to specific requirements that

depend on the developmental state. This further indicates that polydendrocytes at the beginning of myelinogenesis might slow down their glycolytic rate leading to the accumulation of glycolytic intermediates which are necessary for the synthesis of major building blocks of myelin, including fatty acids, cholesterole and phospholipids (Aeberhard and Menkes, 1968; Cuzner and Davison, 1968; Orth and Bellosta, 2012; Saher et al., 2005). For instance, glycerate-3-phosphate is used in a debranching pathway of the glycolysis to produce phospholipids (Newsholme et al., 2003; Mazurek et al., 2005). Moreover, the Pentose-Phosphate-Pathway, another debranching pathway of glycolysis, is indirectly coupled to fatty acid synthesis, due to its delivery of NADPH that is crucial for the production of fatty acids and cholesterol (Baquer et al., 1977, 1988; Mazurek, Boschek, et al., 1997; Wood, 1986). It has to be mentioned that acetyl-CoA is the basic substrate for fatty acid synthesis, which is converted from pyruvate in mitochondria. Thus, mechanisms are required to equilibrate between sufficient NADPH generation and the entry of pyruvate into mitochondria to maintain proper fatty acid production for myelin generation. In contrast, when oligodendrocytes have already synthesized their myelin sheaths, PKM2 might associate to active tetramers promoting glycolysis and thus energy production. According to this, it is conceivable that PKM2 might act as a glycolytic key enzyme balancing between lipid syntheses that are needed for myelination during development and energy production in adulthood.

PKM1 and PKM2 transcripts are alternative splicing products from one gene. PKM1 mRNA levels in optic nerves, a region enriched by oligodendrocytes (Burne et al., 1996; Walhovd et al., 2014) were the lowest at the onset of myelination (P15) and rose with high significance with the peak and further by the termination of myelinogenesis. A continuous raise of PKM1 mRNA expression was as well observed in cortical tissue, but not as strong as in optic nerves. Although cortices are dominated by neurons, there is indeed a considerable residing oligodendrocyte population mediating myelination (Herculano-Houzel and Lent, 2005; Ling and Leblond, 1973). In agreement, PKM2 transcript expression was found to be elevated at P15 in both optic nerves and cortices. That PKM1 expression was comparatively low at P15 and PKM2 mRNA levels elevated at P15 in optic nerve samples suggest a role of PKM2 during the phase of high myelination. However, this analysis gives only a comparison of expression levels during important developmental and adult states of PKM isozymes respectively, but an exact ratio of PKM1 and PKM2 can not be calculated. Since PKM2 can appear as inactive dimers or active tetramers no information about PKM2 activity could be gained by this study. This was overcome by western blot analysis. As expected, PKM1 was found to be more or less equally strongly expressed in white matter tracts including optic nerve and corpus callosum and cortices at P15 and adult tissues. A pronounced enrichment of PKM2 protein concentrations was found in optic nerves and in corpus callosum samples in

comparison to cortices. These findings imply that PKM2 expression can be attributed to oligodendrocytes, because the main difference in cell type composition of white matter tracts and cortical samples is the percentage of oligodendrocytes, which make up to 60% in optic nerve and a clearly minor proportion in cortical fractions (Burne et al., 1996; Herculano-Houzel and Lent, 2005; Mori et al., 2006b; Walhovd et al., 2014; Ling and Leblond, 1973). However, the high expression level of PKM2 in white matter regions of the CNS further indicates that PKM2 seems to have a necessary function regulating the glycolytic flux in these parts of the brain. Investigation whether PKM2 is phosphorylated at the tyrosine residue 105 (p-[Y105]-PKM2) revealed that in comparison to P15 time points p-PKM2 expression was significantly stronger in tissue-matched adult fractions. Phosphorylation at this residue has been shown to disrupt the binding site for its substrate fructose-6-phosphate leading to a decreased growth of cancer cells (Hitosugi et al., 2009). Similarly, phosphorylation at serine 37 of PKM2 was detected to result in the dissociation of active tetramers to dimers (Yang, Zheng, et al., 2012). Furthermore, other studies indicate that acetylation, oxidation and sumoylation are as well involved in PKM2 dimer formation in different cancer cell lines (Anastasiou et al., 2011; Lv et al., 2011; Spoden et al., 2009). The apparent complexity of posttranscriptional modifications of PKM2 that all caused the reduction of PKM2 activity hampers the interpretation of the western blot analysis of p-[Y105]-PKM2. If indeed this modification results in a decreased glycolytic rate, it is conceivable that adult tissues might be stronger exposed to oxidative stress and thus to the production of reactive oxygen species. Slowing down glycolysis favors the PPP, by which NADPH is regenerated necessary for the glutathione-based detoxification of cells (Hirrlinger et al., 2002). However, it has to be mentioned that the true percentage of phosphorylated PKM2 can not be calculated, but when compared to GAPDH signals, only a little ratio of PKM2 seems to be phosphorylated. On the other hand, immunohistological investigations revealed a clear cytoplasmic expression of PKM2 in adult brains. Since PKM2 inactivity is directly associated to a nuclearly localized expression (Lv et al., 2013; Yang et al., 2011; Yang, Zheng, et al., 2012) these results do not support the suggestion that p-[Y105]-PKM2 is inactive.

However, that the embryonic isozyme PKM2 is expressed in a subpopulation of cells in the adult CNS, that do not belong to highly proliferating zones is remarkable. Since there is emerging evidence of an increased glycolysis metabolism in mature oligodendrocytes that is coupled to the maintenance of axonal integrity and regarding the relevance of PKM2 balancing the glycolytic flux denotes the importance to further investigate the role of PKM2 in brain metabolism in the healthy CNS.

6.3 DETAILED SUMMARY

Oligodendrocytes contribute to the maintenance of axonal integrity by shuttling energy-rich glycolytic end-products to neuronal compartments which requires an enhanced glycolytic rate of mature oligodendrocytes that may underlie a 'developmental' switch. This necessitates mechanisms controlling the shift away from mitochondrial respiration towards aerobic glycolysis. In order to determine the metabolic properties of oligodendrocytes, the focus was set on tumor-related key enzymes that are widely debated to be responsible for the glycolytic metabolism in cancer cells.

Therefore, the expression profile of the pyruvate kinase isozyme PKM2 was investigated since the switch from ubiquitous PKM1 to PKM2 expression in tumors is discussed to be an essential mechanism adapting cellular metabolism assuring cancer growth and proliferation. Contrary to the general belief, histological analyses of adult wildtypish mouse brain-sections revealed a robust PKM2 expression in cells with oligodendrocyte-like morphology. In line with this, when compared to cortical regions white matter tract lysates showed a strong PKM2 expression, whereas PKM1 was mainly stably expressed in these tissues. This argues for a crucial role of PKM2 in regulating the glycolytic flux in oligodendrocytes of CNS white matter tracts.

Since PKM2 activity is regulated by various posttranslational modifications, the affinity to its substrate phosphoenolpyruvate is difficult to determine. Indeed, the expression of a presumably inactive PKM2 that is phosphorylated at tyrosine residue 105 was detected in the adult brain, including cortices and white structures. This implied at least one regulatory mechanism controlling PKM2 activity in adulthood. To which extent PKM2 is modulated by specific phosphorylation and whether other modifications contribute to a regulatory network remains to be elusive. However, *in vitro*, practically all main CNS cell-types express PKM2 in this artificial environment. Interestingly, there are indications that during development PKM2 expression partially shifts in cultured oligodendrocytes from nuclear (polydendrocytes) to cytoplasmatic (myelin-forming oligodendrocytes) localization. Since PKM2 translocation is described to correlate with its inactivity, this finding further emphasizes the complexity of control mechanisms mediating the velocity of glycolysis. Further studies are needed to unravel the spectrum of metabolic capabilities of oligodendrocytes to gain more insight about the metabolic interdependency of CNS cell-types and the actual participation of PKM2.

7 MATERIAL AND METHODS

7.1 MATERIALS

7.1.1 CHEMICALS AND KITS

All chemicals were purchased from Sigma-Aldrich GmbH (Munich, Germany), Merck KGaA (Darmstadt, Germany) and SERVA (Heidelberg, Germany) unless stated otherwise. General laboratory materials were from BD Falcon (Heidelberg, Germany), Eppendorf (Hamburg, Germany) Bio-rad (München, Germany) Gilson (Limburg-Offheim, Germany) and Brand (Radebeul, Germany).

Kits

RNA purification 'RNeasy mini prep'   Qiagen (Portland, USA)

DC Protein Assay (Lowry)   Bio-Rad (Munich, Germany)

LSAB$_2$ kit   Dako (Hamburg, Germany)

Vector Elite ABC Kit   Vector Labs (Loerrach, Germany)

DAB Zytomed Kit   Zytomed Systems GmbH (Berlin, Germany)

DeadEnd™ Colorimetric TUNEL System   Promega Corporation (Madison, USA)

AlexaFluor-647 Click-iT EdU Cell Proliferation Assay Kit

Invitrogen, Life Technologies GmbH (Darmstadt, Germany)

7.1.2 MOLECULAR BIOLOGY

Extraction Buffer

0.05 M Tris/HCl, pH 8.8

0.1 M NaCl$_2$

3 mM EDTA

0.5% [v/v] SDS

Proteinase K (10 mg/ml)

Added to Extraction Buffer buffer before use for tail digest

Final concentration 0.5 mg/ ml

10 mM dNTP (50x stock)

2.5 mM each nucleotide (dATP, dCTP, dGTP, dTTP) (Boehringer-Ingelheim, Germany)

200 µM final concentration in a PCR reaction (50 µM each nucleotide)

73

50x Trisacetate EDTA (TAE) buffer

2.0 M Tris/Acetate, pH 8.0

50 mM EDTA

17.5% [v/v] Glacial acetic acid

DNA marker

GeneRuler 100 bp DNA ladder	Thermo Scientific (St. Leon-Rot, Germany)
GeneRuler 1 kp DNA ladder	Thermo Scientific (St. Leon-Rot, Germany)

Enzymes

Proteinase K	Boehringer GmbH (Mannheim, Germany)
GOTaq DNA polymerase	Promega (Mannheim, Germany)
RedTaq DNA polymerase	Sigma-Aldrich (St. Louis, USA)
Superscript III-reverse transcriptase	Invitrogen (Karlsruhe, Germany)
DNase	Roche Diagnostics GmbH (Penzberg, Germany)
Papain	Worthington Biochemical Corp (Lakewood, USA)
Trypsin	Invitrogen (Darmstadt, Germany)

7.1.3 PROTEIN BIOCHEMISTRY BUFFERS

10x Phosphate buffered saline (PBS)

1.7 M NaCl

34 mM KCl

40 mM Na_2HPO_4 x $2H_2O$

18 mM K_2HPO_4

pH 7.2 with 1N NaOH.

10x Tris-buffered saline (TBS)

500 mM Tris/HCl, pH 7.5

1.5 M NaCl

Protein lysis buffer

1x TBS

0.1% [v/v] SDS

0.1% [v/v] Triton X-100

Complete Mini protease inhibitor (Roche Diagnostics GmbH, Mannheim, Germany) was freshly added to the protein lysis buffer (1 tablet/10ml) before use.

SDS separating gel

12% or 10% [v/v] Acrylamid/ Bisacrylamid 29:1

0.4 M Tris/HCl pH 8.8

0.1% [v/v] SDS

0.03% [v/v] APS

0.08% [v/v] TEMED

SDS stacking gel

4% [v/v] Acrylamid/ Bisacrylamid 29:1

125 mM Tris/HCl pH 6.8

0.1% [v/v] SDS

0.05% [v/v] APS

0.1% [v/v] TEMED

4x SDS sample buffer

40% [v/v] Glycerol

240 mM Tris/HCl pH 6.8

8% [v/v] SDS

0.04% [w/v] Bromophenol blue

10x SDS running buffer (Laemmli buffer)

250 mM Tris base

1.92 M Glycine

1% [v/v] SDS

Transfer buffer

96 mM Tris base

78 mM Glycine

10% [v/v] Methanol

20x Tris buffered saline (TBS)

1 M Tris/HCl, pH 7.4

3 M NaCl

1x TBS with Tween-20 (TBST)

50 mM Tris/HCl, pH 7.5

150 mM NaCl

0.05% [v/v] Tween-20

Immunoblot blocking buffer

5% [w/v] non-fat dry milk powder in 1x TBST

or 5% [w/v] BSA powder in 1x TBST

Protein marker

PageRuler Plus Prestained Protein Ladder 10-250K   Fermentas   (St.   Leon-Rot, Germany)

Additional materials

- Enhanced Chemiluminescence (ECL) Immunoblot detection kit Western Lightning™ Plus ECL, Enhanced luminol reagent plus (Perkin Elmer Life Sciences, Inc., Rodgau, Germany).

- ECL-Hyperfilms (Amersham Biosciences, Uppsala, Sweden)

- PVDF membrane Hybond P pore size 0.45 µm (Amersham Biosciences, Uppsala, Sweden)

7.1.4 SOLUTIONS FOR FIXATION

Avertin

2% [w/v] 2,2,2 Tribromethanol 99%

2% [v/v] Amylalkohol

Mixed at 40°C for 30 min while stirring and subsequently filtered

Stored at -20°C

16% [w/v] Paraformaldehye (PFA) stock solution

16% [w/v] Paraformaldehyde cooked at 65°C for 20 min while stirring

5 N NaOH droplets until solution was cleared and then filtered

0.2M Phosphate buffer (fixation buffer)

0.36% [w/v] Sodiumdihydrogenphosphate (NaH_2PO_4)

3.1% [w/v] di-Sodiumhydrogenphosphate (Na_2HPO_4)

1% [w/v] Sodium chloride

4% [v/v] Paraformaldehye (PFA) for immunohistochemistry

4% [v/v] PFA

0.1 M Phosphate buffer

Karlsson-Schultz (K+S) fixative for electron microscopy

4% [w/v] PFA

2.5% [v/v] Glutaraldehyde

0.1 M Phosphate buffer

7.1.5 IMMUNOHISTOCHEMISTRY AND STAINING SOLUTIONS

Phosphate buffer (0.2 M, pH 7.4)

0.04 M Sodiumdihydrogenphosphate (NaH_2PO_4)

0.16 M di-Sodiumhydrogenphosphate (Na_2HPO_4)

Always prepared freshly

Citrate buffer (0.01 M, pH 6.0)

1.8 mM Citric acid ($C_6H_8O_7 * H_2O$)

8.2 mM Sodium citrate ($C_6H_5O_7Na_3 * 2H_2O$)

Always prepared freshly

BSA/PBS

0.04M Sodiumdihydrogenphosphate (NaH_2PO_4)

0.16M di-Sodiumhydrogenphosphate (Na_2HPO_4)

1.8% [w/v] Sodium chloride

1.0% [w/v] Bovines serum albumin (BSA)

Tris buffer (pH 7.6)

50 mM Tris/HCl, pH 7.6

0.9% [w/v] Sodium chloride (NaCl)

Always prepared freshly.

Mayer's haematoxylin solution

0.1% [w/v] Haematoxylin

0.02% [w/v] Sodium iodate

5% [w/v] Potassium aluminium sulphate ($K_2Al_2(SO_4)_4 * 24H_2O$)

Added under constant shaking, solution turned violet blue

5% [w/v] Chloralhydrate

0.1% [w/v] Citric acid added

Added and filtered before use

Eosin solution

0.1% [v/v] Eosin

12 drops of glacial acetic acid in 250ml

Scott's solution

0.2% [w/v] Potassiumhydrogencarbonate

2% [w/v] Magnesium sulphate

HCl-alcohol

0.09% [v/v] HCl

70% [v/v] Ethanol

Gallyas silver impregnation

Incubation solution

0.1% [w/v] Ammonium nitrate

0.1% [w/v] Silver nitrate

12‰ [w/v] Sodium hydroxide (pH 7.5)

Brown precipitate dissolved by shaking, stored for 8-10 weeks.

Physical developer

Solution A 5% [w/v] Sodium carbonate (dehydrated) in H_2O

Solution B 0.2% [w/v] Ammonium nitrate

0.2% [w/v] Silver nitrate

1% [w/v] Wolframosilicic acid (silicotungstic acid)

Solution C 0.2% [w/v] Ammonium nitrate

0.2% [w/v] Silver nitrate

1% [w/v] Wolframosilicic acid (silicotungstic acid)

0.26% [w/v] Paraformaldehyde

To reconstitute physical developer: 70ml of solution B added to 100ml of solution A with constant and gentle shaking and then slowly added to 1000ml solution C.

Fixing solution

2% [w/v] Sodium thiosulphate

Permeabilization and blocking buffer for vibratome sections

5% [v/v] Horse serum

0.3% [v/v] Triton X-100

Dissolved in 1x PBS

Permeabilization and blocking buffer for coverslips

10% [v/v] Horse serum

0.2% [v/v] Tween-20

Dissolved in 1x PBS

Mounting media

Eukitt Kindler (Freiburg, Germany)

Aqua-Poly/Mount Polysciences (Eppelheim, Germany)

7.1.6 ELECTRON MICROSCOPY

Epon

Mixed 30 min before embedding in the following way:

171.3 g Glycidether 100

115 g DDSA (Dodecenyl succinic anhydride)

89 g MNA (Methyl nadic anhydride)

Mixed using magnet stirrer for 10 min and then

6.5 ml DMP-30

Added and mixed using magnet stirrer for 20 min

Methylene blue - Azure II staining solution

Methylene blue

1% [w/v] Na-tetraborat (Borax)

1% [w/v] Methylenblau

Azure II

1% [w/v] Azure II

Methylene blue and Azure II were freshly mixed 1:1 before use.

7.1.7 CELL CULTURE MEDIA AND SOLUTIONS

OPC medium

DMEM (4.5 g glucose/l, Lonza, BioWhittaker)	500 ml
Glutamax-I (100x stock solution, Gibco)	5 ml
Penicillin/Streptomycin (Lonza)	5 ml
Fetal calf serum	50 ml

Neurobasal medium

Neurobasal (- Glutamine, Gibco)	100 ml
Glutamax-I (100x stock solution, Gibco)	1 ml
Penicillin/Streptomycin (Lonza)	1 ml
B27 supplement (50x stock solution, Gibco)	2 ml

HBSS

HBSS (Lonza, BioWhittaker)	99 ml
HEPES (500 mM, sterile filtered)	1 ml

DMEM low glucose

DMEM (1 g glucose/l, Lonza, BioWhittaker)	200 ml
Glutamax-I (100x stock solution, Gibco)	2 ml
Penicillin/Streptomycin (Lonza)	2 ml
B27 supplement (50x stock solution, Gibco)	4 ml
Fetal calf serum	25 ml

Sato medium

DMEM (SIGMA D-6546)	
Streptomycin/ Penicillin (Lonza)	5000 U/ml
L-Glutamine (SIGMA G-6392)	4 mM
Putrescine (SIGMA P-5780)	16 µg/ ml
L-Thyroxine (SIGMA T1775)	400 ng/ ml
Tri-iodothyroxine (SIGMA T-6397)	400 ng/ ml
Progesterone (SIGMA P-8783)	6.2 ng/ ml
Sodium Selenite (SIGMA S-5261)	5 ng/ ml
Bovine Serum Albumin Fraction V (SIGMA A-4919)	100 µg/ ml
Insulin (SIGMA I-0516)	5 µg/ ml
Holo-Transferrin human (SIGMA T-0665)	50 µg/ ml

The medium ist stable for 4 weeks at 4 °C.

Digestion mix

MEM (Invitrogen, 11095-080)	
DNAseI	0.1 mg/ ml
Papaine	1.58 mg/ ml
L-Cysteine	0.24 mg/ ml

7.1.8 ANTIBODIES

<u>Primary antibodies</u>

antibody	dilution and purpose	species	company
APP	1:750 (IHC)	mouse	Chemicon
BrdU	1:200 (IHC)	mouse	Chemicon
CD3	1:150 (IHC)	rat	Serotec
CNP	1:500 (WB)	mouse	SIGMA
Cox4-1	1:1000 (IHC) 1:2000 (WB)	rabbit	Mitoscience
GAPDH	1:200 (IHC) 1:1000 (WB)	mouse	ENZO BioMol
GFAP	1:200 (ICC) 1:200 (IHC)	mouse	Novocastra
GFP	1:1000 (IHC)	goat	Rockland
Mac3	1:400 (IHC)	mouse	Chemicon
MBP	1:200 (ICC)	mouse	Novocastra
NeuN	1:100 (ICC)	mouse	Chemicon
O4	1:50 (ICC)	mouse	Gift of J. Trotter, Mainz
Olig2	1:200 (IHC)	rabbit	Gift of J. Alberta, Harvard
PKM1	1:1000 (WB)	rabbit	Proteintech
PKM2	1:200 (IHC) 1:100 (ICC)	rabbit	SAB

	1:1000 (WB)		
p-PKM2	1:1000 (WB)	rabbit	Cell Signaling
S100ß	1:200 (IHC)	rabbit	Abcam
Tuj-1	1:200 (ICC)	rabbit	Covance
VDAC	1:2000 (WB)	rabbit	Rockland

Secondary antibodies

antibody	dilution	species	company
Alexa488-anti-mouse	1:2000	donkey	Molecular Probes
Alexa488-anti-rabbit	1:2000	donkey	Molecular Probes
Alexa555-anti-rabbit	1:2000	donkey	Molecular Probes

To colabel the nucleus DAPI was co-incubated with the secondary antibody at final a concentration of 0.025 µg/ ml.

7.1.9 OLIGONUCLEOTIDES

Oligonucleotides were synthesized by the service facility of the Max-Planck-Institute for Experimental Medicine.

7.1.9.1 Genotyping primer for used mouse lines

floxed *Cox10* mouse line (Diaz et al., 2005b)

5´- TGAGTAGAATGGCTTCCGGAAGGG -3´

5´- CACTGACGCAGCGCCAGCATCTT -3´

5´- AGCAGCAAAGAGGGCTCACTTCTTGC -3´

CNP1-cre driver mouse line (Lappe-Siefke et al., 2003)

5´- GCCTTCAAACTGTCCATCTC -3´

5´- CCCAGCCCTTTTATTACCAC -3´

5´- CATAGCCTGAAGAACGAGA -3´

PLP1-CreERT2 driver mouse line (Stahl et al., 1990)

5´- TGGACAGCTGGGACAAAGTAAGC -3´

5´- CGTTGCATCGACCGGTAATGCAGGC -3´

CamKinaseIIα-Cre driver mouse line (Minichiello et al., 1999)

5´- GGGAGGTAGGAAGAGCGATG -3´

5´- CCATGAGTGAACGAACCTGG -3´

GLAST-CreERT2 driver mouse line (Mori et al., 2006b)

5´- GAGGCACTTGGCTAGGCTCTGAGGA -3´

5´- GAGGAGATCCTGACCGATCAGTTGG -3´

5´- GGTGTACGGTCAGTAAATTGGACAT -3´

R26R-EYFP mouse line (Srinivas et al., 2001a)

5´- AAAGTCGCTCTGAGTTGTTAT -3´

5´- GCGAAGAGTTTGTCCTCAACC -3´

5´- GGAGCGGGAGAAATGGATATG -3´

7.1.9.2 Quantitative real-time PCR primer
<u>on genomic DNA:</u>

Cox10:   forward 5´- CGGGGATCAATTCGAGCTCGCC -3´

reverse 5´- CACTGACGCAGCGCCAGCATCTT -3´

Neuregulin 1 type III: forward 5´- GTGTGCGGAGAAGGAGAAAACT -3´

reverse 5´- AGGCACAGAGAGGAATTCATTTCTTA -3´

<u>on genomic DNA for quantitative PCR:</u>

Cox10:   forward 5´- CGGGGATCAATTCGAGCTCGCC -5´

reverse 5´- CACTGACGCAGCGCCAGCATCTT -3´

on mRNA for quantitative PCR:

PKM1:	forward 5´- GTTCTCACGGAGTCTGGCA -3´
	reverse 5´- TTCGAGTCACGGCAATGATAG -3´
PKM2:	forward 5´- TACCCTCTGGAGGCTGTTC -3´
	reverse 5´- TCTGCCTCTCGGGCAATCT -3´
PKM total:	forward 5´- CTGGGCTGAGGACGTTGAT -3´
	reverse 5´- TGACCACATCTCCCTTCTTGA -3´
Rpl13a:	forward 5´- ATCCCTCCACCCTATGACAA -3´
	reverse 5´- GCCCCAGGTAAGCAAACTT -3´
Rplp0:	forward 5´- GATGCCCAGGGAAGACAG -3´
	reverse 5´- CACAATGAAGCATTTTGGGTAG -3´

7.2 METHODS

7.2.1 ANIMALS

All animals used in experiments of this thesis were bred and kept in the mouse facility of the Max Planck Institute of Experimental Medicine. All experiments were performed in accordance with the guidelines for German animal welfare. Mice were sacrificed by cervical dislocation or by perfusion using anaesthetics. Animals were maintained on a C57/Bl6 genetic background. All tamoxifen-sensitive mutant and control mice were treated with tamoxifen or the vehicle only. Tamoxifen was dissolved in corn oil to obtain a 10 mg/ml solution. Mice were i.p. injected with a tamoxifen dosage of 100 mg/ kg body weight for 5 consecutive days or 2 weeks (except for the weekends) at P30.

7.2.2 MOLECULAR BIOLOGICAL METHODS

7.2.2.1 Genotyping of mice

0.5 cm long tail tips were taken from P21 young mice. They were digested overnight (o/n) in 400 µl Extraction buffer with 20 µl Proteinase K at 55°C under steady agitation. To extract the DNA 75 µl KAc and 400 µl chloroform were applied and mixed by inversion. To separate

the DNA containing aqueous phase from the chloroform, the sample was centrifuged at 700 x g for 10 min. 200 µl from the supernatant was removed, mixed with 400 µl EtOH for DNA precipitation, followed by a centrifugation step (at 700 x g for 10 min) to pelletise the DNA. The supernatant was carefully and completely removed and after the pellet had been air dried, the DNA was dissolved in 10 mM Tris buffer.

Polymerase chain reaction was used to amplify specific DNA segments (Mullis et al., 1986; Saiki et al., 1988). 1 µl of DNA samples were used per 20 µl PCR reaction. Primers were selected manually using the DNASTAR Lasergene 9 core suite.

For separation of PCR products gels containing 1.5% [w/v] agarose in 1x TAE buffer were used. For DNA visualization 1 µg/ml ethidiumbromide was added to the gel prior to polymerization. 20 µl of PCR samples were loaded and separated at 150V for 45 min in 1x TAE buffer. GeneRuler 100 bp DNA ladder or GeneRuler 1 kp DNA ladder (both Thermo Scientific, St. Leon-Rot, Germany) was used as a marker. For documentation pictures were acquired with the Intas UV system.

7.2.2.2 PCR on genomic DNA

30 µg of total cerebellar and brain purified genomic DNA was used in a PCR reaction to detect the recombined *Cox10* allele with 0.1 µM of following primers TGAGTAGAATGGCTTCCGGAAGGG and AGCAGCAAAGAGGGCTCACTTCTTGC generating a template of 465 bp.

7.2.2.3 Quantitative PCRs on genomic DNA

Sciatic nerves (epineurium was removed), optic nerves and brains were collected from P21 animals and DNA was isolated as usual. Quantitative PCR was performed using 10 ng of sciatic nerve DNA in a 12.5 µl assay using PowerSYBR Green PCR Master Mix (Applied Biosystems) on an Applied Biosystems 7500 Fast real time PCR system in triplicates. A standard curve was generated using DNA from $Cox10^{flox/flox}$, $Cox10^{flox/wt}$, and $Cox10^{wt/wt}$ animals. The values were standardized to an independent genomic marker to correct for small differences in the amount of DNA. Primers CGGGGATCAATTCGAGCTCGCC and CACTGACGCAGCGCCAGCATCTT amplify a 167 bp band specific for the $Cox10^{flox}$ allele. For genomic input control we used an intron-exon stretch of *Neuregulin 1 type III* were used. The percentage of recombination was calculated assuming that every Cre-expressing cell recombines both $Cox10^{flox}$ alleles. The values were shown as histograms using Adobe Illustrator CS3 and p-values were calculated using the Student's t-test of Microsoft Excel 2003. The levels of significance were set as * $p < 0.05$; ** $p < 0.01$; *** $p < 0.001$. Analysis was performed by Dr. Ursula Fünfschilling.

7.2.2.4 RNA isolation ('RNeasy mini prep')

RNA isolation from frozen (-80°C) half brain as well as separated cortex, optic nerve and cerebellum was performed using "Qiagen's RNeasy Mini Prep" kit. The kit is based on a selective binding of RNAs bigger than 200 bases to a silica-gel based membrane under high-salt conditions, which excludes binding of 5S, 5.8S and tRNAs. RNA isolation and purification was carried out following the manufacturer's instructions. Briefly, apart from optic nerves of adult rats that were homogenized in Trizol (Invitrogen, Karlsruhe, Germany) with the Precellys for 3 x 10 sec at 5500 rpm followed by addition of half volume of chloroform, inversion for mixture and an incubation step of 3 min. All other tissue were homogenized in RLT buffer (containing 1% (v/v) ß-Mercaptoethanol). Here, for half brains and cerebella the KINEMATICA AG POLYTRON PT 3000 (1 min at 14.000 rpm) and for the cortices and optic nerves of developing states the Precellys (2 x 10 sec at 5500 rpm) were used. The subsequent steps were for all tissues equally performed. After 15 min certification at 16000 x g (Heraeus Biofuge Pico table centrifuge, 13000 rpm) the upper aqueous phase was transferred to a new 2 ml Eppendorf tube. One volume of ethanol was added to the samples, mixed and applied to RNeasy columns. After 1 min centrifugation at 16000 x g the columns were washed one time with the RW1 buffer and two times with the RPE buffer. The RNA was eluted from the column by adding 20-40µl of RNase-free ddH$_2$O.

7.2.2.5 RNA measurement with Agilent

The quality and the amount of RNA were measured using the Agilent RNA 6000 Nano KIT and the Agilent 2100 Bioanalyzer following the company's instructions. Only RNA samples with a RNA integrity number above 8.5 were further used. The RNA concentration for all samples was adjusted to 100 ng/ µl.

7.2.2.6 cDNA synthesis

cDNA synthesis is based on the characteristic feature of eukaryotic messenger RNAs to harbor defined polyadenylated tail on the 3′ end. First-strand cDNA was mainly synthesized for quantitative RT-PCR. Total RNA is mixed with a random nonamer and oligo-dT primers. The amplification reaction is carried out by Superscript III reverse transcriptase (Kotewicz et al., 1985; Gerard et al., 1986) at 55ºC providing high specificity and yields of cDNA (from 100bp to >12kb). For the cDNA synthesis, 6 pmol of random primers, 0.03 pmol of oligo dT nucleotides were incubated with 400 ng - 1 µg total RNA for 10 min at 70°C and then cooled on ice for 2 min. 2 µl of 5X First-Strand Buffer, 1 µl of 0.1 M DTT, 1 µl of 10 mM dNTP and 1µl of SuperScript™ III RT (200 units/ µl) were added to the tubes. The reaction mixture was incubated in the thermocycler with the following settings: 25°C for 10 min, then 50°C for 45 min, 55°C for 45 min. The cDNA was then used as a template for amplification in PCR.

7.2.2.7 Quantitative real time PCR for mRNA expression

The quantification of amplified gene fragments relied on the usage of the fluorescent dye SYBR Green, which intercalates specifically in double stranded DNA. All reactions were carried out in quadruples. Data evaluation was performed with the 7500 Fast System SDS software Version 1.3 (Applied Biosystems) and Excel 2003. As endogenous gene controls *Rpl13a* and *Rplp0* were used for normalization. Values were further calculated to the P8 time-point of every brain region. The values were shown as histograms using Adobe Illustrator CS3 and p-values were calculated using the Student's t-test of Microsoft Excel 2003. The levels of significance were set as * $p < 0.05$; ** $p < 0.01$; *** $p < 0.001$.

7.2.3 PROTEIN BIOCHEMICAL ANALYSIS

7.2.3.1 Sample preparation

Collected tissue was quickly frozen on dry ice and stored at -80°C. Optic nerves, corpora callosa, cerebella and cortices were homogenized in Lysis buffer using the Tissue Lyser (Peqlab, Erlangen, Germany) at 50 Hz (2 min for optic nerves, for all other tissues 5 min) according to manufactor´s instructions. Half brains were homogenized with the KINEMATICA AG POLYTRON PT 3000 for 1 min at 14.000 rpm as well in Lysis buffer. Lysates were centrifuged for 15 min at 13000 rpm at 4°C. Supernatants were transferred into new tubes and stored at -80°C. Protein concentration was measured and samples were used for SDS Page.

7.2.3.2 Protein concentration measurement by the Lowry method

The Protein concentration was measured using the Bio-Rad DC Protein Assay kit according to the manufacturer's 'microplate assay' protocol. The working principle of the kit is similar to the well-documented Lowry assay (Lowry et al., 1951; Peterson, 1979). The optical density was measured at 650 nm in the microplate reader ThermoMax (Molecular Devices, Biberach, Germany). 10 µg protein of each sample were used for SDS-Page.

7.2.3.3 Separating Proteins using SDS Page

10% [w/v] acrylamid gels were prepared using the Bio-rad system. For this, SDS separating gel mix was casted between a 1.5 mm thick spacer plate and thin coverplates. It was overlaid with isopropanol and polymerized for at least 60 min. The stacking gel mix was added on top after removing the isopropanol. A Teflon comb (10 or 15 wells) was used to generate pockets for the protein samples. After polymerization gels were used immediately or were stored wet at 4°C, but not longer than a week. Proteins were separated using the protocol established by Laemmli (Laemmli, 1970). To denature the proteins, lysates were mixed with 1x SDS sample buffer and 5% [v/v] mercaptoethanol, and heated for 5 min at 95°C. Bio-rad

chambers were used to assemble the gels and filled with 1x Laemmli running buffer. Protein samples were carefully pipetted und were separated by constant current using the Bio-rad power supply (30 mA per gel). After about one and a half hour, gels were removed, incubated for 15 min in transfer buffer and proteins were transferred to a PVDF membrane (immunoblot).

7.2.3.4 Immunoblot

For immunodetection, proteins were transferred to a PVDF membrane as described by Towbin and colleagues (Towbin et al., 1979). Therefore, the wet chamber from Biorad Mini Trans-Blot Ceil was used. The PVDF membrane was activated using 100% [v/v] methanol for 1 min and kept then in transfer buffer. The nitrocellulose membrane, Whatman paper and blotting sponges, that had been pre-soaked in ice cold transfer buffer, were assembled in a Biorad adapter cassette according to manufactor´s instructions. Proteins were transferred at a constant voltage of 200 V and at maximum current of 350 mA for 1 h at 4 °C.

7.2.3.5 Immunodetection of blotted proteins

After the protein transfer, the PVDF membrane was blocked at room temperature (RT) for 1 hour in blocking buffer (usually 5% [w/v] non-fat dry milk in TBST, apart from phospho-antibodies that were blocked in 5% [w/v] BSA in TBST). Primary antibody was diluted in the same blocking buffer and incubated on the membrane o/n at 4°C. Afterwards, the membrane was washed three times in TBST and incubated with the HRP coupled secondary antibody, which was diluted in the blocking buffer, at RT for one hour. After additional washing with TBST (3x), the Enhanced Chemiluminescence Detection (ECL) solution was added according to the manufacturer's recommendations (Western Lightning™, Western Blot Chemiluminescence Reagent Plus, PerkinElmer Life Sciences, Inc., Rodgau, Germany). As protein loading control all membranes were incubated with GAPDH as a standard afterwards. The densitometric analysis of immunoblots was performed using gele analysis of ImageJ. The integrated density or mean grey values for the band of interest was calculated and normalized to the integrated density or mean grey values of GAPDH. The normalized values were shown as histograms using Adobe Illustrator CS3 and p-values were calculated using the Student's t-test of Microsoft Excel 2003. The levels of significance were set as * $p < 0.05$; ** $p < 0.01$; *** $p < 0.001$.

7.2.4 PERFUSION AND FIXATION OF MOUSE TISSUE

Mice were deeply anesthetized by intraperitoneal injection of avertin (0.2 ml per 10 g of body weight). The abdomen was opened and the diaphragm was removed to expose the heart. A butterfly cannula (27G, Venofix) connected to a peristaltic pump was inserted into the left

ventricle, while the right atrium was cut, generating a small opening. The blood was flashed out with HBSS (Invitrogen, Karlsruhe, Germany) until the vessels were cleared. Afterwards ice-cold fixative was used to fix the tissue. Depending on further processing different fixatives were used. All used mice were regenotyped using a tail biopsy.

7.2.5 HISTOLOGY

7.2.5.1 Tissue processing using paraffin wax

Mice were perfused with 4% [v/v] PFA and post-fixed in the same fixative o/n at 4°C. For thin sectioning, brains were embedded in wax (Paraplast, Leica, Wetzlar, Germany) using an automated system (HMP 110, MICROM) with the following program: 50% EtOH for 1 hour, twice in 70% EtOH for 2 hours each, twice in 96% EtOH for 2 hour each and twice in 100% EtOH for 2 hour each, at RT. 100% EtOH was replaced by isopropanol for 1 hour and then incubated twice in Xylene for 2 hours each. Finally brains were impregnated two times with paraplast at 60ºC for 2 hours each. Afterwards, the tissue was placed in metal forms and casted in blocks with 60°C warm wax. Blocks were removed from the molds and can now be stored stably and for years on a dry place at RT.

For further use, the tissue was cut in 5 μm thick paraffin wax sections using a microtome (HM 400, MICROM) and dried at 37°C o/n. Sections were deparaffinized by the following steps: 60°C 10 min, Xylol 2 x 10 min, Xylol/ Isopropanol (1:1) 10 min, 100% [v/v] EtOH 5 min, 90% [v/v] EtOH 5 min, 70% [v/v] EtOH 5 min, 50% [v/v] EtOH 5 min and ddH$_2$O 5 min.

7.2.5.2 Gallyas silver impregnation

Deparaffinized 5 μm brain sections were used to visualize myelin. The technique developed by Gallyas based on binding of colloidal silver particles to myelinated fibers (Gallyas, 1979). First, in order to avoid labelling of other tissue than myelin, the sections were incubated with a 2:1 mixture of pyridine and acetic anhydride for 30 min at RT. Then, tissue was washed with ddH$_2$0 three times 10 min each, incubated in pre-warmed incubation solution for 10 min and washed with 0.5% [v/v] acetic acid three times for 5 min each. Afterwards, sections were incubated in the developer solution for 5–10 min. The extent of silver ion deposition in the developing step was controlled under the microscope and the reaction was stopped by washing in 1.0% [v/v] acetic acid. After additional washing with ddH$_2$O, silver staining was stabilized by incubation with 2% [v/v] sodium thiosulfate solution for 5 min. Tissue was dehydrated by an alcohol gradient (50% [v/v], 70% [v/v], 90% [v/v], and 100% [v/v] for 5 min each), incubated with Xylol/Isopropanol (1:1, 5 min) followed by two times Xylol (5 min) and finally mounted using Eukitt.

7.2.5.3 Detection of apoptotic cells using TUNEL staining

To check for apoptosis, we applied DeadEnd™Colorimetric TUNEL System (Promega) to paraffin-embedded sections (Naruse and Keino, 1995) according to manufactor´s instructions. This method relies on the ability of TdT to label blunt ends of double-stranded DNA breaks and thus the detection of extensive DNA degradation during the late stages of apoptosis. Briefly, after deparaffination and rehydration the sections were washed at first in 0.85% NaCl for 5 min and then for 5 min in 0.1 M PBS, followed by fixation with 4% PFA for 15 min, washing in 1x PBS (twice 5min), permeabilization with 20 µg/ ml Proteinase K in 1x PBS for 10 min and subsequent washing in 1x PBS for 5 min. Then the slides were refixed in 4% PFA for 5 min, washed in PBS (twice 5 min) and equilibrated in Equilibration buffer at RT for 10 min. TdT reaction solution was applied and slides were incubated for 60 min at 37ºC in a humidified chamber. The TdT reaction was stopped by immersion in 2x SSC solution for 15 min, followed by washing in PBS (3x 5min). After blocking in 0.3% hydrogen peroxide for 5 min the slides were washed in PBS (3x 5min) again. Sections were incubated with Streptavidin-HRP (diluted 1:500 in PBS) for 30 min and then washed 3 times in PBS. DAB solution was prepared freshly and applied to the sections for approximately 10 min until there was a light brown background. The slides were rinsed with ddH$_2$O before they were counterstained with Haematoxylin to label nuclei. Therefore they were incubated in 0.1% [w/v] Haematoxylin for 5 min. Blue coloration appears due to the interaction with the basic nuclear compartment. Sections were rinsed with ddH$_2$O, incubated with HCl-Alcohol for 5–10 sec and with Scott's solution for 5 min. This was followed by two rinse with ddH$_2$O. Tissue was dehydrated by an alcohol gradient (50% [w/v], 70% [w/v], 90% [w/v], and 100% [w/v] for 5 min each), incubated with Xylol/ Isopropanol (1:1, 5 min) followed by two times Xylol (5 min) and mounted using Eukitt.

7.2.5.4 Immunohistochemistry of paraffin embedded tissue

5 µm thin sections were deparaffinized and dehydrated and then incubated in citrate buffer for 5 min, followed by a cooking step of 10 min in boiling citrate buffer to permeabilize the tissue (650 watts in microwave oven). After cooling for at least 20 min at RT, sections were rinsed with Tris buffer containing 2% [w/v] milk powder for 5 min. Glass slides were placed into Shandon coverplates (Thermo Scientific, Cheshire, UK) for equal distribution of solutions and rinsed again with Tris buffer containing 2% milk powder. Horse radish peroxidase (HRP) coupled secondary antibodies were used. Therefore, it was necessary to suppress the endogenous peroxidase activity by applying 3% [v/v] hydrogen peroxide for 5 min. After additional washing with Tris buffer containing 2% [w/v] milk powder, slides were incubated in the blocking solution (20% [v/v] goat serum in BSA/PBS) for 30 min at RT. Primary antibodies were diluted in BSA/PBS and incubated o/n at 4°C. Subsequently, slides were washed with Tris buffer containing 2% [w/v] milk powder. For primary antibodies mono

mouse or polyclonal rabbit the LSAB$_2$ kit (Dako, Hamburg, Germany) and for primary antibodies monoclonal rat the Vector Elite ABC Kit (Vector Labs, Loerrach, Germany) was used according to manufactor´s instructions. Then, the coverplates were removed and sections were rinsed with Tris buffer without milk-powder. The HRP substrate 3,3' -Diaminobenzidine (DAB) was applied by using the DAB Zytomed Kit (Zytomed Systems GmbH, Berlin, Germany) and incubated for 10 min. After additional washing with ddH$_2$O, sections were incubated in 0.1% [w/v] Haematoxylin for 5 min to label nuclei. Sections were rinsed with ddH$_2$O, incubated with HCl-Alcohol for 5–10 sec and with Scott's solution for 5 min. This was followed by two rinses with ddH$_2$O. Tissue was dehydrated by an alcohol gradient (50% [w/v], 70% [w/v], 90% [w/v], and 100% [w/v] for 5 min each), incubated with Xylol/Isopropanol (1:1, 5 min) followed by two times Xylol (5 min) and mounted using Eukitt.

7.2.5.5 Imaging and quantification of DAB developed stainings

Tissue was imaged using the Zeiss Axio Z1 and processed with the Zen 2011 software (Zeiss, Oberkochern, Germany). The quantification of positive signal was done with ImageJ. For GFAP the positive area was measured. Therefore, an ImageJ plugin written by Sven Wichert was used. Briefly, the color threshold was transformed to a black and white picture, whereby brown DAB staining as positive black signal appeared. Then the area of the positive black signal was measured and related to the size of the analyzed area. For CD3, Mac3 and APP the Cell Counter plugin of ImageJ was used in order to determine the number of positive cells. The values were shown as histograms using Adobe Illustrator CS3 and p-values were calculated using the Student's t-test of Microsoft Excel 2003.

7.2.5.6 Fluorescent immunodetection on paraffin sections

5 μm thin sections were deparaffinized and dehydrated and then incubated in citrate buffer for 5 min, followed by a cooking step of 10 min in boiling citrate buffer to permeabilize the tissue (650 watts in microwave oven). After cooling for at least 20 min at RT, the sections were rinsed 3 x 5 min in Tris buffer containing 2% milk powder. To minimize the unspecific binding of the antibody and to reduce the background staining the blocking of free sites on sections were carried out by incubating them with goat serum diluted in PBS/BSA (1:5) for 20 min at RT, followed by the incubation with the primary antibody diluted in its appropriate dilution in PBS/BSA o/n at 4°C. Sections were washed 3 x 5 min in Tris buffer containing 2% milk powder. To visualize the site of binding of primary antibodies, sections were incubated with the fluorescently labeled antibodies diluted in PBS/BSA, for about 1 hour at RT. Counterstaining was carried out with DAPI (0.5 μg/ ml final conc.) and was applied together with the secondary antibody. Finally sections were washed 3 x 5 min in Tris buffer without milk powder and were mounted in water based mounting medium such as Aquapoly mount.

The Cell Counter plugin of ImageJ was used in order to determine the number of labelled cells and values were shown as histograms using Adobe Illustrator CS3.

7.2.5.7 Detection of proliferating cells (BrdU staining)

For detection of proliferating cells in vivo BrdU (5-bromo-2'-deoxyuridine) was provided to mice. This is a nucleoside analog that is incorporated into newly synthesized cells during replication and can be detected by specific antibodies. BrdU (Sigma, Germany) was dissolved in 0.9% NaCl and sterile filtered. 16 week old mice received daily intraperitoneal (i.p.) injections of 100 mg/kg body weight (5 days per week) for 4 weeks and were subsequently perfused with 4% (v/v) PFA. Immediately after immunohistochemistry to colabel dividing cells (see protocol for 'Fluorescent immunodetection on paraffin sections'), BrdU was visualized using an antibody specifically directed against BrdU. Sections were kept in dark from now on. First, sections were incubated in 0.2 M Glycine for 30 min, followed by 2 x 5 min washing steps in 1x PBS and the incubation in 2 M HCl at 37°C for 30 min to break open the DNA structure. After rinsing them 2x 5 min in 100 mM Di-Natiumtetraborat (pH 8,5), the sections were washed 3x 5 min in 1x PBS and blocked with 1x PBS containing 10% goat serum for 30 min at RT. Then the tissue was incubated with anti-BrdU (Bioscience) diluted in 2% goat serum in 1x PBS o/n at 4°C followed by 30 min at RT. Sections were washed 3x 5 min in 1x PBS and the secondary antibody was applied in its recommend dilution in 1x PBS containing 2% goat serum and DAPI (0.5 µg/ ml final conc.) for 1 h at RT. After additional wasing in 1x PBS (3x 5 min), the sections were mounted in Aquapoly mount. The Cell Counter plugin of ImageJ was used in order to determine the number of positive cells. The values were shown as histograms using Adobe Illustrator CS3 and p-values were calculated using the Student's t-test of Microsoft Excel 2003.

7.2.5.8 Detection of proliferating cells (EdU staining)

For detection of dividing cells in vivo, EdU (5-ethynyl-2'-deoxyuridine, Invitrogen) was provided to P80 mice in the drinking water at the concentration of 0.2 mg/ml, which was shown to be nontoxic (Young et al., 2013). The water was exchanged every 2 days and mice were exposed to EdU for 14 days in total. EdU is a nucleoside analog for thymidine that incorporates into the DNA of proliferating cells. This method based on click chemistry that relies on covalently coupling an azide with an alkyne. Due to the small size of click detection reagent, no harsh treatment of tissue is required. EdU was visualized using the AlexaFluor-555 Click-iT EdU Cell Proliferation Assay Kit (Molecular Probes, Invitrogen) according to manufactor´s instructions immediately after immunohistochemistry (see protocol for 'Fluorescent immunodetection on paraffin sections'). Paraffin sections were incubated at RT for 60 min in 1x PBS containing 0.5% (v/v) Triton X-100 and 3% horse serum, followed by 2 blocking steps in 3% horse serum diluted in 1x PBS for 10 min at RT each. Then the sections

were transferred to the EdU developing cocktail, incubated in the dark at RT for 45 min, and blocked again 3 times in 3% horse serum in 1x PBS for 10 min each. Cell nuclei were visualized by poststaining with DAPI (0.5 µg/ ml final conc.) and sections were mounted in water based mounting medium (Aquapoly mount). The Cell Counter plugin of ImageJ was used in order to determine the number of labelled cells. The values were shown as histograms using Adobe Illustrator CS3 and p-values were calculated using the Student's t test of Microsoft Excel 2003.

7.2.5.9 Immunohistochemistry of vibratome sections

Mice were perfused with 4% [v/v] PFA, the brain was cut sagittally between the two hemispheres with a razor blade and post-fixed o/n at 4°C. Sagittal sections (25- 30 µm) were sliced using the Leica VT1000S vibratome (Bensheim, Germany), collected in 1x PBS and stored at 4°C till proceeding with fluorescent immunodetection. Therefore sections were incubated in 0.2 % (v/v) Triton X-100 and 10% horse serum in a 24 wells plate. The primary antibody was prepared according to its appropriate dilution in the same solution and was incubated o/n at 4°C. After washing 3x 5 min in 1x PBS the fluorescently labeled antibody was applied in its recommend dilution together wit DAPI (0.5 µg/ ml final conc.) in 2% horse serum in 1x PBS for 1 h at RT, followed by 3 washing steps in 1x PBS for 5 min each. Finally, the sections were mounted in Aquapoly mount. The Cell Counter plugin of ImageJ was used in order to determine the number of positive cells. The values were shown as histograms using Adobe Illustrator CS3 and p-values were calculated using the Student's t-test of Microsoft Excel 2003.

7.2.5.10 Immunohistochemistry of cryosections

Mice were perfused using 4% [v/v] PFA. After fixation, brains and optic nerves were transferred to 10% [w/v] sucrose in 0.1 M phosphate buffer. After 12 hours at 4°C, tissue was first transferred to 20% [w/v] sucrose and then to 30% [w/v] sucrose in 0.1 M phosphate buffer, each o/n at 4°C. Following this cryo-protective step, brains and optic nerves were frozen on dry ice and stored at -80°C. A cryostat (Leica, Wetzlar, Germany) was used to generate 20 µM thick longitudinal or coronar sections of stabilized tissue, which were collected on glass slides, dried at RT and stored at -20°C. For immunofluorescent stainings, tissue was permeabilized and blocked with 0.5% (v/v) Triton X-100 and 10% horse serum in 1x PBS for 1 hour. The primary antibodies were diluted in the same buffer and incubated at 4°C for 40 hours. Afterwards, slides were washed three times for 10 min with 1x PBS and incubated for two hours with the secondary antibodies and DAPI (0.5µg/ ml final conc.) diluted in 0.5% (v/v) Triton X-100 and 10% horse serum in 1x PBS at RT. Tissue was washed 3x 5 min in 1x PBS and mounted using Aquapoly mount.

7.2.5.11 SDH/ COX histochemistry

Mice were perfused with 4% PFA and collected brains were cryoprotected with a descending gradient of sucrose of 10%, 20% and 30% sucrose diluted in 1 x PBS each overnight. 8-mm thick sections were cut using a cryostat and air-dried for 30 min. Sections were exposed to COX medium containing 500 mM cytochrome c, 5 mM diaminobenzidine tetrahydrochloride and 20 mg/ ml catalase at 37 °C for 40 min. Sections were washed three times with 1x PBS and a subsequent incubation with SDH medium containing 130 mM sodium succinate, 200 mM phenazine methosulphate, 1 mM sodium azide, 1.5 mM nitroblue tetrazolium in 0.1M phosphate buffer (pH 7.0) for 30 min at 37 °C. After dual SDH/ COX histochemistry normal immunohistochemistry was performed to identify *Cox10*-deficient oligodendrocytes. Performance and image acquisition were done by Dr. Don Mahad and Graham Campbell.

7.2.6 ELECTRON MICROSCOPY

7.2.6.1 Tissue preparation

Mice were perfused with Karlsson-Schultz fixative (Schultz and Karlsson, 1965), optic nerves, sciatic nerves and cerebella were removed and kept in the same solution for at least 12 h at 4°C. Post-fixed cerebella were cut sagittally into 300 μm thick sections using a vibratome (Leica, VT1000S) and the lobe 3 were punched out before Epon embedding.

7.2.6.2 Epon embedding

Tissues were embedded in Epon using an automated system (EMTP, Leica, Wetzlar, Germany). Steps included osmification, dehydration and Epon impregnation. Briefly, samples were incubated in phosphate buffer 3x for 10 min at 4ºC, followed by 2% [w/v] OsO_4 for 4 hours at 4ºC, 3x ddH_2O 3 for 10 min at 4ºC. Then the samples were treated with an ascending alcohol gradient at 4°C, which included 30% [v/v] EtOH for 20 min, 50% [v/v] EtOH for 20 min, 70% [v/v] EtOH for 20 min, 90% [v/v] EtOH for 20 min and 100% [v/v] EtOH 4x for 10 min. Subsequently, samples were Epon embedded at RT and were incubated with Propylenoxid 3x for 10 min, Propylenoxid/Epon 2:1 for 2 hours, Propylenoxid/Epon 1:1 for 2 hours, Propylenoxid/Epon 1:2 for 4 hours and finally Epon for 4 hours. Tissue was then placed into the Epon filled molds and left o/n at 60ºC for Epon polymerization.

7.2.6.3 Sectioning of Epon embedded samples

Semithin (300 nm) and ultracut sections (50 nm) were cut with a diamond knife (Diatome Ultra 45º) using an Ultramicrotome (Leica, Vienna, Austria) and were collected on a double sized slot grid (2mm-1mm, AGAR scientific, Essex, UK) coated with formvar polyvinyl and contrasted.

7.2.6.4 Staining and analysis of semithin sections

300 nm thin sciatic nerve sections were labeled using the Methylene blue- Azure II stain (Richardson et al., 1960). Sections were dried for 1 min on a 60°C hot plate and then extensively rinsed with ddH$_2$O. After drying, tissue was mounted using Eukitt and imaged with the Zeiss Axio Z1 (Zeiss, Oberkochern, Germany). Schwann cell nuclei were counted using ImageJ and the entire cross sectional area of sciatic nerves was scored. Analysis was performed by Dr. Ursula Fünfschilling.

7.2.6.5 Contrasting of ultra-thin sections

Grids were placed upside-down on drops of the following solutions at RT: 30 min uranyl acetate, 3x 1 min ddH$_2$O, 6 min lead citrate according to Reynolds et al. (1963) and 4x 1 min ddH$_2$O. Grids were carefully dried with a stripe of filter paper.

7.2.6.6 Analysis of EM pictures

Ultrathin sections were analyzed with the Zeiss EM900 (Zeiss, Oberkochen, Germany) and digital pictures were obtained using the wide-angle dual speed 2K-CCD-Camera (TRS, Moorenweis, Germany). Counting of myelinated axons of the sciatic nerve on electron microscopic pictures, all axons in three random fields (5500 µm^2 total) per nerve were traced using ImageJ. Parallel fiber-Purkinje cell synapses were counted using ImageJ and divided by the respective image area. The resulting synapse density was averaged per genotype. The area of Bergmann glial processes was analyzed with the point-hit method (Rabouille et al., 1999) using ImageJ and a grid area of 2.49 µm^2. Bergmann glial processes were identified by their irregular shape and characteristic bundles of intermediate filaments in a comparatively clear cytoplasm (Rubio and Soto, 2001). The values were shown as histograms using Adobe Illustrator CS3 and p-values were calculated using the Student's t test of Microsoft Excel 2003. The levels of significance were set as * $p < 0.05$; ** $p < 0.01$; *** $p < 0.001$. The calculation of the myelinating axon number of sciatic nerves was performed by Dr. Ursula Fünfschilling.

7.2.7 CELL BIOLOGY METHODS

7.2.7.1 Preparation of coverslips

Prior to coating glass coverslips needs to be roughen. This was done by incubating them in 65% HNO$_3$ for 1- 2 h under rotating agitation, followed by several washing steps (5x in dd H$_2$O, 3x in 70% EtOH) and o/n drying at 60°C. Before use coverslips were sterilized by UV light exposure for 10 min.

7.2.7.2 Coating with poly-L-lysin

To enable adherence of primary cells by their negatively charged polysaccharid structures to plastic (flasks) and glass surfaces (coverslips), coating with poly-L-lysin (PLL), which is positively charged, was necessary. 0.1 mg/ ml PLL were diluted in ddH$_2$O for flasks and in boric acid buffer (pH 8.5) for coverslips and incubated for at least 60 min at 37°C, then washed twice with sterile water and air-dried.

7.2.7.3 Preparation of primary rat oligodendrocytes

Protocol was adapted from Eyermann et al., 2012. Briefly, a litter of P2 rats were decapitated. After opening the scull, sagittal brain halves without cerebellum and bulbi were placed in a petridish containing MEM medium. Under a binocular the midbrain, hippocampus and meninges were carefully removed and the cerebra were collected in a 15 ml falcon tube filled with 1 ml MEM at RT. The digestion mix was freshly prepared in 5ml plastic bijoux tube. In order to activate the papaine the digestion solution was preincubated at 37°C, 7.5 % CO$_2$ for 5 min. All further steps were performed under a cell culture hood. The mix was applied to the cerebra by pressing through a filter for sterilization. Then the tissue was homogenized by pipetting up and down several times and put in a cell culture incubator (40–60 min depending on number of cerebra) at 37°C and 7.5 % CO$_2$ for digestion. The digestion was stopped by adding 10 ml OPC medium and subsequent inverting. The cell solution was centrifuged at 1200 rpm for 15–20 min. The supernatant was removed using a glass pipette and fresh OPC medium was added. Each flask was filled with 10 ml already prewarmed and equilibrated OPC medium and 2 ml of the cell suspension was added (2 cerebra per flask). Mixed glial cultures were cultivated at 37°C and 7.5 % CO$_2$ for 10–14 days. Every 2–3 days half of the medium was exchanged. Usually within one week an astrocyte layer was formed with oligodendrocyte precursor cells (OPCs) growing on top of it. Prior to OPC harvest, microglial cells were removed by harsh manual shaking. Afterwards, the OPC medium was replaced by fresh OPC medium and OPCs were enriched in the supernatant by manual shaking (approximately 30 times). The remaining astrocytes were taken for primary astrocytes cultures. The OPCs were pelleted by centrifugation (at 1200 rpm for 20 min) and counted using a Neubauer chamber. Usually, 10000–20000 cells were plated on coverslips in a 24-well format previously coated with PLL (0.1 mg/ ml) in Sato medium for differentiation and further cultivated at 37°C and 7.5 % CO$_2$. Every 2 days a half Sato media change was performed. Within five to six days of culturing *in vitro* most oligodendrocytes had differentiated into a myelin basic protein (MBP)-positive state.

7.2.7.4 Preparation of primary rat astrocytes

For astrocyte cultures the astrocyte layer from the preparation of primary oligodendrocytes were used. First, to get rid of remaining OPCs and microglia the flaks were shaken o/n at

400 rpm and 37°C using the innova 4000 shaker (New Brunswick Scientific). The flasks were washed with OPC media to remove all detached OPCs. In order to loose astrocytes 1x Trypsin containing EDTA was applied and incubated under gentle agitation for 3–5 min at RT. The supernatant was collected and the trypsination was stopped by adding OPC medium containing 10% serum. After centrifugation at 1200 rpm for 15 min, the cell number was calculated using the Neubauer chamber and cells were plated on coverslips in a density of usually 10000–20000 per well in a 24-well format previously coated with PLL (0.1 mg/ ml). Astrocytic cultures were maintained in DMEM containing 10% [v/v] heat-inactivated fetal bovine serum, 1% [v/v] glutamine and 1% [v/v] penicillin/ streptomycin at 37°C and 5% CO_2.

7.2.7.5 Preparation of primary rat cortical neurons

Method based on routine practices for culturing neurons (Meberg and Miller, 2003). Briefly, embryos on embryonal day (E) 17 were dissected, decapitated and stored in HBSS+. Meninges and hippocampi from 2–3 brains were carefully removed and cortices were isolated under a binocular. The tissue was transferred into 15 ml falcons containing HBSS+. After washing 2x with HBSS, the cortices were digested with 2.5 % Trypsin in HBSS for 20 min at 37°C under gentle agitation. Then the medium (as much as possible) was removed and the trypsination was stopped by adding DMEM medium containing 10 % FCS, followed by an incubation step with DNAse (2 % in DMEM) for 5 min at RT and 3 washing steps with DMEM medium. Afterwards the supernatant was removed and 2 ml fresh DMEM was applied. Then the tissue was titruated by performing a liquid stream using a firepolished pasteur pipette und the supernatant (cell solution) was let flow through a cell strainer into a 50 ml falcon tube. The cell strainer was washed with additional 2 ml DMEM. The cell number was determined using a Neubauer chamber. Usually, 10000–20000 cells were plated on coverslips per well in a 24-well format previously coated with PLL (0.1 mg/ ml) in DMEM medium. Cells were cultivated at 37°C and 5% CO_2. The next day the entire media was exchanged to Neurobasal medium and from there on every 3–4 days a half medium change was performed. To obtain pure neuronal cultures AraC was added (to a final concentration of 5 µM) at DIV4 and DIV8 to kill postmitotic glial cells. Usually, neuronal cultures were used for experiments at 10 DIV.

7.2.7.6 Rotenone treatment

Rotenone treatments were induced at astrocyte DIV 25 and neuron DIV 10. The duration of all experiments was 24 h. Fresh rotenone powder (Sigma) was diluted in dimethyl suloxide (DMSO) to a 10 mM dilution. The final rotenone concentrations used in each experiment are indicated in the figures.

7.2.7.7 Trypan blue exclusion

Cells were cultured as stated above and treated in the presence or absence of rotenone. Subsequently, they were harvested by light trypsinization and suspended in a defined medium volume. Cells were incubated in 0.2% [v/v] trypan blue solution and the number of trypan blue negative cells was counted using a hemocytometer to determine viable cells per coverslip (Ø 13 mm, 132.7 µm^2).

7.2.7.8 Immunocytochemistry

Cells were washed with 1x PBS (pH 7.4) and fixed with 4% [v/v] paraformaldehyde at 37°C. Cells were washed 3 times in 1x PBS and permeabilized with 0.2% [v/v] Triton X-100, 10% [v/v] horse serum in 1x PBS for 1 h at RT. Primary antibodies were incubated o/n at 4°C in the same solution. Secondary antibodies were incubated in 2 % horse serum or PBS/ BSA for 1 h at RT. For nuclei labelling DAPI (0.025 µg/ ml final concentration) was added to the secondary antibody. Sections were mounted using Aqua-Polymount (Eppelheim).

7.2.8 ELECTROPHYSIOLOGY

7.2.8.1 Nerve conduction velocity measurements

Mice were anesthetized with Xylacin and Ketamin intraperitoneally. Two recording electrodes were inserted into the intrinsic foot muscle. Distal stimulation electrodes were inserted at the ankle and the proximal stimulation electrodes were inserted at the sciatic notch. Compound muscle action potentials (CMAPs) were recorded with a Jaeger-Toennies Neuroscreen (Würzburg, Germany) instrument. Nerve conduction velocities were calculated from the distance between proximal and distal stimulation electrodes and the latency difference between the CMAPs after successive proximal and distal stimulation. CMAP amplitudes were calculated peak to peak. Analysis was performed by Dr. Bastian Brinkmann.

7.2.9 MAGNETIC RESONANCE SPECTROSCOPY

MRI/MRS was performed on *CNP1$^{Cre/+}$ * Cox10$^{flox/flox}$* mice and *CNP1$^{Cre/+}$ * Cox10$^{flox/+}$* mice as controls at the age of 4 to 5 (n = 6/6) and 6 to 7 months (n = 7/7). Mice were initially anesthetized with 5% isoflurane, subsequently intubated and kept under anesthesia with 1.75% isoflurane in ambient air. In 4 mice additional spectra were obtained without anesthesia. In these mice, pancuronium (15 mg/kg) was administrated 15 min before switching off the isoflurane supply to avoid movement artifacts.

In vivo localized proton MRS (STEAM, TR/TE/TM = 6000/10/10 ms) in different regions of the brain (cortex: 3.9 x 0.7 x 3.2 mm^3, NA = 160; corpus callosum: 2.5 x 1.0 x 2.0 mm^3,

NA = 160; striatum: 1.2 x 1.4 x 2.0 mm^3, NA = 160; cerebrum: 4 x 3 x 4 mm^3, NA = 32) was performed at 9.4 T (Bruker Biospin GmbH, Germany). For a proper positioning of the volumes of interest T2-weighted images (2D FSE, TR/TE = 4200/43 ms, 8 echoes, resolution 100 x 100 µm^2, slice thickness 300 µm) were obtained in axial and horizontal orientation. Metabolite quantification involved spectral evaluation by LCModel (Provincher, 1993) and calibration with brain water concentration. Metabolites with Cramer-Rao lower bonds above 20% were excluded from further analyses unless noted otherwise. Analysis was performed by Prof. Susann Boretius and Prof. Jens Frahm.

8 REFERENCES

Aeberhard, E., and Menkes, J.H., 1968, Biosynthesis of long chain fatty acids by subcellular particles of mature brain: The Journal of Biological Chemistry, v. 243, p. 3834–3840.

Aggarwal, S., Yurlova, L., and Simons, M., 2011, Central nervous system myelin: structure, synthesis and assembly: Trends in Cell Biology, v. 21, p. 585–593, doi: 10.1016/j.tcb.2011.06.004.

Altenberg, B., and Greulich, K.O., 2004, Genes of glycolysis are ubiquitously overexpressed in 24 cancer classes: Genomics, v. 84, p. 1014–1020, doi: 10.1016/j.ygeno.2004.08.010.

Anastasiou, D., Poulogiannis, G., Asara, J.M., Boxer, M.B., Jiang, J., Shen, M., Bellinger, G., Sasaki, A.T., Locasale, J.W., Auld, D.S., Thomas, C.J., Vander Heiden, M.G., and Cantley, L.C., 2011, Inhibition of pyruvate kinase M2 by reactive oxygen species contributes to cellular antioxidant responses: Science (New York, N.Y.), v. 334, p. 1278–1283, doi: 10.1126/science.1211485.

Antonicka, H., Leary, S.C., Guercin, G.-H., Agar, J.N., Horvath, R., Kennaway, N.G., Harding, C.O., Jaksch, M., and Shoubridge, E.A., 2003, Mutations in COX10 result in a defect in mitochondrial heme A biosynthesis and account for multiple, early-onset clinical phenotypes associated with isolated COX deficiency: Human Molecular Genetics, v. 12, p. 2693–2702, doi: 10.1093/hmg/ddg284.

Araque, A., Carmignoto, G., Haydon, P.G., Oliet, S.H.R., Robitaille, R., and Volterra, A., 2014, Gliotransmitters travel in time and space: Neuron, v. 81, p. 728–739, doi: 10.1016/j.neuron.2014.02.007.

Attwell, D., Buchan, A.M., Charpak, S., Lauritzen, M., Macvicar, B.A., and Newman, E.A., 2010, Glial and neuronal control of brain blood flow: Nature, v. 468, p. 232–243, doi: 10.1038/nature09613.

Bak, L.K., Schousboe, A., and Waagepetersen, H.S., 2006, The glutamate/GABA-glutamine cycle: aspects of transport, neurotransmitter homeostasis and ammonia transfer: Journal of Neurochemistry, v. 98, p. 641–653, doi: 10.1111/j.1471-4159.2006.03913.x.

Baquer, N.Z., Hothersall, J.S., and McLean, P., 1988, Function and regulation of the pentose phosphate pathway in brain: Current Topics in Cellular Regulation, v. 29, p. 265–289.

Baquer, N.Z., Hothersall, J.S., McLean, P., and Greenbaum, A.L., 1977, Aspects of carbohydrate metabolism in developing brain: Developmental Medicine and Child Neurology, v. 19, p. 81–104.

Baumann, N., and Pham-Dinh, D., 2001, Biology of oligodendrocyte and myelin in the mammalian central nervous system: Physiological Reviews, v. 81, p. 871–927.

Beattie, D.S., Basford, R.E., and Koritz, S.B., 1967, The turnover of the protein components of mitochondria from rat liver, kidney, and brain: The Journal of Biological Chemistry, v. 242, p. 4584–4586.

Bélanger, M., Allaman, I., and Magistretti, P.J., 2011, Brain energy metabolism: focus on astrocyte-neuron metabolic cooperation: Cell Metabolism, v. 14, p. 724–738, doi: 10.1016/j.cmet.2011.08.016.

Black, J.A., and Waxman, S.G., 1988, The perinodal astrocyte: Glia, v. 1, p. 169–183, doi: 10.1002/glia.440010302.

Bluemlein, K., Grüning, N.-M., Feichtinger, R.G., Lehrach, H., Kofler, B., and Ralser, M., 2011, No evidence for a shift in pyruvate kinase PKM1 to PKM2 expression during tumorigenesis: Oncotarget, v. 2, p. 393–400.

Boumezbeur, F., Petersen, K.F., Cline, G.W., Mason, G.F., Behar, K.L., Shulman, G.I., and Rothman, D.L., 2010, The contribution of blood lactate to brain energy metabolism in humans measured by dynamic 13C nuclear magnetic resonance spectroscopy: The Journal of Neuroscience: The Official Journal of the Society for Neuroscience, v. 30, p. 13983–13991, doi: 10.1523/JNEUROSCI.2040-10.2010.

Bouzier-Sore, A.-K., Voisin, P., Bouchaud, V., Bezancon, E., Franconi, J.-M., and Pellerin, L., 2006, Competition between glucose and lactate as oxidative energy substrates in both neurons and astrocytes: a comparative NMR study: The European Journal of Neuroscience, v. 24, p. 1687–1694, doi: 10.1111/j.1460-9568.2006.05056.x.

Brady, S.T., and Lasek, R.J., 1981, Nerve-specific enolase and creatine phosphokinase in axonal transport: soluble proteins and the axoplasmic matrix: Cell, v. 23, p. 515–523.

Brown, A.M., 2004, Brain glycogen re-awakened: Journal of Neurochemistry, v. 89, p. 537–552, doi: 10.1111/j.1471-4159.2004.02421.x.

Brown, A.M., Sickmann, H.M., Fosgerau, K., Lund, T.M., Schousboe, A., Waagepetersen, H.S., and Ransom, B.R., 2005, Astrocyte glycogen metabolism is required for neural activity during aglycemia or intense stimulation in mouse white matter: Journal of Neuroscience Research, v. 79, p. 74–80, doi: 10.1002/jnr.20335.

Bunge, R.P., 1968, Glial cells and the central myelin sheath: Physiological Reviews, v. 48, p. 197–251.

Burne, J.F., Staple, J.K., and Raff, M.C., 1996, Glial cells are increased proportionally in transgenic optic nerves with increased numbers of axons: The Journal of Neuroscience: The Official Journal of the Society for Neuroscience, v. 16, p. 2064–2073.

Cahoy, J.D., Emery, B., Kaushal, A., Foo, L.C., Zamanian, J.L., Christopherson, K.S., Xing, Y., Lubischer, J.L., Krieg, P.A., Krupenko, S.A., Thompson, W.J., and Barres, B.A., 2008, A Transcriptome Database for Astrocytes, Neurons, and Oligodendrocytes: A New Resource for Understanding Brain Development and Function: The Journal of Neuroscience, v. 28, p. 264–278, doi: 10.1523/JNEUROSCI.4178-07.2008.

Cairns, R.A., Harris, I.S., and Mak, T.W., 2011, Regulation of cancer cell metabolism: Nature Reviews. Cancer, v. 11, p. 85–95, doi: 10.1038/nrc2981.

Capaldi, R.A., 1990, Structure and function of cytochrome c oxidase: Annual Review of Biochemistry, v. 59, p. 569–596, doi: 10.1146/annurev.bi.59.070190.003033.

Cavanagh, J.B., and Harding, B.N., 1994, Pathogenic factors underlying the lesions in Leigh's disease. Tissue responses to cellular energy deprivation and their clinico-pathological consequences: Brain: A Journal of Neurology, v. 117 (Pt 6), p. 1357–1376.

Chandross, K.J., Cohen, R.I., Paras, P., Gravel, M., Braun, P.E., and Hudson, L.D., 1999, Identification and characterization of early glial progenitors using a transgenic

selection strategy: The Journal of Neuroscience: The Official Journal of the Society for Neuroscience, v. 19, p. 759–774.

Chang, C.Y., Choi, D.-K., Lee, D.K., Hong, Y.J., and Park, E.J., 2013, Resveratrol Confers Protection against Rotenone-Induced Neurotoxicity by Modulating Myeloperoxidase Levels in Glial Cells: PLoS ONE, v. 8, p. e60654, doi: 10.1371/journal.pone.0060654.

Chen, N., Sugihara, H., Sharma, J., Perea, G., Petravicz, J., Le, C., and Sur, M., 2012, Nucleus basalis-enabled stimulus-specific plasticity in the visual cortex is mediated by astrocytes: Proceedings of the National Academy of Sciences of the United States of America, v. 109, p. E2832–2841, doi: 10.1073/pnas.1206557109.

Cheon, J.-E., Kim, I.-O., Hwang, Y.S., Kim, K.J., Wang, K.-C., Cho, B.-K., Chi, J.G., Kim, C.J., Kim, W.S., and Yeon, K.M., 2002, Leukodystrophy in children: a pictorial review of MR imaging features: Radiographics: A Review Publication of the Radiological Society of North America, Inc, v. 22, p. 461–476, doi: 10.1148/radiographics.22.3.g02ma01461.

Christofk, H.R., Vander Heiden, M.G., Harris, M.H., Ramanathan, A., Gerszten, R.E., Wei, R., Fleming, M.D., Schreiber, S.L., and Cantley, L.C., 2008, The M2 splice isoform of pyruvate kinase is important for cancer metabolism and tumour growth: Nature, v. 452, p. 230–233, doi: 10.1038/nature06734.

Cuzner, M.L., and Davison, A.N., 1968, The lipid composition of rat brain myelin and subcellular fractions during development: The Biochemical Journal, v. 106, p. 29–34.

Dani, J.W., Chernjavsky, A., and Smith, S.J., 1992, Neuronal activity triggers calcium waves in hippocampal astrocyte networks: Neuron, v. 8, p. 429–440.

Davalos, D., Grutzendler, J., Yang, G., Kim, J.V., Zuo, Y., Jung, S., Littman, D.R., Dustin, M.L., and Gan, W.-B., 2005, ATP mediates rapid microglial response to local brain injury in vivo: Nature Neuroscience, v. 8, p. 752–758, doi: 10.1038/nn1472.

David, C.J., Chen, M., Assanah, M., Canoll, P., and Manley, J.L., 2010, HnRNP proteins controlled by c-Myc deregulate pyruvate kinase mRNA splicing in cancer: Nature, v. 463, p. 364–368, doi: 10.1038/nature08697.

Diaz, F., Garcia, S., Hernandez, D., Regev, A., Rebelo, A., Oca-Cossio, J., and Moraes, C.T., 2008, Pathophysiology and fate of hepatocytes in a mouse model of mitochondrial hepatopathies: Gut, v. 57, p. 232–242, doi: 10.1136/gut.2006.119180.

Diaz, F., Garcia, S., Padgett, K.R., and Moraes, C.T., 2012, A defect in the mitochondrial complex III, but not complex IV, triggers early ROS-dependent damage in defined brain regions: Human Molecular Genetics, v. 21, p. 5066–5077, doi: 10.1093/hmg/dds350.

Diaz, F., Thomas, C.K., Garcia, S., Hernandez, D., and Moraes, C.T., 2005, Mice lacking COX10 in skeletal muscle recapitulate the phenotype of progressive mitochondrial myopathies associated with cytochrome c oxidase deficiency: Human Molecular Genetics, v. 14, p. 2737–2748, doi: 10.1093/hmg/ddi307.

Dibaj, P., Nadrigny, F., Steffens, H., Scheller, A., Hirrlinger, J., Schomburg, E.D., Neusch, C., and Kirchhoff, F., 2010, NO mediates microglial response to acute spinal cord injury under ATP control in vivo: Glia, v. 58, p. 1133–1144, doi: 10.1002/glia.20993.

Dienel, G.A., and Cruz, N.F., 2003, Neighborly interactions of metabolically-activated astrocytes in vivo: Neurochemistry International, v. 43, p. 339–354.

DiMauro, S., Servidei, S., Zeviani, M., DiRocco, M., DeVivo, D.C., DiDonato, S., Uziel, G., Berry, K., Hoganson, G., and Johnsen, S.D., 1987, Cytochrome c oxidase deficiency in Leigh syndrome: Annals of Neurology, v. 22, p. 498–506, doi: 10.1002/ana.410220409.

Dombrauckas, J.D., Santarsiero, B.D., and Mesecar, A.D., 2005, Structural basis for tumor pyruvate kinase M2 allosteric regulation and catalysis: Biochemistry, v. 44, p. 9417–9429, doi: 10.1021/bi0474923.

Domingo, M., Einig, C., Eigenbrodt, E., and Reinacher, M., 1992, Immunohistological demonstration of pyruvate kinase isoenzyme type L in rat with monoclonal antibodies: The Journal of Histochemistry and Cytochemistry: Official Journal of the Histochemistry Society, v. 40, p. 665–673.

Dringen, R., Gebhardt, R., and Hamprecht, B., 1993, Glycogen in astrocytes: possible function as lactate supply for neighboring cells: Brain Research, v. 623, p. 208–214.

Dringen, R., Hoepken, H.H., Minich, T., and Ruedig, C., 2007, 1.3 Pentose Phosphate Pathway and NADPH Metabolism, in Lajtha, A., Gibson, G.E., and Dienel, G.A. eds., Handbook of Neurochemistry and Molecular Neurobiology, Springer US, p. 41–62.

Duong, T.Q., 2007, Cerebral blood flow and BOLD fMRI responses to hypoxia in awake and anesthetized rats: Brain Research, v. 1135, p. 186–194, doi: 10.1016/j.brainres.2006.11.097.

Dziedzic, T., Metz, I., Dallenga, T., König, F.B., Müller, S., Stadelmann, C., and Brück, W., 2010, Wallerian degeneration: a major component of early axonal pathology in multiple sclerosis: Brain Pathology (Zurich, Switzerland), v. 20, p. 976–985, doi: 10.1111/j.1750-3639.2010.00401.x.

Edgar, J.M., McCulloch, M.C., Thomson, C.E., and Griffiths, I.R., 2008, Distribution of mitochondria along small-diameter myelinated central nervous system axons: Journal of Neuroscience Research, v. 86, p. 2250–2257, doi: 10.1002/jnr.21672.

Edgar, J.M., McLaughlin, M., Werner, H.B., McCulloch, M.C., Barrie, J.A., Brown, A., Faichney, A.B., Snaidero, N., Nave, K.-A., and Griffiths, I.R., 2009, Early ultrastructural defects of axons and axon-glia junctions in mice lacking expression of Cnp1: Glia, v. 57, p. 1815–1824, doi: 10.1002/glia.20893.

Edgar, J.M., McLaughlin, M., Yool, D., Zhang, S.-C., Fowler, J.H., Montague, P., Barrie, J.A., McCulloch, M.C., Duncan, I.D., Garbern, J., Nave, K.A., and Griffiths, I.R., 2004, Oligodendroglial modulation of fast axonal transport in a mouse model of hereditary spastic paraplegia: The Journal of Cell Biology, v. 166, p. 121–131, doi: 10.1083/jcb.200312012.

El Waly, B., Macchi, M., Cayre, M., and Durbec, P., 2014, Oligodendrogenesis in the normal and pathological central nervous system: Frontiers in Neuroscience, v. 8, p. 145, doi: 10.3389/fnins.2014.00145.

Eyermann, C., Czaplinski, K., and Colognato, H., 2012, Dystroglycan promotes filopodial formation and process branching in differentiating oligodendroglia: Journal of Neurochemistry, v. 120, p. 928–947, doi: 10.1111/j.1471-4159.2011.07600.x.

Fantin, V.R., St-Pierre, J., and Leder, P., 2006, Attenuation of LDH-A expression uncovers a link between glycolysis, mitochondrial physiology, and tumor maintenance: Cancer Cell, v. 9, p. 425–434, doi: 10.1016/j.ccr.2006.04.023.

Feltri, M.L., D'antonio, M., Quattrini, A., Numerato, R., Arona, M., Previtali, S., Chiu, S.Y., Messing, A., and Wrabetz, L., 1999, A novel P0 glycoprotein transgene activates expression of lacZ in myelin-forming Schwann cells: The European Journal of Neuroscience, v. 11, p. 1577–1586.

Foran, D.R., and Peterson, A.C., 1992, Myelin acquisition in the central nervous system of the mouse revealed by an MBP-Lac Z transgene: The Journal of Neuroscience: The Official Journal of the Society for Neuroscience, v. 12, p. 4890–4897.

Fox, P.T., and Raichle, M.E., 1986, Focal physiological uncoupling of cerebral blood flow and oxidative metabolism during somatosensory stimulation in human subjects: Proceedings of the National Academy of Sciences of the United States of America, v. 83, p. 1140–1144.

Fox, P.T., Raichle, M.E., Mintun, M.A., and Dence, C., 1988, Nonoxidative glucose consumption during focal physiologic neural activity: Science (New York, N.Y.), v. 241, p. 462–464.

Frezza, C., and Gottlieb, E., 2009, Mitochondria in cancer: Not just innocent bystanders: Seminars in Cancer Biology, v. 19, p. 4–11, doi: 10.1016/j.semcancer.2008.11.008.

Fukui, H., Diaz, F., Garcia, S., and Moraes, C.T., 2007, Cytochrome c oxidase deficiency in neurons decreases both oxidative stress and amyloid formation in a mouse model of Alzheimer's disease: Proceedings of the National Academy of Sciences of the United States of America, v. 104, p. 14163–14168, doi: 10.1073/pnas.0705738104.

Fünfschilling, U., Supplie, L.M., Mahad, D., Boretius, S., Saab, A.S., Edgar, J., Brinkmann, B.G., Kassmann, C.M., Tzvetanova, I.D., Möbius, W., Diaz, F., Meijer, D., Suter, U., Hamprecht, B., et al., 2012, Glycolytic oligodendrocytes maintain myelin and long-term axonal integrity: Nature, v. 485, p. 517–521, doi: 10.1038/nature11007.

Gandhi, G.K., Cruz, N.F., Ball, K.K., and Dienel, G.A., 2009, Astrocytes are poised for lactate trafficking and release from activated brain and for supply of glucose to neurons: Journal of Neurochemistry, v. 111, p. 522–536, doi: 10.1111/j.1471-4159.2009.06333.x.

Gao, X., Wang, H., Yang, J.J., Liu, X., and Liu, Z.-R., 2012, Pyruvate kinase M2 regulates gene transcription by acting as a protein kinase: Molecular Cell, v. 45, p. 598–609, doi: 10.1016/j.molcel.2012.01.001.

Genoud, C., Quairiaux, C., Steiner, P., Hirling, H., Welker, E., and Knott, G.W., 2006, Plasticity of astrocytic coverage and glutamate transporter expression in adult mouse cortex: PLoS biology, v. 4, p. e343, doi: 10.1371/journal.pbio.0040343.

Gerard, G.F., D'Alessio, J.M., Kotewicz, M.L., and Noon, M.C., 1986, Influence on stability in Escherichia coli of the carboxy-terminal structure of cloned Moloney murine leukemia virus reverse transcriptase: DNA (Mary Ann Liebert, Inc.), v. 5, p. 271–279.

Giaume, C., Fromaget, C., el Aoumari, A., Cordier, J., Glowinski, J., and Gros, D., 1991, Gap junctions in cultured astrocytes: single-channel currents and characterization of channel-forming protein: Neuron, v. 6, p. 133–143.

Gordon, G.R.J., Mulligan, S.J., and MacVicar, B.A., 2007, Astrocyte control of the cerebrovasculature: Glia, v. 55, p. 1214–1221, doi: 10.1002/glia.20543.

Gourine, A.V., Kasymov, V., Marina, N., Tang, F., Figueiredo, M.F., Lane, S., Teschemacher, A.G., Spyer, K.M., Deisseroth, K., and Kasparov, S., 2010, Astrocytes control breathing through pH-dependent release of ATP: Science (New York, N.Y.), v. 329, p. 571–575, doi: 10.1126/science.1190721.

Gravel, M., Di Polo, A., Valera, P.B., and Braun, P.E., 1998, Four-kilobase sequence of the mouse CNP gene directs spatial and temporal expression of lacZ in transgenic mice: Journal of Neuroscience Research, v. 53, p. 393–404.

Griffiths, I., Klugmann, M., Anderson, T., Yool, D., Thomson, C., Schwab, M.H., Schneider, A., Zimmermann, F., McCulloch, M., Nadon, N., and Nave, K.-A., 1998, Axonal Swellings and Degeneration in Mice Lacking the Major Proteolipid of Myelin: Science, v. 280, p. 1610–1613, doi: 10.1126/science.280.5369.1610.

Gui, D.Y., Lewis, C.A., and Vander Heiden, M.G., 2013, Allosteric regulation of PKM2 allows cellular adaptation to different physiological states: Science Signaling, v. 6, p. pe7, doi: 10.1126/scisignal.2003925.

Hacker, H.J., Steinberg, P., and Bannasch, P., 1998, Pyruvate kinase isoenzyme shift from L-type to M2-type is a late event in hepatocarcinogenesis induced in rats by a choline-deficient/DL-ethionine-supplemented diet: Carcinogenesis, v. 19, p. 99–107.

Halestrap, A.P., and Wilson, M.C., 2012, The monocarboxylate transporter family--role and regulation: IUBMB life, v. 64, p. 109–119, doi: 10.1002/iub.572.

Hamilton, N.B., and Attwell, D., 2010, Do astrocytes really exocytose neurotransmitters? Nature Reviews. Neuroscience, v. 11, p. 227–238, doi: 10.1038/nrn2803.

Herculano-Houzel, S., and Lent, R., 2005, Isotropic fractionator: a simple, rapid method for the quantification of total cell and neuron numbers in the brain: The Journal of Neuroscience: The Official Journal of the Society for Neuroscience, v. 25, p. 2518–2521, doi: 10.1523/JNEUROSCI.4526-04.2005.

Herrero-Mendez, A., Almeida, A., Fernández, E., Maestre, C., Moncada, S., and Bolaños, J.P., 2009, The bioenergetic and antioxidant status of neurons is controlled by continuous degradation of a key glycolytic enzyme by APC/C-Cdh1: Nature Cell Biology, v. 11, p. 747–752, doi: 10.1038/ncb1881.

Hirrlinger, J., Resch, A., Gutterer, J.M., and Dringen, R., 2002, Oligodendroglial cells in culture effectively dispose of exogenous hydrogen peroxide: comparison with cultured neurones, astroglial and microglial cells: Journal of Neurochemistry, v. 82, p. 635–644.

Hitosugi, T., Kang, S., Vander Heiden, M.G., Chung, T.-W., Elf, S., Lythgoe, K., Dong, S., Lonial, S., Wang, X., Chen, G.Z., Xie, J., Gu, T.-L., Polakiewicz, R.D., Roesel, J.L., et al., 2009, Tyrosine phosphorylation inhibits PKM2 to promote the Warburg effect and tumor growth: Science Signaling, v. 2, p. ra73, doi: 10.1126/scisignal.2000431.

Ikeda, Y., and Noguchi, T., 1998, Allosteric regulation of pyruvate kinase M2 isozyme involves a cysteine residue in the intersubunit contact: The Journal of Biological Chemistry, v. 273, p. 12227–12233.

Itoh, Y., Esaki, T., Shimoji, K., Cook, M., Law, M.J., Kaufman, E., and Sokoloff, L., 2003, Dichloroacetate effects on glucose and lactate oxidation by neurons and astroglia in vitro and on glucose utilization by brain in vivo: Proceedings of the National Academy of Sciences of the United States of America, v. 100, p. 4879–4884, doi: 10.1073/pnas.0831078100.

Jahn, O., Tenzer, S., and Werner, H.B., 2009, Myelin proteomics: molecular anatomy of an insulating sheath: Molecular Neurobiology, v. 40, p. 55–72, doi: 10.1007/s12035-009-8071-2.

Kacem, K., Lacombe, P., Seylaz, J., and Bonvento, G., 1998, Structural organization of the perivascular astrocyte endfeet and their relationship with the endothelial glucose transporter: a confocal microscopy study: Glia, v. 23, p. 1–10.

Kang, J.-S., Tian, J.-H., Pan, P.-Y., Zald, P., Li, C., Deng, C., and Sheng, Z.-H., 2008, Docking of axonal mitochondria by syntaphilin controls their mobility and affects short-term facilitation: Cell, v. 132, p. 137–148, doi: 10.1016/j.cell.2007.11.024.

Kotewicz, M.L., D'Alessio, J.M., Driftmier, K.M., Blodgett, K.P., and Gerard, G.F., 1985, Cloning and overexpression of Moloney murine leukemia virus reverse transcriptase in Escherichia coli: Gene, v. 35, p. 249–258.

Kumakura, A., Asada, J., Okumura, R., Fujisawa, I., and Hata, D., 2009, Diffusion-weighted imaging in preclinical Leigh syndrome: Pediatric Neurology, v. 41, p. 309–311, doi: 10.1016/j.pediatrneurol.2009.04.028.

Kumar, Y., Tapuria, N., Kirmani, N., and Davidson, B.R., 2007, Tumour M2-pyruvate kinase: a gastrointestinal cancer marker: European Journal of Gastroenterology & Hepatology, v. 19, p. 265–276, doi: 10.1097/MEG.0b013e3280102f78.

Lappe-Siefke, C., Goebbels, S., Gravel, M., Nicksch, E., Lee, J., Braun, P.E., Griffiths, I.R., and Nave, K.-A., 2003, Disruption of Cnp1 uncouples oligodendroglial functions in axonal support and myelination: Nature Genetics, v. 33, p. 366–374, doi: 10.1038/ng1095.

Larsson, N.G., Wang, J., Wilhelmsson, H., Oldfors, A., Rustin, P., Lewandoski, M., Barsh, G.S., and Clayton, D.A., 1998, Mitochondrial transcription factor A is necessary for mtDNA maintenance and embryogenesis in mice: Nature Genetics, v. 18, p. 231–236, doi: 10.1038/ng0398-231.

Lebre, A.S., Rio, M., Faivre d'Arcier, L., Vernerey, D., Landrieu, P., Slama, A., Jardel, C., Laforêt, P., Rodriguez, D., Dorison, N., Galanaud, D., Chabrol, B., Paquis-Flucklinger, V., Grévent, D., et al., 2011, A common pattern of brain MRI imaging in mitochondrial diseases with complex I deficiency: Journal of Medical Genetics, v. 48, p. 16–23, doi: 10.1136/jmg.2010.079624.

Lee, M., Brennan, A., Blanchard, A., Zoidl, G., Dong, Z., Tabernero, A., Zoidl, C., Dent, M.A., Jessen, K.R., and Mirsky, R., 1997, P0 is constitutively expressed in the rat neural crest and embryonic nerves and is negatively and positively regulated by axons to generate non-myelin-forming and myelin-forming Schwann cells, respectively: Molecular and Cellular Neurosciences, v. 8, p. 336–350.

Lee, Y., Morrison, B.M., Li, Y., Lengacher, S., Farah, M.H., Hoffman, P.N., Liu, Y., Tsingalia, A., Jin, L., Zhang, P.-W., Pellerin, L., Magistretti, P.J., and Rothstein, J.D., 2012, Oligodendroglia metabolically support axons and contribute to neurodegeneration: Nature, v. 487, p. 443–448, doi: 10.1038/nature11314.

Leist, M., Single, B., Castoldi, A.F., Kühnle, S., and Nicotera, P., 1997, Intracellular Adenosine Triphosphate (ATP) Concentration: A Switch in the Decision Between Apoptosis and Necrosis: The Journal of Experimental Medicine, v. 185, p. 1481–1486, doi: 10.1084/jem.185.8.1481.

Li, X., Fang, P., Mai, J., Choi, E.T., Wang, H., and Yang, X., 2013, Targeting mitochondrial reactive oxygen species as novel therapy for inflammatory diseases and cancers: Journal of Hematology & Oncology, v. 6, p. 19, doi: 10.1186/1756-8722-6-19.

Ling, E.A., and Leblond, C.P., 1973, Investigation of glial cells in semithin sections. II. Variation with age in the numbers of the various glial cell types in rat cortex and corpus callosum: The Journal of Comparative Neurology, v. 149, p. 73–81, doi: 10.1002/cne.901490105.

Li, C., Patel, S., Auerbach, E.J., and Zhang, X., 2013, Dose-dependent effect of isoflurane on regional cerebral blood flow in anesthetized macaque monkeys: Neuroscience letters, v. 541, p. 58–62, doi: 10.1016/j.neulet.2013.02.007.

Lovatt, D., Sonnewald, U., Waagepetersen, H.S., Schousboe, A., He, W., Lin, J.H.-C., Han, X., Takano, T., Wang, S., Sim, F.J., Goldman, S.A., and Nedergaard, M., 2007, The transcriptome and metabolic gene signature of protoplasmic astrocytes in the adult murine cortex: The Journal of Neuroscience: The Official Journal of the Society for Neuroscience, v. 27, p. 12255–12266, doi: 10.1523/JNEUROSCI.3404-07.2007.

Lowry, O.H., Rosebrough, N.J., Farr, A.L., and Randall, R.J., 1951, Protein measurement with the Folin phenol reagent: The Journal of Biological Chemistry, v. 193, p. 265–275.

Lv, L., Li, D., Zhao, D., Lin, R., Chu, Y., Zhang, H., Zha, Z., Liu, Y., Li, Z., Xu, Y., Wang, G., Huang, Y., Xiong, Y., Guan, K.-L., et al., 2011, Acetylation targets the M2 isoform of pyruvate kinase for degradation through chaperone-mediated autophagy and promotes tumor growth: Molecular Cell, v. 42, p. 719–730, doi: 10.1016/j.molcel.2011.04.025.

Lv, L., Xu, Y.-P., Zhao, D., Li, F.-L., Wang, W., Sasaki, N., Jiang, Y., Zhou, X., Li, T.-T., Guan, K.-L., Lei, Q.-Y., and Xiong, Y., 2013, Mitogenic and oncogenic stimulation of K433 acetylation promotes PKM2 protein kinase activity and nuclear localization: Molecular Cell, v. 52, p. 340–352, doi: 10.1016/j.molcel.2013.09.004.

Magistretti, P.J., Sorg, O., and Martin, J.-L., 1993, Regulation of glycogen metabolism in astrocytes: physiological, pharmacological and pathological aspects: Astrocytes: pharmacology and function, p. 243–265.

Mahad, D.J., Ziabreva, I., Campbell, G., Laulund, F., Murphy, J.L., Reeve, A.K., Greaves, L., Smith, K.J., and Turnbull, D.M., 2009, Detection of cytochrome c oxidase activity and mitochondrial proteins in single cells: Journal of Neuroscience Methods, v. 184, p. 310–319, doi: 10.1016/j.jneumeth.2009.08.020.

Mahad, D.J., Ziabreva, I., Campbell, G., Lax, N., White, K., Hanson, P.S., Lassmann, H., and Turnbull, D.M., 2009, Mitochondrial changes within axons in multiple sclerosis: Brain, v. 132, p. 1161–1174, doi: 10.1093/brain/awp046.

Majumder, P.K., Febbo, P.G., Bikoff, R., Berger, R., Xue, Q., McMahon, L.M., Manola, J., Brugarolas, J., McDonnell, T.J., Golub, T.R., Loda, M., Lane, H.A., and Sellers, W.R., 2004, mTOR inhibition reverses Akt-dependent prostate intraepithelial neoplasia

through regulation of apoptotic and HIF-1-dependent pathways: Nature Medicine, v. 10, p. 594–601, doi: 10.1038/nm1052.

Matthieu, J.M., Widmer, S., and Herschkowitz, N., 1973, Biochemical changes in mouse brain composition during myelination: Brain Research, v. 55, p. 391–402.

Mazurek, S., 2011, Pyruvate kinase type M2: a key regulator of the metabolic budget system in tumor cells: The International Journal of Biochemistry & Cell Biology, v. 43, p. 969–980, doi: 10.1016/j.biocel.2010.02.005.

Mazurek, S., Boschek, C.B., and Eigenbrodt, E., 1997, The role of phosphometabolites in cell proliferation, energy metabolism, and tumor therapy: Journal of Bioenergetics and Biomembranes, v. 29, p. 315–330.

Mazurek, S., Boschek, C.B., Hugo, F., and Eigenbrodt, E., 2005, Pyruvate kinase type M2 and its role in tumor growth and spreading: Seminars in Cancer Biology, v. 15, p. 300–308, doi: 10.1016/j.semcancer.2005.04.009.

Mazurek, S., and Eigenbrodt, E., 2003, The tumor metabolome: Anticancer Research, v. 23, p. 1149–1154.

Mazurek, S., Grimm, H., Wilker, S., Leib, S., and Eigenbrodt, E., 1998, Metabolic characteristics of different malignant cancer cell lines: Anticancer Research, v. 18, p. 3275–3282.

Mazurek, S., Michel, A., and Eigenbrodt, E., 1997, Effect of extracellular AMP on cell proliferation and metabolism of breast cancer cell lines with high and low glycolytic rates: The Journal of Biological Chemistry, v. 272, p. 4941–4952.

McKeehan, W.L., 1982, Glycolysis, glutaminolysis and cell proliferation: Cell Biology International Reports, v. 6, p. 635–650.

Meberg, P.J., and Miller, M.W., 2003, Culturing Hippocampal and Cortical Neurons, *in* Biology, B.-M. in C. ed., Academic Press, p. 111–127.

Menzies, R.A., and Gold, P.H., 1971, The turnover of mitochondria in a variety of tissues of young adult and aged rats: The Journal of Biological Chemistry, v. 246, p. 2425–2429.

Merezhinskaya, N., and Fishbein, W.N., 2009, Monocarboxylate transporters: past, present, and future: Histology and Histopathology, v. 24, p. 243–264.

Minichiello, L., Calella, A.M., Medina, D.L., Bonhoeffer, T., Klein, R., and Korte, M., 2002, Mechanism of TrkB-Mediated Hippocampal Long-Term Potentiation: Neuron, v. 36, p. 121–137, doi: 10.1016/S0896-6273(02)00942-X.

Mori, T., Tanaka, K., Buffo, A., Wurst, W., Kühn, R., and Götz, M., 2006, Inducible gene deletion in astroglia and radial glia--a valuable tool for functional and lineage analysis: Glia, v. 54, p. 21–34, doi: 10.1002/glia.20350.

Morrison, B.M., Lee, Y., and Rothstein, J.D. (2013). Oligodendroglia: metabolic supporters of axons. Trends Cell Biol. *23*, 644–651

Morland, C., Henjum, S., Iversen, E.G., Skrede, K.K., and Hassel, B., 2007, Evidence for a higher glycolytic than oxidative metabolic activity in white matter of rat brain: Neurochemistry International, v. 50, p. 703–709, doi: 10.1016/j.neuint.2007.01.003.

Morris, R.L., and Hollenbeck, P.J., 1993, The regulation of bidirectional mitochondrial transport is coordinated with axonal outgrowth: Journal of Cell Science, v. 104 (Pt 3), p. 917–927.

Mullis, K., Faloona, F., Scharf, S., Saiki, R., Horn, G., and Erlich, H., 1986, Specific enzymatic amplification of DNA in vitro: the polymerase chain reaction: Cold Spring Harbor Symposia on Quantitative Biology, v. 51 Pt 1, p. 263–273.

Nagy, J.I., Ionescu, A.V., Lynn, B.D., and Rash, J.E., 2003, Connexin29 and connexin32 at oligodendrocyte and astrocyte gap junctions and in myelin of the mouse central nervous system: The Journal of Comparative Neurology, v. 464, p. 356–370, doi: 10.1002/cne.10797.

Nakao, J., Shinoda, J., Nakai, Y., Murase, S., and Uyemura, K., 1997, Apoptosis regulates the number of Schwann cells at the premyelinating stage: Journal of Neurochemistry, v. 68, p. 1853–1862.

Nave, K.-A., 2010, Myelination and the trophic support of long axons: Nature Reviews. Neuroscience, v. 11, p. 275–283, doi: 10.1038/nrn2797.

Newsholme, P., Lima, M.M.R., Procopio, J., Pithon-Curi, T.C., Doi, S.Q., Bazotte, R.B., and Curi, R., 2003, Glutamine and glutamate as vital metabolites: Brazilian Journal of Medical and Biological Research = Revista Brasileira De Pesquisas Médicas E Biológicas / Sociedade Brasileira De Biofísica ... [et Al.], v. 36, p. 153–163.

Nimmerjahn, A., Mukamel, E.A., and Schnitzer, M.J., 2009, Motor behavior activates Bergmann glial networks: Neuron, v. 62, p. 400–412, doi: 10.1016/j.neuron.2009.03.019.

Nishino, I., Spinazzola, A., and Hirano, M., 1999, Thymidine phosphorylase gene mutations in MNGIE, a human mitochondrial disorder: Science (New York, N.Y.), v. 283, p. 689–692.

Noguchi, T., Inoue, H., and Tanaka, T., 1986, The M1- and M2-type isozymes of rat pyruvate kinase are produced from the same gene by alternative RNA splicing: The Journal of Biological Chemistry, v. 261, p. 13807–13812.

Oblinger, M.M., Foe, L.G., Kwiatkowska, D., and Kemp, R.G., 1988, Phosphofructokinase in the rat nervous system: regional differences in activity and characteristics of axonal transport: Journal of Neuroscience Research, v. 21, p. 25–34, doi: 10.1002/jnr.490210105.

Ohno, N., Kidd, G.J., Mahad, D., Kiryu-Seo, S., Avishai, A., Komuro, H., and Trapp, B.D., 2011, Myelination and axonal electrical activity modulate the distribution and motility of mitochondria at CNS nodes of Ranvier: The Journal of Neuroscience: The Official Journal of the Society for Neuroscience, v. 31, p. 7249–7258, doi: 10.1523/JNEUROSCI.0095-11.2011.

Orth, M., and Bellosta, S., 2012, Cholesterol: its regulation and role in central nervous system disorders: Cholesterol, v. 2012, p. 292598, doi: 10.1155/2012/292598.

Panatier, A., Theodosis, D.T., Mothet, J.-P., Touquet, B., Pollegioni, L., Poulain, D.A., and Oliet, S.H.R., 2006, Glia-derived D-serine controls NMDA receptor activity and synaptic memory: Cell, v. 125, p. 775–784, doi: 10.1016/j.cell.2006.02.051.

Panatier, A., Vallée, J., Haber, M., Murai, K.K., Lacaille, J.-C., and Robitaille, R., 2011, Astrocytes are endogenous regulators of basal transmission at central synapses: Cell, v. 146, p. 785–798, doi: 10.1016/j.cell.2011.07.022.

Parpura, V., Basarsky, T.A., Liu, F., Jeftinija, K., Jeftinija, S., and Haydon, P.G., 1994, Glutamate-mediated astrocyte-neuron signalling: Nature, v. 369, p. 744–747, doi: 10.1038/369744a0.

Pellerin, L., and Magistretti, P.J., 1994, Glutamate uptake into astrocytes stimulates aerobic glycolysis: a mechanism coupling neuronal activity to glucose utilization: Proceedings of the National Academy of Sciences of the United States of America, v. 91, p. 10625–10629.

Pellerin, L., Pellegri, G., Martin, J.L., and Magistretti, P.J., 1998, Expression of monocarboxylate transporter mRNAs in mouse brain: support for a distinct role of lactate as an energy substrate for the neonatal vs. adult brain: Proceedings of the National Academy of Sciences of the United States of America, v. 95, p. 3990–3995.

Perrot, R., and Julien, J.-P., 2009, Real-time imaging reveals defects of fast axonal transport induced by disorganization of intermediate filaments: The FASEB Journal, v. 23, p. 3213–3225, doi: 10.1096/fj.09-129585.

Peters, A., 1966, The node of Ranvier in the central nervous system: Quarterly Journal of Experimental Physiology and Cognate Medical Sciences, v. 51, p. 229–236.

Peterson, G.L., 1979, Review of the Folin phenol protein quantitation method of Lowry, Rosebrough, Farr and Randall: Analytical Biochemistry, v. 100, p. 201–220.

Peterson, J.W., Bö, L., Mörk, S., Chang, A., and Trapp, B.D., 2001, Transected neurites, apoptotic neurons, and reduced inflammation in cortical multiple sclerosis lesions: Annals of Neurology, v. 50, p. 389–400.

Pierre, K., Magistretti, P.J., and Pellerin, L., 2002, MCT2 is a major neuronal monocarboxylate transporter in the adult mouse brain: Journal of Cerebral Blood Flow and Metabolism: Official Journal of the International Society of Cerebral Blood Flow and Metabolism, v. 22, p. 586–595, doi: 10.1097/00004647-200205000-00010.

Pierre, K., and Pellerin, L., 2005, Monocarboxylate transporters in the central nervous system: distribution, regulation and function: Journal of Neurochemistry, v. 94, p. 1–14, doi: 10.1111/j.1471-4159.2005.03168.x.

Pierre, K., Pellerin, L., Debernardi, R., Riederer, B.M., and Magistretti, P.J., 2000, Cell-specific localization of monocarboxylate transporters, MCT1 and MCT2, in the adult mouse brain revealed by double immunohistochemical labelling and confocal microscopy: Neuroscience, v. 100, p. 617–627.

Reinacher, M., and Eigenbrodt, E., 1981, Immunohistological demonstration of the same type of pyruvate kinase isoenzyme (M2-Pk) in tumors of chicken and rat: Virchows Archiv. B, Cell Pathology Including Molecular Pathology, v. 37, p. 79–88.

Reitzer, L.J., Wice, B.M., and Kennell, D., 1979, Evidence that glutamine, not sugar, is the major energy source for cultured HeLa cells: The Journal of Biological Chemistry, v. 254, p. 2669–2676.

Rinholm, J.E., Hamilton, N.B., Kessaris, N., Richardson, W.D., Bergersen, L.H., and Attwell, D., 2011, Regulation of oligodendrocyte development and myelination by glucose and

lactate: The Journal of Neuroscience: The Official Journal of the Society for Neuroscience, v. 31, p. 538–548, doi: 10.1523/JNEUROSCI.3516-10.2011.

Rodriguez-Horche, P., Luque, J., Perez-Artes, E., Pineda, M., and Pinilla, M., 1987, Comparative kinetic behaviour and regulation by fructose-1,6-bisphosphate and ATP of pyruvate kinase from erythrocytes, reticulocytes and bone marrow cells: Comparative Biochemistry and Physiology. B, Comparative Biochemistry, v. 87, p. 553–557.

Rosenbluth, J., 1980, Central myelin in the mouse mutant shiverer: The Journal of Comparative Neurology, v. 194, p. 639–648, doi: 10.1002/cne.901940310.

Rossner, M.J., Hirrlinger, J., Wichert, S.P., Boehm, C., Newrzella, D., Hiemisch, H., Eisenhardt, G., Stuenkel, C., Ahsen, O. von, and Nave, K.-A., 2006, Global Transcriptome Analysis of Genetically Identified Neurons in the Adult Cortex: The Journal of Neuroscience, v. 26, p. 9956–9966, doi: 10.1523/JNEUROSCI.0468-06.2006.

Rothstein, J.D., Dykes-Hoberg, M., Pardo, C.A., Bristol, L.A., Jin, L., Kuncl, R.W., Kanai, Y., Hediger, M.A., Wang, Y., Schielke, J.P., and Welty, D.F., 1996, Knockout of glutamate transporters reveals a major role for astroglial transport in excitotoxicity and clearance of glutamate: Neuron, v. 16, p. 675–686.

Saab, A.S., Neumeyer, A., Jahn, H.M., Cupido, A., Šimek, A.A.M., Boele, H.-J., Scheller, A., Le Meur, K., Götz, M., Monyer, H., Sprengel, R., Rubio, M.E., Deitmer, J.W., De Zeeuw, C.I., et al., 2012, Bergmann glial AMPA receptors are required for fine motor coordination: Science (New York, N.Y.), v. 337, p. 749–753, doi: 10.1126/science.1221140.

Saher, G., Brügger, B., Lappe-Siefke, C., Möbius, W., Tozawa, R., Wehr, M.C., Wieland, F., Ishibashi, S., and Nave, K.-A., 2005, High cholesterol level is essential for myelin membrane growth: Nature Neuroscience, v. 8, p. 468–475, doi: 10.1038/nn1426.

Saiki, R.K., Gelfand, D.H., Stoffel, S., Scharf, S.J., Higuchi, R., Horn, G.T., Mullis, K.B., and Erlich, H.A., 1988, Primer-directed enzymatic amplification of DNA with a thermostable DNA polymerase: Science, v. 239, p. 487–491, doi: 10.1126/science.2448875.

Saiki, K., Mogi, T., Hori, H., Tsubaki, M., and Anraku, Y., 1993, Identification of the functional domains in heme O synthase. Site-directed mutagenesis studies on the cyoE gene of the cytochrome bo operon in Escherichia coli: The Journal of Biological Chemistry, v. 268, p. 26927–26934.

Sancho, S., Young, P., and Suter, U., 2001, Regulation of Schwann cell proliferation and apoptosis in PMP22-deficient mice and mouse models of Charcot-Marie-Tooth disease type 1A: Brain: A Journal of Neurology, v. 124, p. 2177–2187.

Sandell, J.H., and Peters, A., 2002, Effects of age on the glial cells in the rhesus monkey optic nerve: The Journal of Comparative Neurology, v. 445, p. 13–28.

Scherer, S.S., Braun, P.E., Grinspan, J., Collarini, E., Wang, D.Y., and Kamholz, J., 1994, Differential regulation of the 2',3'-cyclic nucleotide 3'-phosphodiesterase gene during oligodendrocyte development: Neuron, v. 12, p. 1363–1375.

Schultz, R.L., and Karlsson, U., 1965, FIXATION OF THE CENTRAL NERVOUS SYSTEM FOR ELECTRON MICROSCOPY BY ALDEHYDE PERFUSION. II. EFFECT OF

OSMOLARITY, PH OF PERFUSATE, AND FIXATIVE CONCENTRATION: Journal of Ultrastructure Research, v. 12, p. 187–206.

Sherwood, C.C., Stimpson, C.D., Raghanti, M.A., Wildman, D.E., Uddin, M., Grossman, L.I., Goodman, M., Redmond, J.C., Bonar, C.J., Erwin, J.M., and Hof, P.R., 2006, Evolution of increased glia-neuron ratios in the human frontal cortex: Proceedings of the National Academy of Sciences of the United States of America, v. 103, p. 13606–13611, doi: 10.1073/pnas.0605843103.

Shigetomi, E., Jackson-Weaver, O., Huckstepp, R.T., O'Dell, T.J., and Khakh, B.S., 2013, TRPA1 channels are regulators of astrocyte basal calcium levels and long-term potentiation via constitutive D-serine release: The Journal of Neuroscience: The Official Journal of the Society for Neuroscience, v. 33, p. 10143–10153, doi: 10.1523/JNEUROSCI.5779-12.2013.

Skoff, R.P., Toland, D., and Nast, E., 1980, Pattern of myelination and distribution of neuroglial cells along the developing optic system of the rat and rabbit: The Journal of Comparative Neurology, v. 191, p. 237–253, doi: 10.1002/cne.901910207.

Snaidero, N., Möbius, W., Czopka, T., Hekking, L.H.P., Mathisen, C., Verkleij, D., Goebbels, S., Edgar, J., Merkler, D., Lyons, D.A., Nave, K.-A., and Simons, M., 2014, Myelin membrane wrapping of CNS axons by PI(3,4,5)P3-dependent polarized growth at the inner tongue: Cell, v. 156, p. 277–290, doi: 10.1016/j.cell.2013.11.044.

Sokoloff, L., Reivich, M., Kennedy, C., Des Rosiers, M.H., Patlak, C.S., Pettigrew, K.D., Sakurada, O., and Shinohara, M., 1977, The [14C]deoxyglucose method for the measurement of local cerebral glucose utilization: theory, procedure, and normal values in the conscious and anesthetized albino rat: Journal of Neurochemistry, v. 28, p. 897–916.

Spoden, G.A., Rostek, U., Lechner, S., Mitterberger, M., Mazurek, S., and Zwerschke, W., 2009, Pyruvate kinase isoenzyme M2 is a glycolytic sensor differentially regulating cell proliferation, cell size and apoptotic cell death dependent on glucose supply: Experimental Cell Research, v. 315, p. 2765–2774, doi: 10.1016/j.yexcr.2009.06.024.

Srinivas, S., Watanabe, T., Lin, C.S., William, C.M., Tanabe, Y., Jessell, T.M., and Costantini, F., 2001, Cre reporter strains produced by targeted insertion of EYFP and ECFP into the ROSA26 locus: BMC developmental biology, v. 1, p. 4.

Stahl, N., Harry, J., and Popko, B., 1990, Quantitative analysis of myelin protein gene expression during development in the rat sciatic nerve: Brain Research. Molecular Brain Research, v. 8, p. 209–212.

Sturrock, R.R., 1980, Myelination of the mouse corpus callosum: Neuropathology and Applied Neurobiology, v. 6, p. 415–420.

Sun, Q., Chen, X., Ma, J., Peng, H., Wang, F., Zha, X., Wang, Y., Jing, Y., Yang, H., Chen, R., Chang, L., Zhang, Y., Goto, J., Onda, H., et al., 2011, Mammalian target of rapamycin up-regulation of pyruvate kinase isoenzyme type M2 is critical for aerobic glycolysis and tumor growth: Proceedings of the National Academy of Sciences of the United States of America, v. 108, p. 4129–4134, doi: 10.1073/pnas.1014769108.

Suzuki, A., Stern, S.A., Bozdagi, O., Huntley, G.W., Walker, R.H., Magistretti, P.J., and Alberini, C.M., 2011, Astrocyte-neuron lactate transport is required for long-term memory formation: Cell, v. 144, p. 810–823, doi: 10.1016/j.cell.2011.02.018.

Tanaka, T., Harano, Y., Sue, F., and Morimura, H., 1967, Crystallization, characterization and metabolic regulation of two types of pyruvate kinase isolated from rat tissues: Journal of Biochemistry, v. 62, p. 71–91.

Tekkök, S.B., Brown, A.M., Westenbroek, R., Pellerin, L., and Ransom, B.R., 2005, Transfer of glycogen-derived lactate from astrocytes to axons via specific monocarboxylate transporters supports mouse optic nerve activity: Journal of Neuroscience Research, v. 81, p. 644–652, doi: 10.1002/jnr.20573.

Towbin, H., Staehelin, T., and Gordon, J., 1979, Electrophoretic transfer of proteins from polyacrylamide gels to nitrocellulose sheets: procedure and some applications: Proceedings of the National Academy of Sciences of the United States of America, v. 76, p. 4350–4354.

Trapp, B.D., Peterson, J., Ransohoff, R.M., Rudick, R., Mörk, S., and Bö, L., 1998, Axonal transection in the lesions of multiple sclerosis: The New England Journal of Medicine, v. 338, p. 278–285, doi: 10.1056/NEJM199801293380502.

Ullian, E.M., Sapperstein, S.K., Christopherson, K.S., and Barres, B.A., 2001, Control of Synapse Number by Glia: Science, v. 291, p. 657–661, doi: 10.1126/science.291.5504.657.

Valnot, I., von Kleist-Retzow, J.C., Barrientos, A., Gorbatyuk, M., Taanman, J.W., Mehaye, B., Rustin, P., Tzagoloff, A., Munnich, A., and Rötig, A., 2000, A mutation in the human heme A:farnesyltransferase gene (COX10) causes cytochrome c oxidase deficiency: Human Molecular Genetics, v. 9, p. 1245–1249.

Vander Heiden, M.G., Cantley, L.C., and Thompson, C.B., 2009, Understanding the Warburg effect: the metabolic requirements of cell proliferation: Science (New York, N.Y.), v. 324, p. 1029–1033, doi: 10.1126/science.1160809.

Vander Heiden, M.G., Locasale, J.W., Swanson, K.D., Sharfi, H., Heffron, G.J., Amador-Noguez, D., Christofk, H.R., Wagner, G., Rabinowitz, J.D., Asara, J.M., and Cantley, L.C., 2010, Evidence for an alternative glycolytic pathway in rapidly proliferating cells: Science (New York, N.Y.), v. 329, p. 1492–1499, doi: 10.1126/science.1188015.

Vannucci, S.J., and Simpson, I.A., 2003, Developmental switch in brain nutrient transporter expression in the rat: American Journal of Physiology. Endocrinology and Metabolism, v. 285, p. E1127–1134, doi: 10.1152/ajpendo.00187.2003.

Viader, A., Golden, J.P., Baloh, R.H., Schmidt, R.E., Hunter, D.A., and Milbrandt, J., 2011, Schwann cell mitochondrial metabolism supports long-term axonal survival and peripheral nerve function: The Journal of Neuroscience: The Official Journal of the Society for Neuroscience, v. 31, p. 10128–10140, doi: 10.1523/JNEUROSCI.0884-11.2011.

Viader, A., Sasaki, Y., Kim, S., Strickland, A., Workman, C.S., Yang, K., Gross, R.W., and Milbrandt, J., 2013, Aberrant Schwann cell lipid metabolism linked to mitochondrial deficits leads to axon degeneration and neuropathy: Neuron, v. 77, p. 886–898, doi: 10.1016/j.neuron.2013.01.012.

Walhovd, K.B., Johansen-Berg, H., and Káradóttir, R.T., 2014, Unraveling the secrets of white matter--bridging the gap between cellular, animal and human imaging studies: Neuroscience, v. 276, p. 2–13, doi: 10.1016/j.neuroscience.2014.06.058.

Wood, T., 1986, Physiological functions of the pentose phosphate pathway: Cell Biochemistry and Function, v. 4, p. 241–247, doi: 10.1002/cbf.290040403.

Wyss, M.T., Jolivet, R., Buck, A., Magistretti, P.J., and Weber, B., 2011, In vivo evidence for lactate as a neuronal energy source: The Journal of Neuroscience: The Official Journal of the Society for Neuroscience, v. 31, p. 7477–7485, doi: 10.1523/JNEUROSCI.0415-11.2011.

Xanthos, D.N., and Sandkühler, J., 2014, Neurogenic neuroinflammation: inflammatory CNS reactions in response to neuronal activity: Nature Reviews. Neuroscience, v. 15, p. 43–53, doi: 10.1038/nrn3617.

Yamada, K., and Noguchi, T., 1999, Regulation of pyruvate kinase M gene expression: Biochemical and Biophysical Research Communications, v. 256, p. 257–262, doi: 10.1006/bbrc.1999.0228.

Yang, Y., Ge, W., Chen, Y., Zhang, Z., Shen, W., Wu, C., Poo, M., and Duan, S., 2003, Contribution of astrocytes to hippocampal long-term potentiation through release of D-serine: Proceedings of the National Academy of Sciences of the United States of America, v. 100, p. 15194–15199, doi: 10.1073/pnas.2431073100.

Yang, W., Xia, Y., Cao, Y., Zheng, Y., Bu, W., Zhang, L., You, M.J., Koh, M.Y., Cote, G., Aldape, K., Li, Y., Verma, I.M., Chiao, P.J., and Lu, Z., 2012, EGFR-induced and PKCε monoubiquitylation-dependent NF-κB activation upregulates PKM2 expression and promotes tumorigenesis: Molecular Cell, v. 48, p. 771–784, doi: 10.1016/j.molcel.2012.09.028.

Yang, W., Xia, Y., Ji, H., Zheng, Y., Liang, J., Huang, W., Gao, X., Aldape, K., and Lu, Z., 2011, Nuclear PKM2 regulates β-catenin transactivation upon EGFR activation: Nature, v. 480, p. 118–122, doi: 10.1038/nature10598.

Yang, W., Zheng, Y., Xia, Y., Ji, H., Chen, X., Guo, F., Lyssiotis, C.A., Aldape, K., Cantley, L.C., and Lu, Z., 2012, ERK1/2-dependent phosphorylation and nuclear translocation of PKM2 promotes the Warburg effect: Nature Cell Biology, v. 14, p. 1295–1304, doi: 10.1038/ncb2629.

Yeung, M.S.Y., Zdunek, S., Bergmann, O., Bernard, S., Salehpour, M., Alkass, K., Perl, S., Tisdale, J., Possnert, G., Brundin, L., Druid, H., and Frisén, J., 2014, Dynamics of oligodendrocyte generation and myelination in the human brain: Cell, v. 159, p. 766–774, doi: 10.1016/j.cell.2014.10.011.

Yin, X., Crawford, T.O., Griffin, J.W., Tu, P. h, Lee, V.M., Li, C., Roder, J., and Trapp, B.D., 1998, Myelin-associated glycoprotein is a myelin signal that modulates the caliber of myelinated axons: The Journal of Neuroscience: The Official Journal of the Society for Neuroscience, v. 18, p. 1953–1962.

Yiş, U., Seneca, S., Dirik, E., Kurul, S.H., Ozer, E., Cakmakçi, H., and De Meirleir, L., 2009, Unusual findings in Leigh syndrome caused by T8993C mutation: European journal of paediatric neurology: EJPN: official journal of the European Paediatric Neurology Society, v. 13, p. 550–552, doi: 10.1016/j.ejpn.2008.10.009.

Young, E.A., Fowler, C.D., Kidd, G.J., Chang, A., Rudick, R., Fisher, E., and Trapp, B.D., 2008, Imaging correlates of decreased axonal Na+/K+ ATPase in chronic multiple sclerosis lesions: Annals of Neurology, v. 63, p. 428–435, doi: 10.1002/ana.21381.

Yuan, A., Mills, R.G., Bamburg, J.R., and Bray, J.J., 1999, Cotransport of glyceraldehyde-3-phosphate dehydrogenase and actin in axons of chicken motoneurons: Cellular and Molecular Neurobiology, v. 19, p. 733–744.

Zalc, B., Goujet, D., and Colman, D., 2008, The origin of the myelination program in vertebrates: Current Biology, v. 18, p. R511–R512, doi: 10.1016/j.cub.2008.04.010.

Zhuang, Z., Yang, B., Theus, M.H., Sick, J.T., Bethea, J.R., Sick, T.J., and Liebl, D.J., 2010, EphrinBs regulate D-serine synthesis and release in astrocytes: The Journal of Neuroscience: The Official Journal of the Society for Neuroscience, v. 30, p. 16015–16024, doi: 10.1523/JNEUROSCI.0481-10.2010.

Zwerschke, W., Mazurek, S., Massimi, P., Banks, L., Eigenbrodt, E., and Jansen-Dürr, P., 1999, Modulation of type M2 pyruvate kinase activity by the human papillomavirus type 16 E7 oncoprotein: Proceedings of the National Academy of Sciences of the United States of America, v. 96, p. 1291–1296.

Zwerschke, W., Mazurek, S., Stöckl, P., Hütter, E., Eigenbrodt, E., and Jansen-Dürr, P., 2003, Metabolic analysis of senescent human fibroblasts reveals a role for AMP in cellular senescence: The Biochemical Journal, v. 376, p. 403–411, doi: 10.1042/BJ20030816.

9 ACKNOWLEDGEMENTS

I wish to express my deepest appreciation to my supervisor Prof. Dr. Klaus-Armin Nave for his overall support and that he always took the time to discuss ideas and shared his scientific expertise with me. I am very grateful and indepted for the opportunity and his trust to work freely on these challenging projects.

I would like to thank the members of my thesis committee, Prof. E. Wimmer and Prof. M. Rossner for their support during my thesis. I thank Prof. H. Ehrenreich, Prof. R. Heinrich, Dr. M. Schmidt and Prof. M. Sereda for their willingness to extend my examination board.

Special thanks go to all co-authors. I would like to emphasize Dr. Ursula Fünfschilling who contributes a lot of data and ideas, Dr. Don Mahad and Dr. Graham Campbell for the performance of the SDH/ COX histochemistry as well as Prof. Dr. Susann Boretius and Prof. Dr. Jens Frahm who did the NMR experiments.

I thank all members of the Neurogenetics department for generating a very friendly working atmosphere and for being always open for discussions and their cooperativeness.

I like to express my gratitude to Aiman Saab who supported me with invaluable advices and shared a lot of scientific knowledge with me in the beginning of my PhD thesis. I would like to thank Torben Ruhwedel and Dr. Wiebke Möbius for their help with the electron microscopy and as well Annette Fahrenholz and Verena Meywirth for their constant support with histological issues. Dr. Iva Tzvetanova taught me culturing primary cells and Ulli Bode was often my contact person concerning technical questions or troubles in science. Thanks a lot for this. I am very grateful to Dr. Ben Brankatschk, Dr. Sven Wichert and Dr. Bastian Brinkmann for helping me in any technical problems and experimental tips and tricks. Special thanks go to Tim Düking, who experimentally supported me in one part of my thesis and especially for his trust in allowing me as his mentor. Many thanks go to Dr. Iva Tzvetanova and Christof as well as Hannah for proof-reading my PhD thesis.

I would like to extend my gratitude to our animal caretakers, especially Conny Casper and Tanja Freerk, for providing an excellent mouse house and for being always very cooperative. I thank Hajo Horn, Rolf Merker and Lothar Demel for solving computer-related problems.

I am deeply thankful to Gabi Endo and Ela Schmalstieg for their immense care and support, also beyond bureaucratic hurdles. Without you the lab wouldn´t be so funny anymore.

Resi, Sarah, Uli Hannah and Elina, it was really great to have you around in the lab. Thank you for your technical and mental support in daily lab routine and the fun we had together during and after work. It is amazing to have friends like you.

I wish to thank my flat-mates and friends, especially Usching, Rosa, Kristin, Christof, Sören, Batti and Beckbert for reminding me of other important things in life, but also for their support and love.

Above all, I want to thank my family for keeping me constantly grounded, your love and encouragement and that you are always there for me.

10 CURRICULUM VITAE

Personal details

Surname:	Supplie
Forename:	Lotti Marianna
Nationality:	German
Date and place of birth:	November 1th, 1983, Burg, Germany

Work address:	Department of Neurogenetics
	Max Planck Institute of Experimental Medicine
	Hermann-Rein-Str. 3
	37075, Göttingen, Germany

Email address:	supplie@em.mpg.de

Scientific education

Jan. 2010 – present	PhD student (Doktorandin),
	Department of Neurogenetics,
	Max Planck Institute of Experimental Medicine,
	Göttingen, Germany
Apr. 2009 – Jan. 2010	Diploma thesis, Research project
	Project title "Analyse des Zerebellums Konditionaler
	NeuroD Mausmutanten"
	MPI of Exp. Medicine, Göttingen, Germany
Oct. 2004 – Jan. 2010	Biologie Studium (Studies in Biology)
	Georg-August-Universität Göttingen, Germany
	Graduation date: 22.02.2010
	Average grade: 1.4 (very good)

Oct. 2003 – Oct. 2004   Job training to "pharmaceutic-technical assistance"

Berufsbildende Schule "Dr. Otto Schlein"

Magdeburg, Germany

School education

June 2003   Abitur, Erlangung der Allgemeinen Hochschulreife

University Entrance Qualification

Gymnasium Burg, Burg

39288, Germany

Average grade: 2.0 (good)

Poster presentation

Supplie LM, Düking T, Moraes CT, Mahad D, and Nave KA. Survival of respiration-deficient astrocytes by aerobic glycolysis *in vivo*. 5th Axon Degeneration Meeting, Berlin, Germany, 2014

Publications

Fünfschilling U[#], **Supplie LM**[#], Mahad D[#], Boretius S[#], Saab AS, Edgar J, Brinkmann BG, Kassmann CM, Tzvetanova ID, Möbius W, Diaz F, Meijer D, Suter U, Hamprecht B, Sereda MW, Moraes CT, Frahm J, Goebbles S, and Nave KA. (2012), Glycolytic oligodendrocytes maintain myelin and long-term axonal integrity. Nature *485*, 517–521. [#] equal contribution

Supplie LM, Düking T, Campbell G, Diaz F, Moraes CT, Hamprecht B, Götz M, Mahad D and Nave KA. (2015), Survival of respiration-deficient astrocytes by aerobic glycolysis *in vivo*. Glia (in preparation).